AN EXPERIMENTAL STUDY OF DISCHARGE MECHANISM IN ECDM

By
Anjali V. Kulkarni

DEPARTMENT OF ELECTRICAL ENGINEERING
INDIAN INSTITUTE OF TECHNOLOGY KANPUR
July, 2000

AN EXPERIMENTAL STUDY OF DISCHARGE MECHANISM IN ECDM

A Thesis Submitted
In Partial Fulfillment of the Requirements
for the Degree of
MASTER OF TECHNOLOGY

By

Anjali V. Kulkarni
9710425

to the

DEPARTMENT OF ELECTRICAL ENGINEERING
INDIAN INSTITUTE OF TECHNOLOGY KANPUR

July, 2000

TH

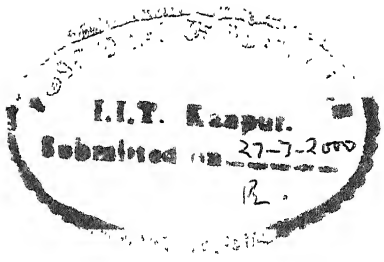

Certificate

This is to certify that the present work entitled "**AN EXPERIMENTAL STUDY OF DISCHARGE MECHANISM IN ECDM**" has been carried out by Anjali V. Kulkarni under our supervision and that this work has not been submitted elsewhere for a degree.

R. Sharan
Professor
Electrical Engineering Dept.
I.I.T. Kanpur

G.K. Lal
Professor
Mechanical Engineering Dept.
I.I.T. Kanpur

July, 2000

ACKNOWLEDGEMENTS

I express my deep sense of gratitude towards Prof. R. Sharan of Electrical Engineering Department and Prof. G..K. Lal of Mechanical Engineering Department, for their valuable suggestions and inspiring guidance throughout the work.

I am grateful to Prof. A. Ghosh of Mechanical Engineering Department (presently Director, I.I.T., Kharagpur) for introducing me to this interesting field of research of electrochemical discharge machining (ECDM) and for his encouragement, advice and suggestions. I am thankful to Prof. V.K. Jain of Mechanical Engineering Department for many valuable discussions and for his advice and suggestions. I am thankful to Prof. H. Hatwal, and Dr. Bhaskar Dasgupta of Mechanical Engineering Department, Prof. Kripashanker of Industrial Management Engineering Department and Dr. Amitabh Mukerjee of Computer Science Engineering Departement for their advice and help.

I am grateful to Dr. Sanjay Gupta of ACMS for providing me the pyrometer for carrying out temperature measurements and for giving me full liberty to tamper with it to explore and modify its working. I am thankful to Mr. B.K. Jain of ACMS for getting the optical photographs of the samples.

Shri. R.M. Jha, Shri. Namdeo Murkhe, Shri. Sharma and Shri. Anil Jha of the Manufacturing Laboratory have helped in fabricating several components required for experiments. I gratefully acknowledge their help.

I am thankful to Shri. S. Sen of Centre for Robotics, for many valuable suggestions. My special thanks are due to Smt. Madhuri Karnik for her whole hearted help in carrying out the experiments. I am also thankful to Shri. Rajendra, Shri. Vivek Shukla, Shri. R.S. Gupta and Shri Pannalal of the Centre for Robotics for their timely help.

I express my deep sense of gratitude towards my parents, my in-laws and my younger brothers Abhay and Anand for their encouragement, help and affection which was a constant source of inspiration for me. I lovingly thank my daughters Vedricha and Apoorva for their stoic forbearance.

Finally, I thank the Department of Science and Technology, New Delhi, for financial support.

श्री

।। ॐ तत्सत् ब्रह्मार्पणमस्तु ।।

CONTENTS

LIST OF FIGURES **p.n.**

LIST OF TABLES

LIST OF PHOTOGRAPHS

ABSTRACT

Electrical discharge associated with the electrolysis process causes material removal and can be effectively used for machining of conducting as well as non conducting materials. Theses processes are known as electrochemical discharge machining (ECDM) processes Although ECDM is commercially in use, the basic mechanism of the process is not yet completely understood and is still a matter of research investigations. The present work has attempted to measure the time varying temperature and current in the process to reveal the basic mechanism of temperature rise and material removal and to calculate the efficiency of the process.

Experiments are performed using different workpiece materials viz, copper, brass, silicon and tantalum. In the case of copper, experiments have been performed using the fractional method scheme with supply voltage ranging from 130V-180V and HCl electrolyte concentration from 1%-5% in volume. For other materials, experiments are performed at supply voltage of 155V and 3% electrolyte concentration. A novel way has been developed to remotely sense the time varying temperature of workpiece using a radiation pyrometer. In addition the temperature at different locations in ECDM cell and on the workpiece surface are measured using immersion thermocouples, and conventional thermocouples during the ECDM process.

The surface features of the discharge treated workpiece have been observed under an optical microscope which show the effect of an individual discharge on the workpiece and clearly indicate melting and solidification of the material in the discharge affected zone.

Energy analysis is performed by comparing the total input energy with that associated with the electrolyte in raising its temperature and the total energy associated with the workpiece (required to raise the temperature of the workpiece and for transformation of the workpiece material). The energy associated with the workpiece gives the measure of the efficiency of the process which turn s out to be low - of the order of 2-6 %.

On the basis of the time varying current, a mechanism is proposed for the occurrence and the effects of the discharges. This mechanism provides a consistent reasoning for the use of ECDM process for microwelding purposes.

Chapter 1

INTRODUCTION

1.1 Background

Our standard of living depends on the quality of goods. Virtually all products we use daily are manufactured or processed by converting materials from one form to another. Amongst many manufacturing processes, electrochemical processes have become widespread during the last few decades. Conventionally these processes viz., electrolysis, electroplating, electropolishing, etc. are used for plating, electrolytic production of aluminum, making of batteries and fuel cells, etc. In modern day technology, these processes are generally known as electrochemical machining (ECM) processes and are emerging as 'advanced machining techniques' in manufacturing industry. The application of these processes have been extended to perform various operations such as electrochemical boring, drilling, grinding, milling, micro-machining, sawing, turning, etc. [1].

1.2 Electrochemical Machining (ECM) Processes

ECM has been developed for machining of metals, alloys which are difficult to machine. Faraday's laws of electrolysis are the basis for this phenomenon. Electrolysis is a chemical process which occurs when an electric current is passed between two electrodes dipped into an electrolyte. Electrolyte is a solution which carries current by means of ions. Ions which carry positive charges move through the electrolyte in the direction of the positive current towards the cathode and are called as 'cations'. Similarly the negatively charged ions travel towards anode and are called 'anions'. The system of electrodes and electrolyte is called as the electrolytic cell. The movement of the ions is accompanied by the flow of electrons in the opposite sense outside the cell as shown in Figure 1.1. Both these actions are the consequence of the applied voltage to the cell. The chemical reactions which occur at the electrodes are called anodic and cathodic reactions or processes.

The electrolysis of copper sulphate solution is described with the help of Figure 1.1. The negative electron on the cathode neutralizes a cation reaching the cathode. For copper cathode,

$$Cu^{++} + 2e \rightarrow Cu \qquad \text{(at cathode)}$$

where e is one electron.

To maintain the cathodic reaction, electrons are required to pass round the circuit. These are obtained from the atoms of the metal anode. These atoms thus become the positively charged cations which pass into solution. The reaction for copper anode is

$$Cu \rightarrow Cu^{++} + 2e \qquad \text{(at anode)}$$

The electrolyte in its bulk must be electrically neutral; i.e. there must be an equal number of opposite charges within it, and thus there must be equal amounts of reaction at both the electrodes. Therefore, in the electrolysis of copper sulphate solution with copper electrodes, the overall cell reaction is the transfer of copper metal from the anode to the cathode. This is called the electroplating process. Current densities used in electroplating are of the order of $2 \times 10^{-2} A/cm^2$ and the thickness of the coating is of the order of $10\mu m$. Electropolishing is another application of electrolysis. The workpiece which is to be polished is made the anode in an electrolyte cell. Irregularities on its surface are dissolved and surface becomes flat and polished. A typical current density in this operation would be $10^{-1} A/cm^2$ and the irregularities removed are of $10^{-2}\mu m$ [2].

ECM is similar to the electropolishing, as it is an anodic dissolution process, where electrical energy causes a chemical reaction which in turn, dissolves metal from the workpiece (anode) into an electrolyte. In Figure 1.2, anode iron is used with NaCl as the electrolyte. Cathode is made up of an inert material. On applying a voltage between anode and cathode, high-density current passes through electrically conductive electrolyte solution. The dissolution of iron at anode gives

$$Fe \rightarrow Fe^{++} + 2e \qquad \text{(at anode)}$$

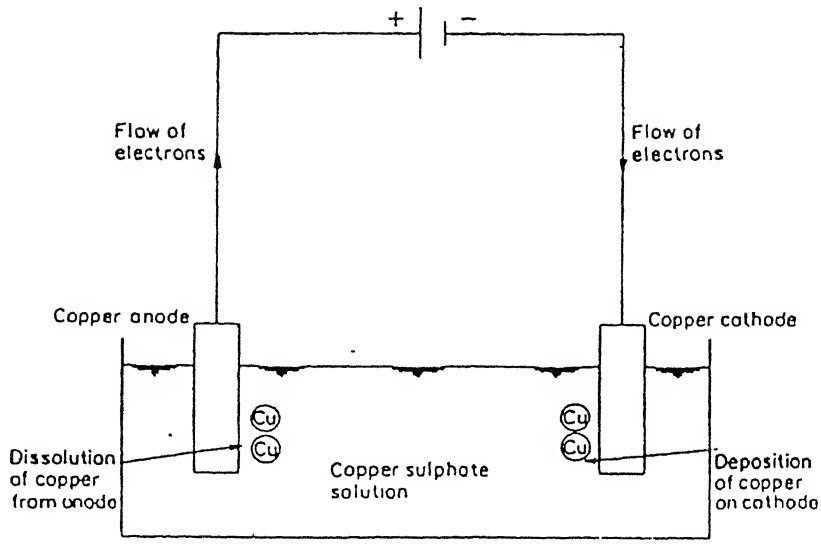

Figure1.1 Electrolysis of Copper Sulphate Solution [1]

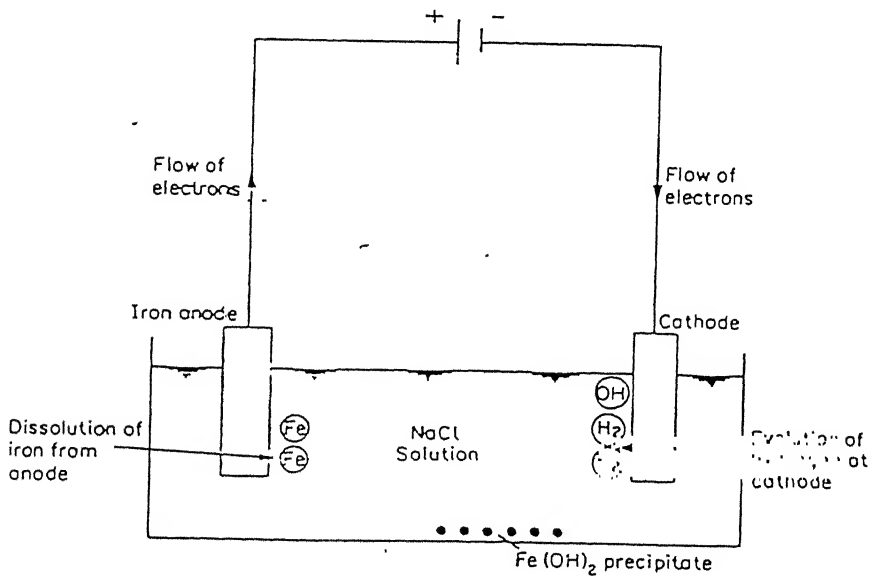

Figure1.2 Electrolytic dissolution of Iron [1]

and the electrolyte gains electrons. Generation of hydrogen gas and production of hydroxyl ions take place at the cathode, i.e.,

$$2H_2O + 2e \rightarrow H_2 + 2OH^- \qquad \text{(at cathode)}$$

The result of this electrochemical reaction is that the iron ions combine with the hydroxyl ions to precipitate out as iron hydroxide. Similarly, the ECM process is used for metal. machining. The rates of removal are considerably higher in machining than in electropolishing.

1.3 Electrical Discharge Machining (EDM) Process

EDM is a machining process to produce intricate shapes on any conducting metal and alloy irrespective of its hardness. It involves controlled erosion of electrically conducting materials by the initiation of rapid and repetitive electrical spark discharge between the tool (cathode) and the workpiece (anode) separated by a dielectric fluid medium as shown in Figure 1.3. A suitable gap known as 'spark gap' is maintained between the tool and the workpiece to cause the spark discharge. The amount of energy contained in each spark is discrete in nature. The temperature of the spot hit by the spark may rise up to 10,000 ^{0}C causing the work surface to melt and vaporize. It takes the form of a sphere and gets quenched by the surrounding dielectric fluid [3]. The dielectrics, which are commonly used, are paraffin, kerosene, etc.

Considering different aspects, such as, material removal characteristics, achievable accuracy and shape capabilities both ECM and EDM have large potential. Unfortunately, these processes have a major limitation that only electrically conducting materials can be machined. In order to overcome this limitation, electrochemical discharge machining (ECDM) process has been developed. This is a hybrid process combining ECM and EDM.

1.4 Electrochemical Discharge Machining (ECDM) Process

Basically ECDM is an extension of the ECM process. The electrolyte cell is similar to that used in ECM process. In this the two electrodes are grossly different in size as shown in Figure 1.4. Anode is made up of inert material and cathode normally is made up of copper. HCl is used as the electrolyte. The electrochemical reaction such as reduction of electrolyte at cathode takes place when a voltage is applied to the cell in proper polarity. Thus

$$2\ H_2O + 2\ e \rightarrow H_2 + 2\ OH^- \quad \text{(at cathode)}$$

When the applied voltage is increased further, hydrogen gas bubbles evolve more in number at the tip of the cathode and they grow in size. Their nucleation site density increases, current path gets restricted between the cathode and electrolyte interface causing discharge to occur at this interface instantly. The discharge always occurs at the interface of smaller electrode (cathode) and the electrolyte interface when voltage in an electrolytic cell is increased beyond a threshold value.

Unlike ECM, which is a continuous process, ECDM is a time varying phenomenon. The tool-electrolyte interface resistance goes on changing from a lower value to a large dynamic value. This changes the current in the circuit. When discharge takes place, there is an abrupt change in the current.

ECDM appears to have potential for machining of low machinability, high strength electrically conducting as well as non-conducting materials. It may turn out to be a powerful technique for machining of materials, such as tantalum, tungsten, fiber-reinforced composites, ceramics, etc, which can not be machined using conventional methods. Using this phenomenon Allesu [4] has developed a scheme for scribing on non-conducting materials [Figure 1.5]. ECDM phenomenon can be used for micro-welding also. Figure 1.6 shows how micro welding of a fine thermocouple can be performed using the heat generated by ECDM [4,5]. The process can also be useful for surface treatment

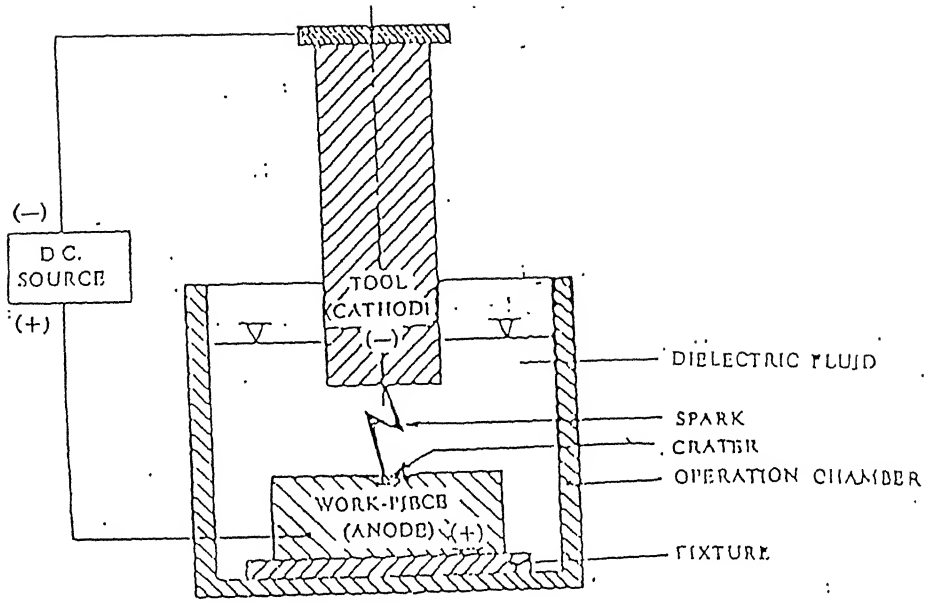

Figure1.3 Basic scheme of EDM process [2]

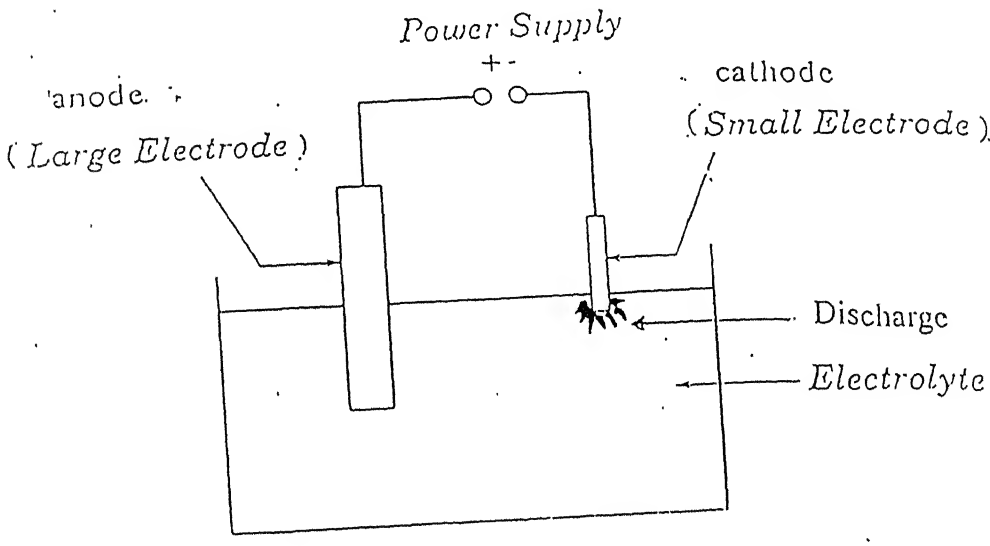

Figure1.4 Schematic diagram of an ECDM cell [3]

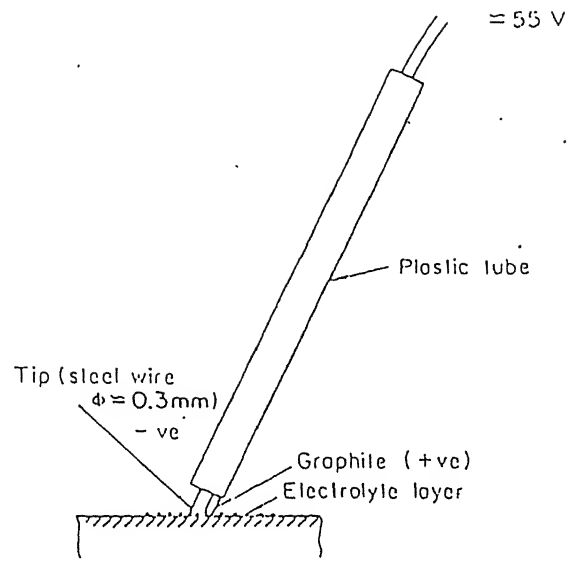

Figure1.5 Scribing pen using ECDM [4]

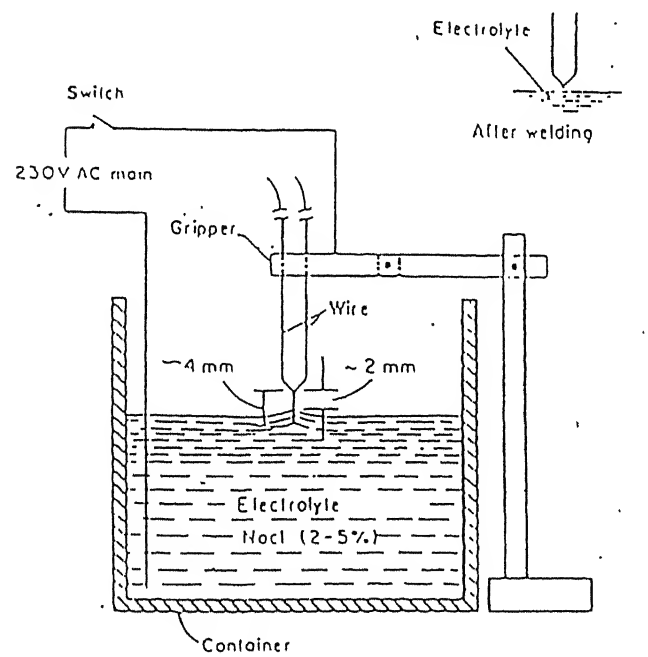

Figure1.6 Micro welding of thermocouple using ECDM [4,5]

and low budget rapid prototyping with fused deposition of very thin metallic wire [6] as indicated schematically in Figure 1.7.

The basics of ECDM are yet to be understood completely. Various researchers have put forth explanations of ECDM phenomenon based on their experimental studies. McGough and co-researchers [7] concluded that electrical discharge between cathode tool and electrolyte interface occurs due to

(i) Electrolytic gas generation at the surface of electrodes,

(ii) Growth of layers of low ionic concentration near the electrodes and formation of the oxide films on the anode surface, and

(iii) Local variations in the electrolyte flow pattern caused by flow stagnation and eddy.

They performed streak photography to get insight into the various stages of discharge on applying a 85 Volt pulse for a duration of 200 μsec. Basak [8] treats the discharge phenomenon as a 'switching off' of bubble bridges due to intense thermal heating (Figure 1.8). Jain et al. [9] has put forward 'valve theory' considering each gas bubble as a valve (Figure 1.9), which after its breakdown due to high electric field produces discharge in the form of arc.

1.5 Experimental Measurements

There are four primary reasons for making measurements in any process:

- Performance evaluation to ascertain that the process is functioning properly.
- Parametric study to know the dominant parameters which influence the process.
- Process control in which an arrangement is made to sense some critical parameters and use these to control the process.
- Measurements done to get insight into the working of the process, e.g. measurements to check energy balance.

These measurements provide insight that helps in improvement of the process.

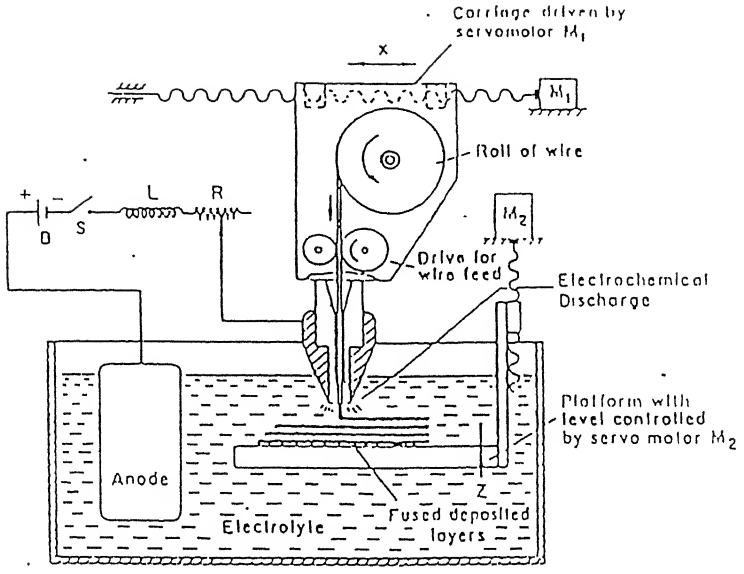

Figure1.7 Scheme of ECDM Fused Deposition Modeling [6]

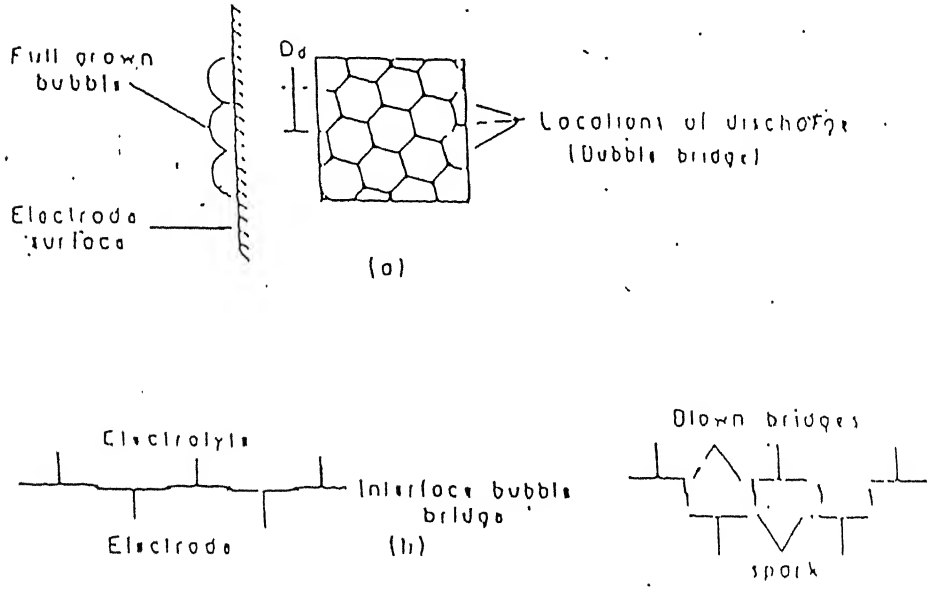

Figure1.8 'Switching off' model of the ECDM process [8]

Though ECDM process appears to have potential for machining materials, it has very limited acceptance partially because of its limited capacity and partially because of complicated phenomena associated with it. As mentioned earlier, limited literature is available on the phenomena of discharge in electrolyte. To improve the process capability of ECDM it is essential to understand the basic mechanism and to identify the process parameters correctly. This leads to a natural choice of measurements of process parameters such as temperature, current, etc.

Basak [10] measured the temperature of the cathode tip by using thermocouple itself as a cathode. The plot of temperature versus applied voltage for different electrolytes is shown in Figure 1.10. He presented a thermal model to estimate metal removal rate (MRR) analytically. Jain et al [9] compute MRR and the temperature distribution in the workpiece using the finite element analysis. Parija [5] has computed the time taken to form a thermocouple bead by solving the heat equation. The temperature of discharge itself has been estimated by emission spectroscopy by Reghuram [11] and was found to be in the range of 8000-10000 K.

It appears that no attempt has been made to measure the temperature of the workpiece and temperature distribution within the electrolyte bath. The present work is carried out with in situ measurements of electrical and thermal parameters of the ECDM system as the main objective. These measurements, it is hoped, will help in developing a close loop control of the process.

1.6 Present Work

To gain insight into the ECDM process for micro welding, it was decided to measure the temperature of a small area of the workpiece at the discharge affected zone. In addition the temperature at two different places on the workpiece surface along the same line is measured. Also the temperature of electrolyte at two different locations within the cell are measured. Simultaneously, the time varying current is monitored which helps in analyzing the mechanism of discharge. Measurement of these parameters help in understanding the mechanisms involved in ECDM. Also a

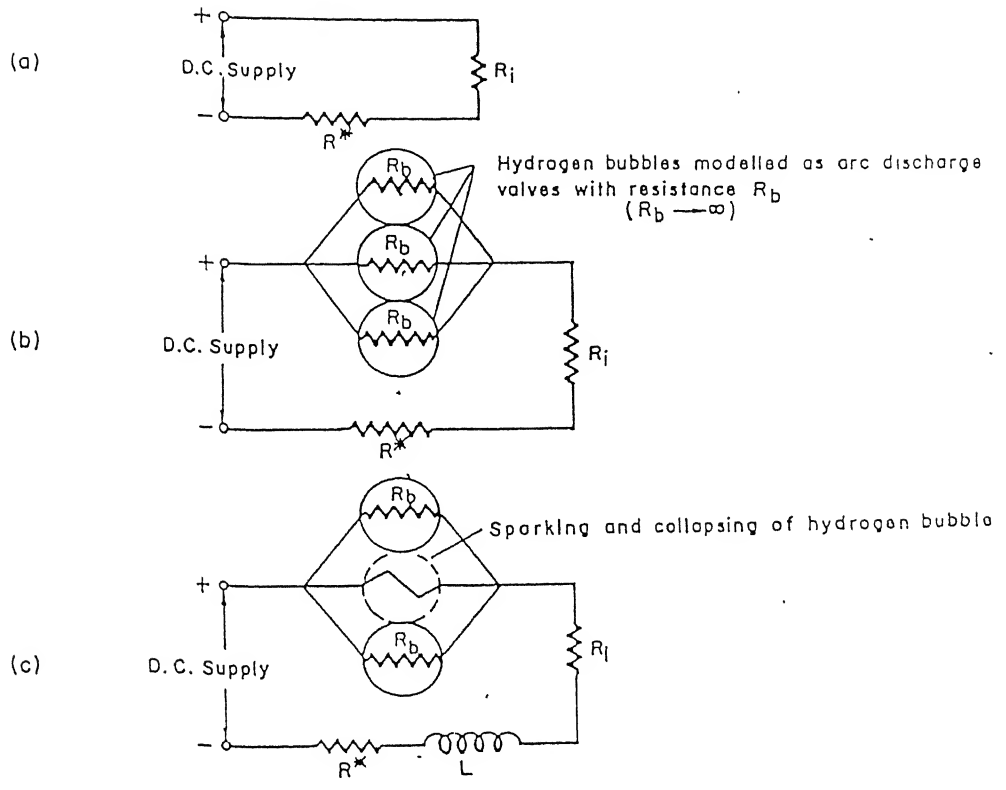

Figure1.9 'Valve' model of ECDM process [9]

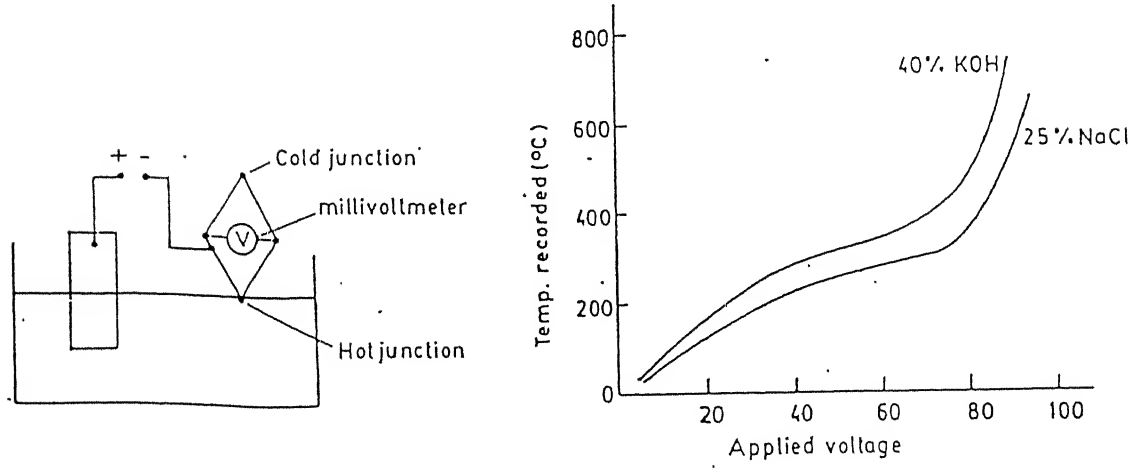

Figure1.10 Arrangement for measuring cathode temperature using thermocouple as cathode and its results[10]

comparison of the energies associated with different mechanisms involved in ECDM indicate the process efficiency and feasibility of the process for other applications. The methodology has been summarized in the form of a flow diagram in Figure 1.11. The important steps involved in carrying out this are summarized below:

- Measure time varying current and temperature in the ECDM system.
- Analyze the time varying current pulses measured using Cathode Ray Oscilloscope (CRO) to identify the discharge mechanism involved in ECDM.
- Measure the temperature distribution using contact type sensors in the electrolyte cell using immersion probes and on the workpiece surface by using thin chromel-alumel thermocouples.
- Measure the temperature of the workpiece close to the machining area using radiation pyrometer as a non-contact type sensor.
- Estimate the input energy, energy associated with the electrolyte and that with the workpiece using current and temperature data.
- Perform the energy analysis of the process by comparing the input and total output energies.
- Draw inferences about the ECDM process.

One important contribution of the present work is the development of a model of the discharge phenomenon.

1.7 Proposed Mechanism of ECDM

Discharge in ECDM is a complicated phenomenon involving various mechanisms. In this thesis, it is proposed that the discharge between the cathode electrode and electrolyte occur mainly due to electrolytic gas generation at the surface of tool (cathode) electrode. This assumption also makes the visualization simple and the discharge phenomena can be compared to that with the discharge in gases.

Unlike ECM, which is a continuous machining process, ECDM is a time varying process wherein machining takes place during the discharge period. For discharge to occur, the supply voltage is increased beyond a threshold value. Though we

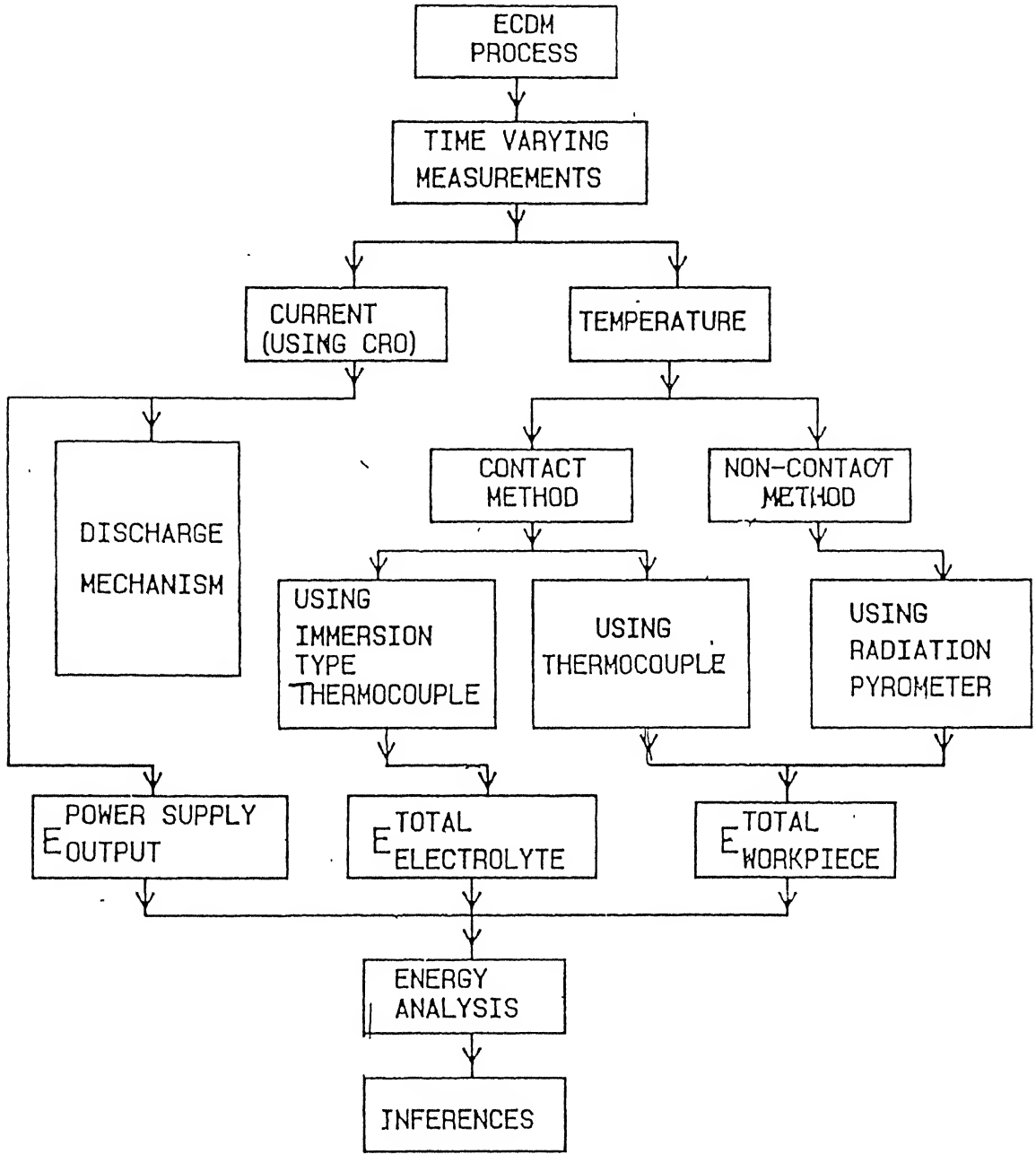

Figure1.11 Flow diagram showing the methodology of the present work

see a continuos discharge, the actual discharge is a time varying one. The time dependence of the discharge is due to the formation of dynamic resistance at the cathode-electrolyte interface. Further, the discharge process by and large appears to be statistical in nature as it depends on various parameters such as density of hydrogen gas bubbles, electrolyte concentration, voltage, inter electrode gap, etc. These parameters are interdependent.

It was strongly felt that a high electric field gets generated locally across the gas bubbles bridging the gap between the tool and the workpiece and momentarily a large current spike would result in breakdown of the gas bubbles. Observing the time varying current validated this. The current spikes of small but varying duration (in ms) were observed. Study of the current provides a new dimension to the discharge studies. On the basis of these observations a theory is proposed which explains the phenomenon. This is further discussed in Chapter 4.

1.8 Organization of the Thesis

The thesis is organized in five chapters. The present chapter i.e. Chapter 1 introduces the electrochemical discharge machining processes and provides the details of the process available in the literature. The need for experimental measurements is also elaborated. The concluding part outlines the main objectives on which the emphasis is given in this thesis. Chapter 2 describes the experimental details, giving information about various types of temperature sensors together with the selection of appropriate sensors for a particular measurement, their characteristics, etc. The experimental set-up to measure the response time of the pyrometer is included therein. Results are discussed in Chapter 3 giving details of energy balance. Chapter 4 presents the mechanism of ECDM discharge phenomenon. Conclusions are drawn in chapter 5 mentioning the scope for the future studies.

Chapter 2

EXPERIMENTAL DETAILS

2.1 Introduction

In the ECDM process, there are various process parameters, which can be measured to control and automate the system. Amongst these the important ones are, temperature, current, immersion depth of tool in the electrolyte, hydrogen bubble generation rate, hydrogen bubble diameter, etc. which directly affect the throughput of the system (MRR and deposition rate). These parameters also reflect on the tool wear rate (TWR). In the present work the two crucial parameters i.e., time varying temperature and current are measured. A novel way has been developed to remotely sense the workpiece temperature using a radiation pyrometer. No reports appear to be available in the literature on the measurement of this time varying temperatures. Figure 2.1 shows the details of the ECDM process and its parameters which is a part of the flow diagram shown earlier in Figure 1.11. The following section describes the experimental set up showing the use of various kinds of temperature sensors together with the instruments used for the measurements.

2.2 Experimental Set-up and Instrumentation

An experimental set-up has been designed and developed for time varying temperature and current measurements. Temperature measurements on the workpiece surface, in the vicinity of the discharge, and in the electrolyte have been carried out. These measurements are done to carry out energy analysis of the ECDM process and for estimating the efficiency of the process. In addition, these measurements will be useful for developing the feedback mechanism for controlling the process.

The ECDM cell has been fabricated using a boro-sillicate glass flask of 10 cm diameter. The arrangement of the cathode, anode, and workpiece is shown in Figure. 2.2. Photograph 2.1 shows the arrangement of the experimental set up. A DC regulated power

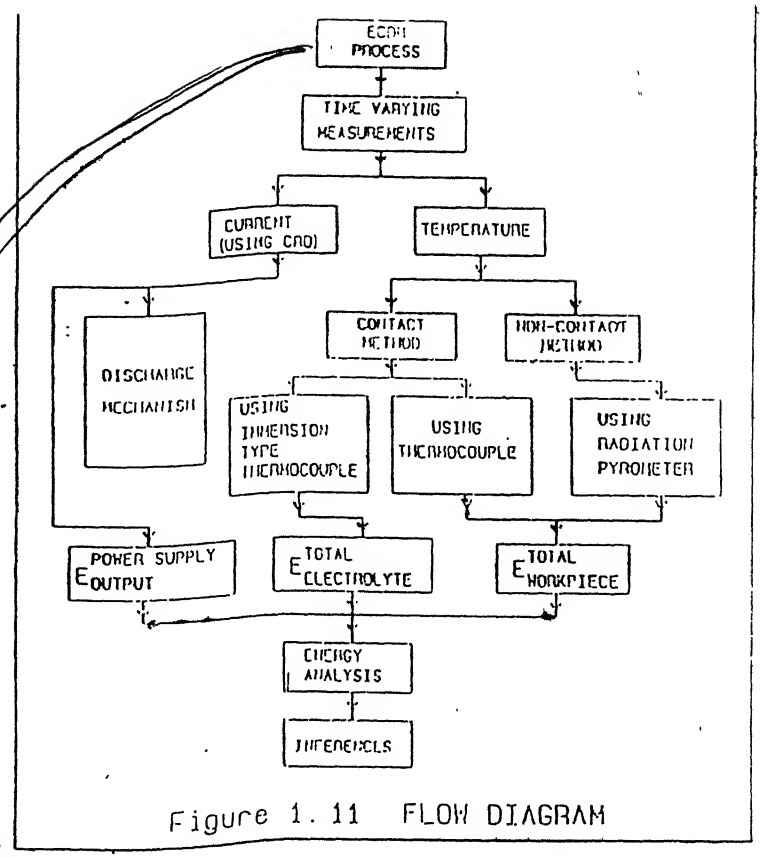

Figure 1.11 FLOW DIAGRAM

ECDM PROCESS

- PROCESS PARAMETERS
  - DC VOLTAGE (130-180V)
  - ELECTROLYTE CONCENTRATION (1-5%)
- TRANSIENT MEASUREMENTS
  - CURRENT
  - ELECTROLYTE TEMPERATURE
  - WORKPIECE TEMPERATURE at WORKPIECE EDGE
  - WORKPIECE TEMPERATURE at MACHINING ZONE

Figure 2.1 Flow diagram highlighting the process parameters

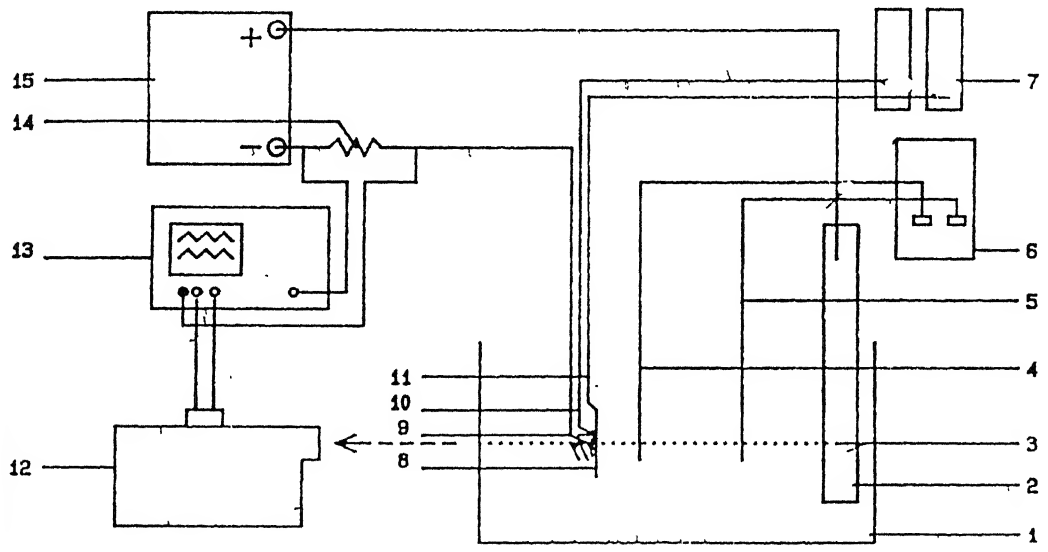

1-ECDM cell. 2-Anode, 3-Electrolyte
4-Immersion probe1, 5-Immersion probe2,
6-Digital Thermometer, 7-Multimeters,
8-**Workpiece**, 9-Cathode with Discharge at its tip,
10-Thermocouple1, 11-Thermocouple2
12-Pyrometer, 13-Oscilloscope,
14-Resistor, 15-DC Power Supply

Figure 2.2 Experimental Set up
(Not to the scale)

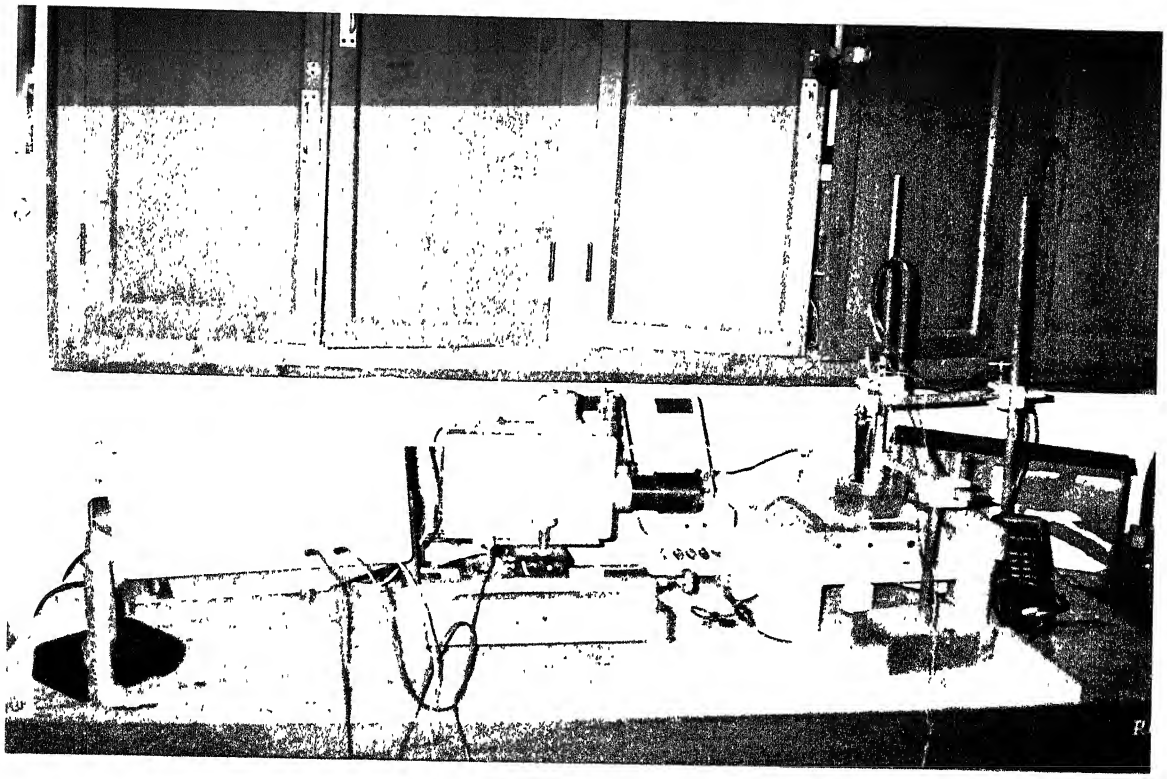

Photograph 2.1 Experimental set up.

supply (0-200V, 5A) has been used. In the present experiment, mixture of hydrochloric acid with distilled water in various concentrations (1, 1.5, 3, 4.5 and 5%) has been used as electrolyte. A jig arrangement has been made to position the chromel _alumel (K type) thermocouples on the workpiece surface at two different places . Their output voltages are recorded with the help of two digital multimeters (DM-375). A standard conversion chart is used to convert the voltage readings to temperature readings. Two immersion thermocouples have been used to register the temperature of the electrolyte solution. These are also K type thermocouples with special coatings to make them suitable for work under harsh conditions, i.e., in electrolytes. The thermocouples are positioned with their tip immersed in the electrolyte with the help of another jig arrangement. The readings are displayed on a digital thermometer (Fluke-52 K/J) in scan mode. The tip of the cathode tool is bent slightly, and workpiece is mounted vertically just near the cathode tip. The separation between the cathode tip and the workpiece is of the order of 400-500μm. The depth of cathode inside the electrolyte is also maintained at a fix distance where one gets the spark. The distance between cathode and anode is kept fixed at 3cm in all the experiments.

The temperature of workpiece where the discharge strikes, is measured by a non-contact type radiation pyrometer placed externally without disturbing the process. It is mounted on a x-y table with fine adjustments for focusing purposes. This pyrometer gives the temperature of the target area of around 1 mm^2. Workpiece is radiating the heat by virtue of its temperature. The radiated power is very small as compared to the conducted one, but it is possible to measure the corresponding temperature of the workpiece using a sensitive sensor like pyrometer. Since the discharge is a non-thermal radiation, radiation pyrometer can not be used to sense the temperature of the discharge. In the present set-up, the pyrometer is focused at the workpiece where the discharge strikes its surface and its output is monitored on one of the channels of the digital storage oscilloscope (KIKUSUI 60 MHz, 4 channel). The waveform is stored in one of the four locations. Its photograph is taken by a digital camera (Sony 10X Digital Mavica, MVC-FD7, Still camera). This camera stores the image in 'jpg' format on a floppy. Using 'Photo shop' software, these images are viewed and printed using a Pentium II personal computer

(PC). The calibration of the pyrometer in terms of voltage and temperature is discussed later.

To measure the current through the ECDM cell, a 1 Ω, 5W resistance in series with the cathode electrode is used. The time varying voltage across this resistance is traced on one of the channel of the storage oscilloscope. This voltage is analogues to the current through the circuit. The time varying current has thrown light on developing a model of discharge mechanism. The following section describes the planning for experiments.

2.3 Design of Experiments

Experiments were planned according to the technique given in 'Experimental design' [12]. The voltage ($130<V<180$) and the electrolyte concentration ($1<C<5$) were the independent variables to plan the experiments. The method is called factorial method and is used to test one factor over different levels of another factor. The scheme of the experiments is as shown in Table 2.1. The responses, which are of importance in this work, are the time varying surface temperature measured with pyrometer, the temperature of the electrolyte, the workpiece temperature recorded with thermocouples, the time varying current. These are measured for different combinations of voltage and electrolyte concentration.

Use of HCl as an electrolyte was preferred due to its higher activity and as the present work was undertaken in continuation with the work reported in reference [13]. Another main reason for using HCl as the electrolyte in present experiments is its lower absorbvity at 900nm wavelength as shown in Figure 2.3. This makes it suitable for measuring the workpiece temperature by the pyrometer which uses a sensor working at 900nm.

Copper is used for making the tool in the form of 2mm thick wire. Copper, brass, tantalum and silicon were used as workpiece materials.

S.N.	Voltage (V)	Concentration (% by volume)
1	137	1.5
2	173	1.5
3	137	4.5
4	173	4.5
5	130	3
6	180	3
7	155	1
8	155	5
9	155	3
10	155	3
11	155	3
12	155	3
13	155	3

Table 2.1 The scheme of the experiments.

In the following section a brief description of various types of temperature sensors is given along with the rational for their selection in the present study.

2.4 Temperature sensing

The measurement of temperature is the most fundamental and important thermal measurement. Temperature is a measure of atomic and molecular kinetic energy of a substance. From engineering point of view, temperature or more specifically a temperature difference, is an indication of heat transfer. Heat is closely related to temperature and heat transfer takes place by three mechanisms viz. conduction, convection and radiation.

Temperature is an intensive quantity. We make use of zeroth law of thermodynamics while measuring the temperature. This is the basis used for fixed points in the International Practical Temperature Scale and IPTS-68 is the standard for calibration based on the material properties.

There are various types of temperature sensors. The choice of a particular temperature sensor is based on the following characteristics:

- Sensitivity
- Stability
- Temperature range
- Sensor size
- Response time
- Working environment
- Melting temperature of the sensor material

As mentioned earlier, the objectives, has been to measure temperature at different places in the ECDM process. Thus it becomes necessary to use different kinds of temperature sensors. The following section describes about selection criterion of sensors giving brief description of the types of temperature sensors.

2.4.1 Various Types of Temperature Sensors

Any object that has a property influenced by temperature is a thermometer or temperature sensor. The effect may be a one or more of the following:

(i) Change in physical / chemical state of an object.

(ii) Change in Dimensions: Expansion gas or liquid thermometers (Bi-metallic strip, Mercury-in-glass)

(iii) Change in electrical properties: Thermocouples, Resistance temperature detectors (RTD), Thermistors, etc.

(iv) Radiation: Pyrometers and Spectrometers.

(v) Others: Johnson' noise thermometer, Integrated circuit (IC) thermometer, etc.

These can be broadly divided into two categories of sensors; the contact type and the non-contact type. Category (i), (ii), (iii) and (v) are the contact type of sensors, while category (iv) is the non-contact type.

Thermistors, RTDs, thermocouples are briefly compared in Figure 2.4 [14]. Amongst these, thermocouples are most versatile, inexpensive temperature sensors used for entire temperature range. Thermocouples are also suitable for measuring time varying temperatures. Thermistors are highly nonlinear in nature, their accuracy is less, and has negative resistance coefficient of temperature. Response time of RTDs is longer than thermocouples due to their higher thermal mass. RTDs are subject to self heating errors because a current is needed to bias the RTD, this causes i^2R heating in the sensing element. Thus RTDs are less rugged and more expensive than thermocouples. Hence thermocouples are chosen for the measurement purposes. The details of thermocouple are given in Appendix A.

For measuring the temperature at various locations in the ECDM cell, K type thermocouples of two different varieties are chosen. Thus to measure the temperature within the electrolyte cell, immersion thermocouple probes with digital thermometer are preferred. To measure the temperature at workpiece surface chromel_alumel

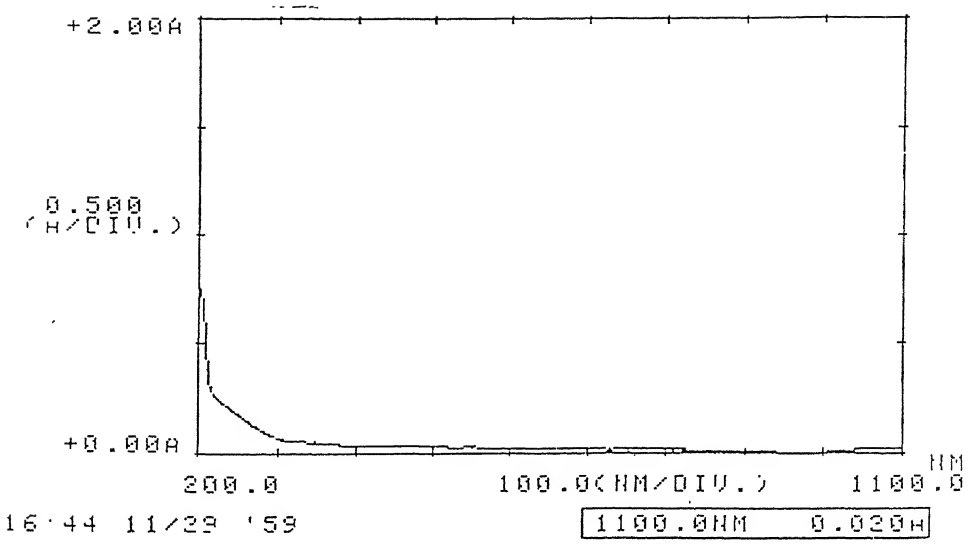

Figure 2.3 Absorbvity of HCl solution

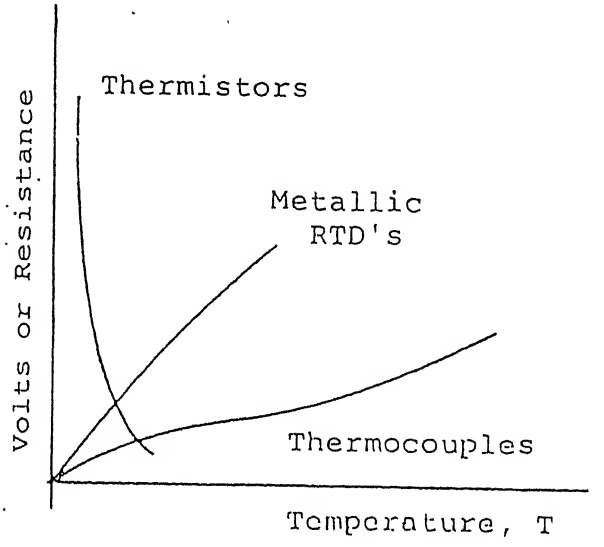

Figure 2.4 Comparison of sensors [14]

thermocouples are preferred. These are fabricated with chromel_alumel wires of 24 gage. The bead diameter is 1.4mm. This ensures smaller thermal mass and hence shorter response time. The wires are individually insulated and wrapped in a sheath that serves to hold the wires together ensuring the stability of the sensor. This protects the wires from the harsh environment as in the ECDM cell Approximate physical properties of type K thermocouples are listed in Appendix A.

Radiation thermometer is the only and right choice for sensing high temperature of the workpiece at the machining zone in a non-intrusive way Further, in this work, we have appropriately modified a commercial pyrometer to measure time varying temperature. The details of the radiation thermometer are given in Appendix B.

The particular pyrometer, which is used for measurements, is a German make, 'Dr. George Maurer GmbH, D-7441, Kohelberg'. The working temperature range for it is mentioned as 815 °C - 1700 °C. The technical details of this instrument such as response time, conversion time, etc., are not available.

2.5 Calibration of Pyrometer

To test for its calibration, a tungsten bulb (24V, 150W) is used. A resistor of 1 Ω, 10W is connected in series with the bulb as shown in Figure 2.5. By varying the voltage across this series combination (3-9V), V_1 and V_2 (V_2 is equivalent to the current flowing through the bulb) were noted. The product of V_1 and V_2 gives the electrical power provided to the bulb. It is assumed that all of the electrical power supplied to the bulb is utilized for producing the radiation. The pyrometer was focused at the middle region of the tungsten filament of the bulb. Corresponding temperature readings of pyrometer were noted down after steady temperature. In this set-up pyrometers digital temperature meter is used to read the temperature values directly. The Stefan-Boltzmann's relation was established by plotting ln (P) versus ln (T). The same experiment was carried out by placing the bulb in an empty boro-sillicate glass flask and flask filled with the electrolyte to be used in the ECDM process to check for the suitability of this pyrometer for remote temperature measurements in the ECDM process. Figure 2.6 shows the plot of ln (P)

versus ln (T) in this situation, this linear plot shows an agreement with the Stefan-Boltazmann's relation. The input power is proportional to the fourth power of the temperature and the pyrometer can be used to sense the temperature of the workpiece immersed in the electrolyte.

In spite of checking for the suitability of pyrometer for measuring steady temperatures in electrolyte bath, it was found unsuitable to sense the time varying temperature of the workpiece in the localized region of the discharge. By performing various experiments in this regard, it was concluded that the response time of the pyrometer is longer. The reason has attributed to the conversion module in the pyrometer, which takes longer time than that for sensing, signal processing etc. The digital temperature meter would take longer to display the temperature conversion, hence the pyrometer would not be able to track the time varying phenomena correctly. Tapping the signal lines as input to this module isolated the digital temperature meter. These signal lines (output voltage) now are connected to the oscilloscope directly A look up table (Table 2.2) is developed for output voltage with corresponding temperature reading by using the calibration method explained above. Also the calibration of the pyrometer is cross-checked by measuring the temperature of a furnace with known temperature. This shows a good agreement with the results developed in look up table.

An attempt has been made to calculate the response time by performing an experiment as discussed in the next section.

2.6 Response Time Measurements

As described in the previous section, response time is an important parameter in many temperature measurement applications. If the temperature to be measured is changing rapidly, the temperature sensor must have a fast response in order to track the temperature accurately.

The response time is determined for a step change in temperature. To introduce the step change in temperature a mechanical chopper is devised. The technique used is

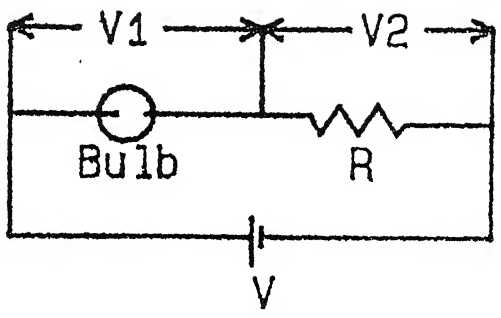

Figure 2.5 Circuit used for Calibration of Pyrometer

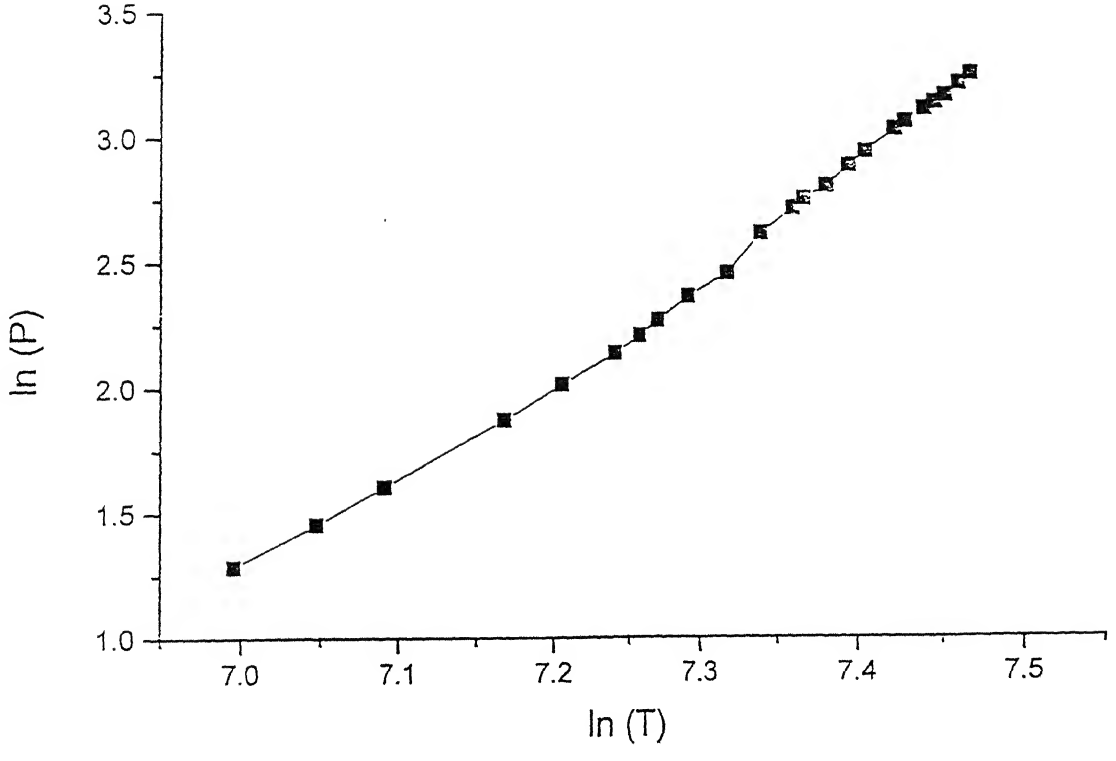

Figure 2.6 Plot of ln(P) vs. ln(T) for the tungsten bulb In borosillicate flask filled with HCl

S.N.	Voltage (V)	Temperature (^{0}C)
1	0.821	820
2	0.852	850
3	0.962	960
4	0.971	972
5	1.018	1016
6	1.084	1086
7	1.134	1138
8	1.192	1195
9	1.236	1238
10	1.292	1294
11	1.325	1327
12	1.374	1375
13	1.507	1509
14	1.538	1540
15	1.562	1565
16	1.635	1637
17	1.683	1685
18	1.702	1704
19	12	>1705

Table 2.2 Look up table showing Voltage values and corresponding Temperature readings

similar to that used for motor encoder for calculating the speed. A CD is used for the purpose. Sixteen equi-spaced holes of 5 mm diameter are drilled on the periphery of the CD. The drilling of holes is performed with the help of an indexing head to maintain the precision. This CD is mounted on a shaft of a DC motor with a special mounting that will take care of voblling problem to some extent. The motor is rotated with a known speed with the help of its controller and driver circuit. The tungsten bulb is mounted at the back of the CD. Pyrometer is focused on the middle portion of the filament through a hole on the CD. Photograph 2.2 shows the set up. When the CD is moving with the motor shaft, the light from the bulb is alternately falling on pyrometer sensor when the hole is facing it, and it gets obstructed when there is no hole. The output from the pyrometer is connected to the storage oscilloscope. Figure 2.7 (a) shows the curve for the response time of the order of 20 ms. To make the observation simpler and reliable, a single hole is used. Now the output of the pyrometer is recorded with respect to the encoder waveform giving the speed of the motor. The pulses are observed for increasing speed of the motor. It is observed that pyrometer responds for each pulse which is at least 10 ms apart (Figure 2.7 b). So the response time is around 10 ms. The discharge frequency also varies from 12-100 Hz as discussed in section 3.3.2. This makes the pyrometer suitable for time varying temperature measurements in this work.

The results based on the measurements of temperature and current performed as described in this chapter are presented in the next chapter. Energy balance is described with the discussion of the results therein.

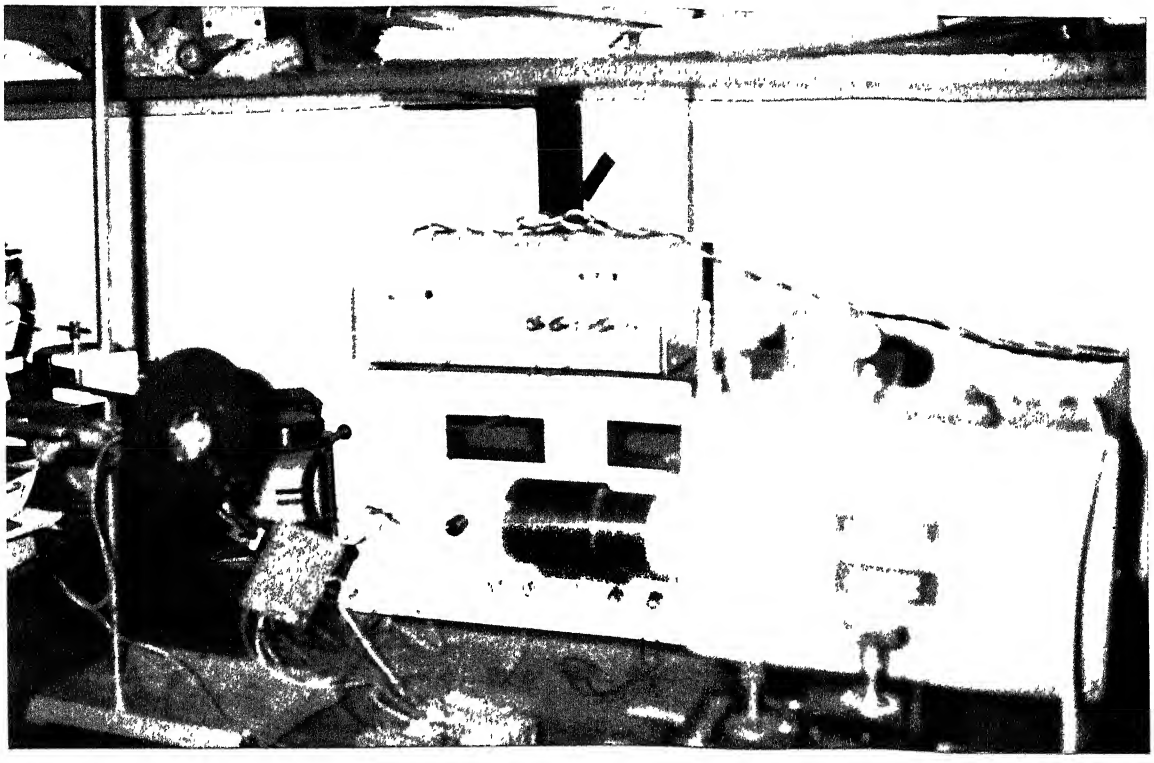

Photograph 2.2 Set up for the measurement of response time of the pyrometer

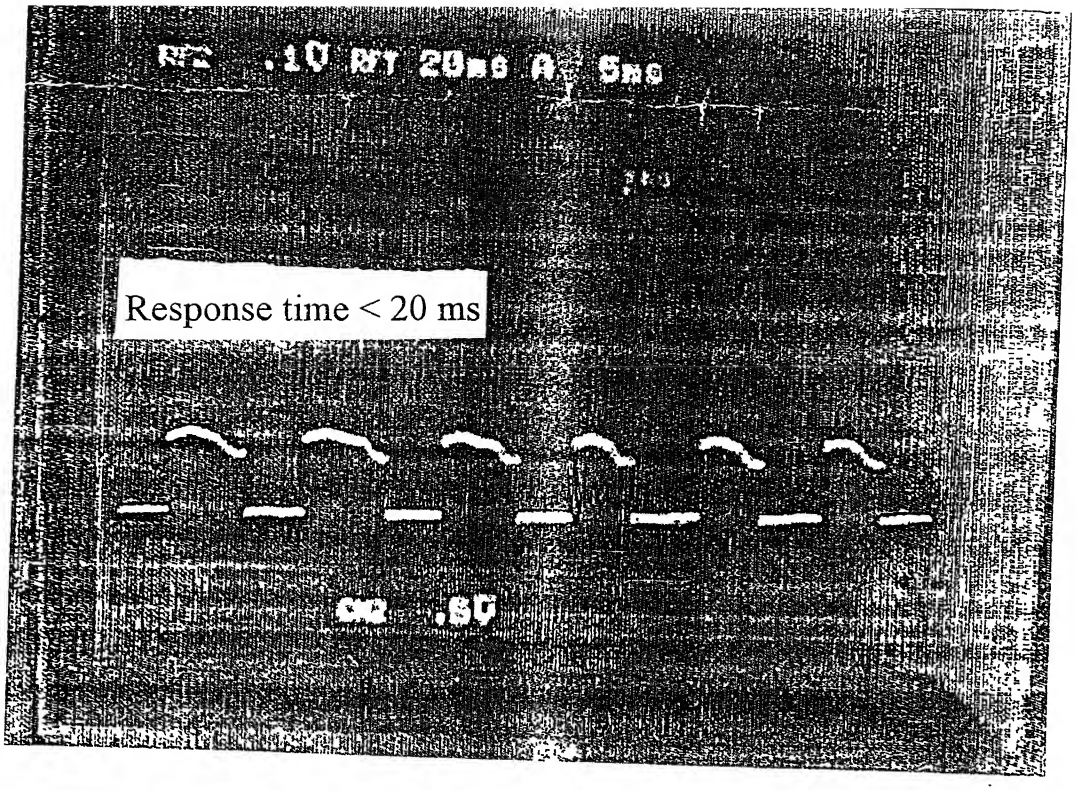

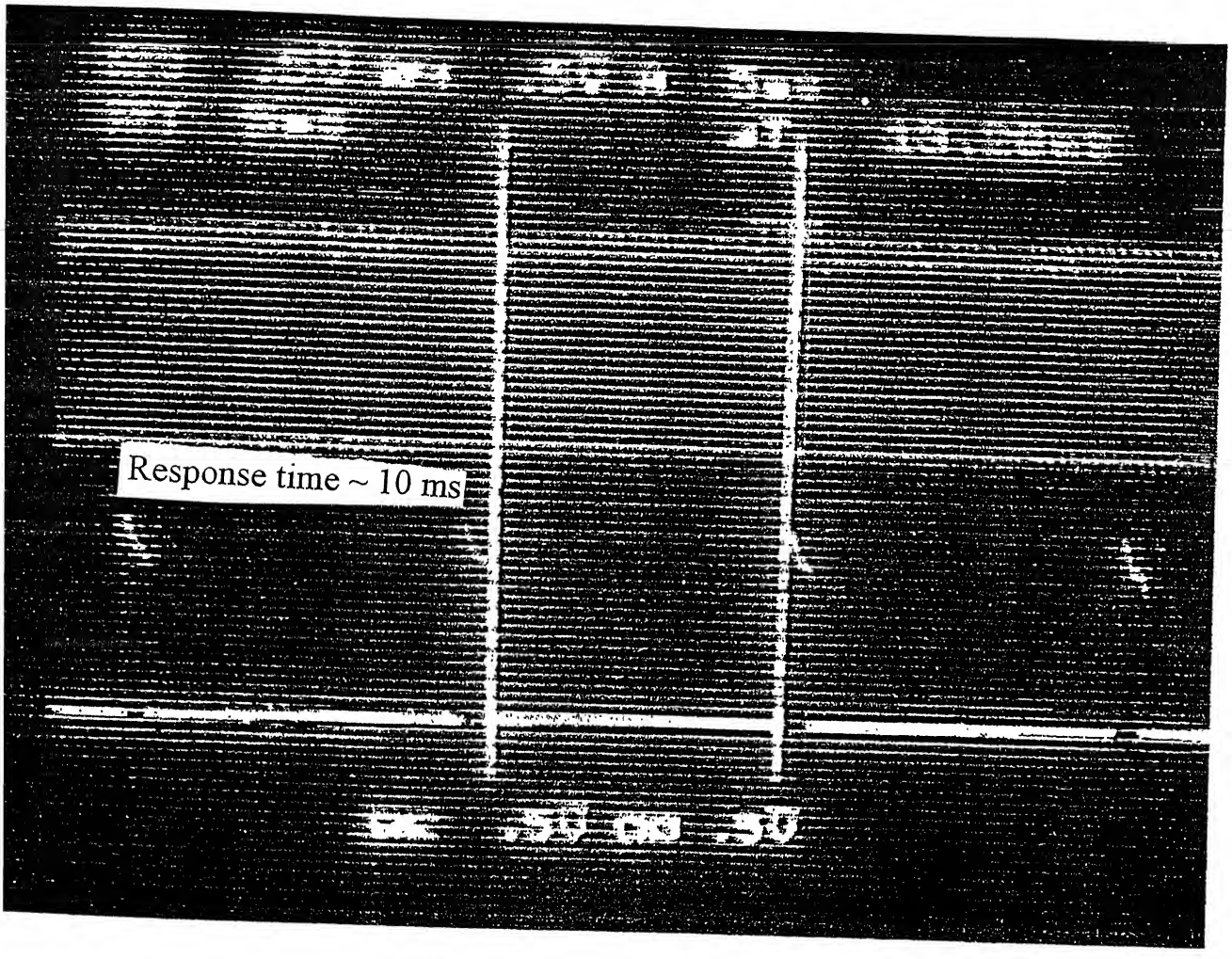

Figure 2.7 Plots showing Response time of the pyrometer

Chapter 3

RESULTS AND DISCUSSION

3.1 Introduction

This chapter presents the results of measurements described in Chapter 2 and elaborates on the analysis of energy balance in ECDM process. The experiments are performed using different workpiece materials viz., copper (melting point 1083^0C), brass (melting point 996^0C), silicon (melting point 1410^0C) and tantalum (melting point 2996^0C). In the case of copper, experiments have been performed using the fractional method scheme [12] with supply voltage ranging from 130V-180V and the HCl electrolyte concentration from 1%-5% in volume. For other materials, experiments are performed at supply voltage of 155V and 3% electrolyte concentration. At the beginning of each experiment, initial temperature, weight of electrolyte, and weight of the workpiece are recorded. During the experiments, average current is monitored and the time varying current and temperature pulses are recorded. After carrying out the experiment for approximately 60 seconds, the final temperature readings are monitored. Also the weight of the workpiece is measured.

The surface features of the workpiece have been observed under the optical microscope and are presented in section 3.7. Measurements of time varying current pulses are useful in understanding the mechanism of ECDM. This is discussed in the next chapter.

3.2 Temperature

The temperature at different locations in the ECDM cell and on the workpiece surface are measured using immersion thermocouples, conventional thermocouples and pyrometer during the ECDM process. The locations of these measurements are illustrated in Figure 3.1 (a) and (b). Figure 3.1 (a) gives the front view while Figure 3.1 (b) shows the side view. The cell is 10cm in diameter, and the workpiece is a square of

2.5cmX2.5cm with 0.6mm thickness. Pyrometer is focused at the center point of the workpiece. The location of conventional thermocouples and immersion thermocouples are visible in the figure. Two thermocouples are placed on the workpiece surface by a jig arrangement. The first one is at a distance of 4mm away from the discharge affecting zone and the second one is 6mm further away along the same line.

3.2.1 Copper Workpiece

The temperature measurements for copper workpiece are performed as explained earlier. Change in initial and final temperature readings at four different locations and temperature measured by the pyrometer are given in Table 3.1 for various combinations of supply voltage in the range of 130-180V and electrolyte concentration in the range of 1-5%.

The time varying temperature recorded by the pyrometer in the discharge zone increases by increasing the supply voltage from 130-180V for the same electrolyte concentration. The overall temperature rise ranges from 815^0C-1000^0C (as shown in column 3 of Table 3.1). The change in temperature at the lower concentration (1.5%) is from 880^0C to 895^0C which is about 15^0C. The same change is from 920^0C to 1000^0C which is about 80^0C for 4.5% concentration. For 130V, 3% electrolyte concentration pyrometer did not show the reading as the temperature is below 815^0C.

Energy released per spark is not always the same but it varies and the discharge location keeps changing. As a result the temperature attained by the workpiece in the discharge affected zone is not always the same for the same values of voltage and concentration of the electrolyte.

The region at a distance of 4mm away from the discharge zone on the workpiece attains a temperature in the range of 55-200^0C in all the experiments (shown in column 4 in Table 3.1). The highest change of 200^0C was recorded for 155V and 5% electrolyte concentration. At a distance of 10mm away from the discharge zone on the workpiece surface, the temperature attains a value in the range of 30-60^0C (shown in column 5 in

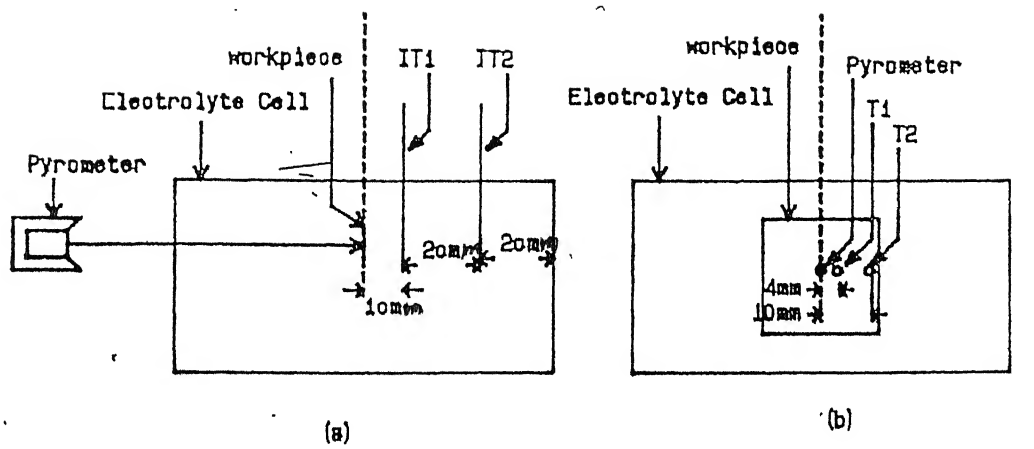

Figure 3.1 Various Locations in the ECDM cell where temperatures are measured
(a) Front View (b) Side View

Table 3.1). The average of these two values is used for the estimation of energy required for raising the temperature of the workpiece (workpiece stored energy).

The temperature of the electrolyte cell, 10mm away from the workpiece center (at the backside) increases from 5.5 to 16^0C (shown in column 6 in Table 3.1). Similarly the temperature of the electrolyte 30mm away along the same line, increases from 2.5 to 13^0C (shown in column 4 in Table 3.1). The average of these two readings is used to determine the overall temperature rise to estimate the rise in stored energy associated with the electrolyte.

3.2.2 Comparison with Other Workpiece Materials

Similar experiments are carried out at 155V and 3% electrolyte concentration with brass, silicon and tantalum as workpiece materials. The measurements are presented in Table 3.2. The temperature recorded by the pyrometer is around 1000^0C for brass, around 1360^0C for silicon and around 1640^0C for tantalum. The temperature at the workpiece surface recorded by thermocouples show increase in the temperature in the range of 20 to 40^0C. The electrolyte temperature varies in the range from 4 to 11^0C. The average current in the case of brass is higher than the other three materials.

MRR of brass is around 0.275mg/sec. In the case of silicon, calculation of MRR could not be carried out as the sample broke. In the case of tantalum, MRR is of the order of 0.2mg/sec. It is observed that MRR highly depends on the spacing between the cathode and the workpiece. If the spacing is decreased, MRR increases.

3.3 Current

The average current and the time varying current are recorded during the ECDM process using a DM-375 multimeter and a KIKUSUI 60 MHz, 4 channel storage oscilloscope respectively.

Voltage (V)	C (%v)	Pyrometer ** Reading (^{0}C)	T_1 (^{0}C)	T_2 (^{0}C)	IT_1 (^{0}C)	IT_2 (^{0}C)
137	1.5	880	55	30	5.5	2.5
173	1.5	895	65	40	6	4
137	4.5	920	70	44	7	6
173	4.5	1000	80	60	3.5	0.5
130	3	--	74	60	6	5
180	3	815	70	55	16	12
155	1	815	100	50	13	12
155	5	850	200	50	16	13
155	3	850	150	50	10	6
155	3	875	75	50	9	7
155	3	835	75	50	8	5
155	3	900	80	55	8	6
155	3	875	85	50	7	4

Table 3.1 Results of temperature measurements for Copper workpiece using various probes measured at various locations.

(Note: ** These are time varying values and are discussed in section 3.2.1 and section 3.5).

-Pyrometer focused at the center of the workpiece where the discharge strikes,
-T_1 is at a distance of 4 mm away from the discharge affected zone,
-T_2 is at a distance of 10 mm away from the discharge affected zone,
-IT_1 is at a distance of 1 cm from the workpiece (at its back side) in the cell, and
-IT_2 is at a distance of 3 cm from the workpiece (at its back side) in the cell.

Material	Pyrometer ** Reading (^{0}C)	ΔT_1 (^{0}C)	ΔT_2 (^{0}C)	ΔIT_1 (^{0}C)	ΔIT_2 (^{0}C)	Current (A)	MRR (mg/sec)
Brass	1000	35	20	11	7	1.4	0.275
Silicon	1360	35	22	6	5	0.48	--
Tantalum	1640	40	34	6	4	0.7	0.2

Table 3 2 Temperatures, average current and MRR for Brass, Silicon and Tantalum

(Note: ** This time varying response is discussed in section 3.2.2 and section 3.5)

3.3.1 Average Current

As expected, the average current increases as a function of supply voltage. It ranges from 0.35A (at 137V, 1.5% concentration) to 1.1A (155V, 3% concentration). Table 3.3 shows the variation of current with system parameters. This average value of current is used in the calculation of energy supplied to the ECDM system.

3.3.2 Time Varying Current

While observing the time varying current, large spikes are seen at the time of each discharge. These current spikes show peak values in the range of 32A with a duration of a fraction of a millisecond. The nature of the current spikes is same for all four materials used but the values differ in magnitude. This is depicted in Figure 3.2 for copper, brass, silicon and tantalum workpieces for the supply voltage of 155V and electrolyte concentration of 3%.

In Figure 3.2 (a), the current pulses for copper workpiece are indicated. The peak value of the spike is greater than 16A. The duration between first two spikes is around 18.4ms and that between the other two spikes is around 13.4ms. The total pulse duration is about 1.6ms.

For brass, the two peaks rise up to 3A and the duration between them is around 75ms as seen in Figure 3.2 (b). The total pulse duration is about 17ms. In the case of silicon, the current spikes are of smaller values than those for other three materials. The spikes are rising up to around 0.5A as seen in Figure 3.2 (c). The delay between the two spikes is of the order of 10-30ms. The pulse duration is around 2ms. For tantalum the current spikes are of greater value. Theses are attaining values greater than 28.5A as can be seen in Figure 3.2 (d). The delay is ranging from 10-16ms. The pulse duration is around 4ms. Thus discharge frequency for copper, silicon and tantalum material is comparable and is ranging from 30-100Hz. It is around 12-13Hz for brass material.

Voltage (V)	C (%v)	Current (A)
137	1.5	0.35
173	1.5	0.5
137	4.5	0.7
173	4.5	0.8
130	3	0.5
180	3	1
155	1	1
155	5	1.1
155	3	0.75
155	3	0.7
155	3	0.6
155	3	0.7

Table 3.3 Average current for copper workpiece.

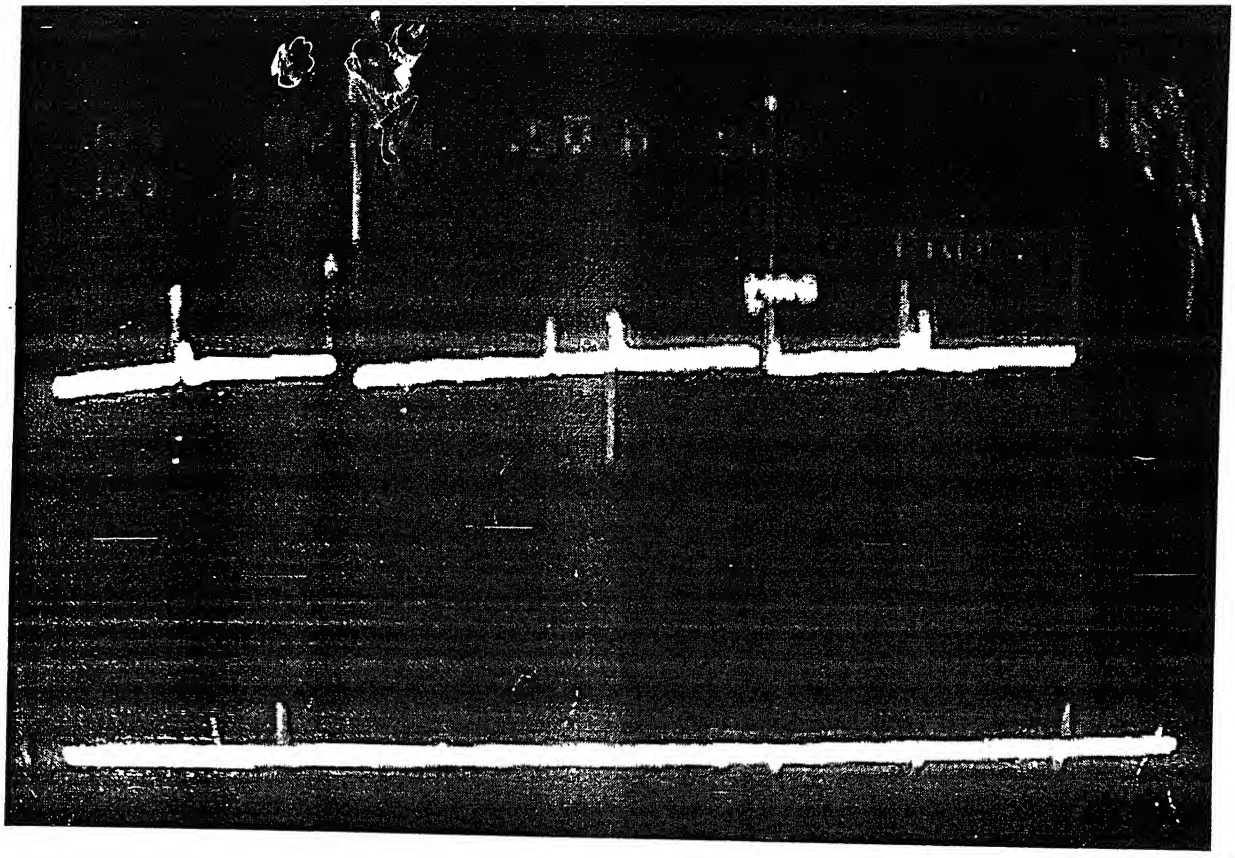

Curren

(a) Copper

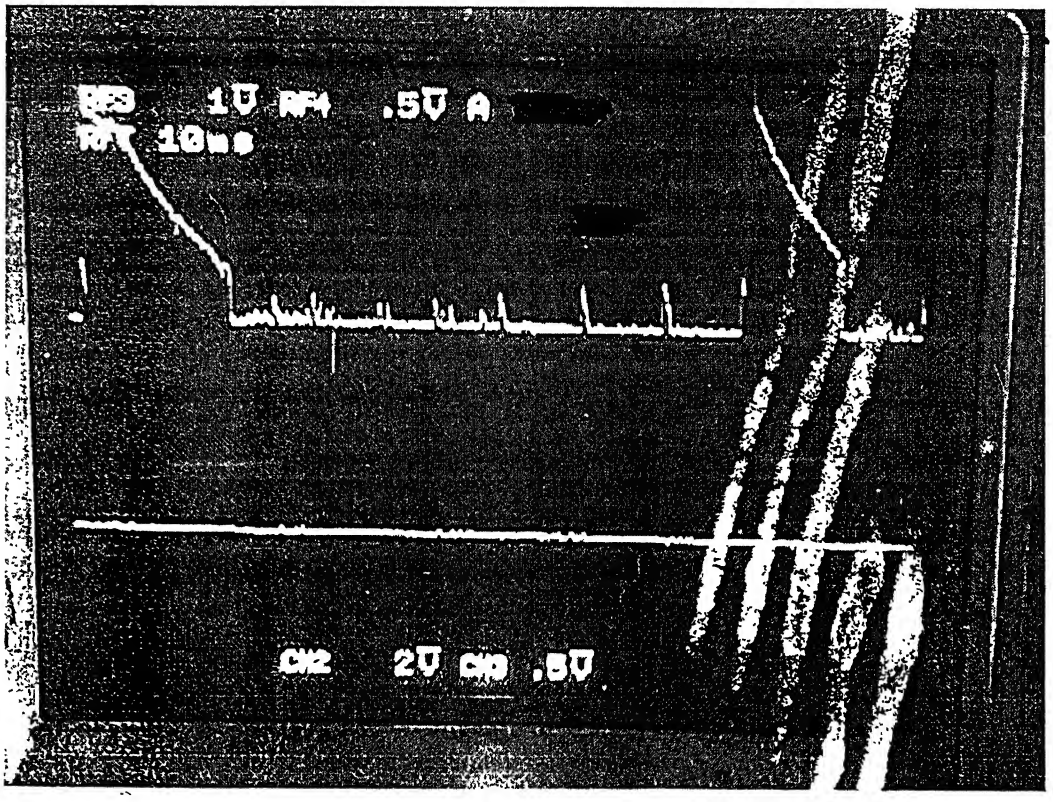

Current

(b) Brass

Figure 3 2 Time varying current at 155 V, 5 % HCl

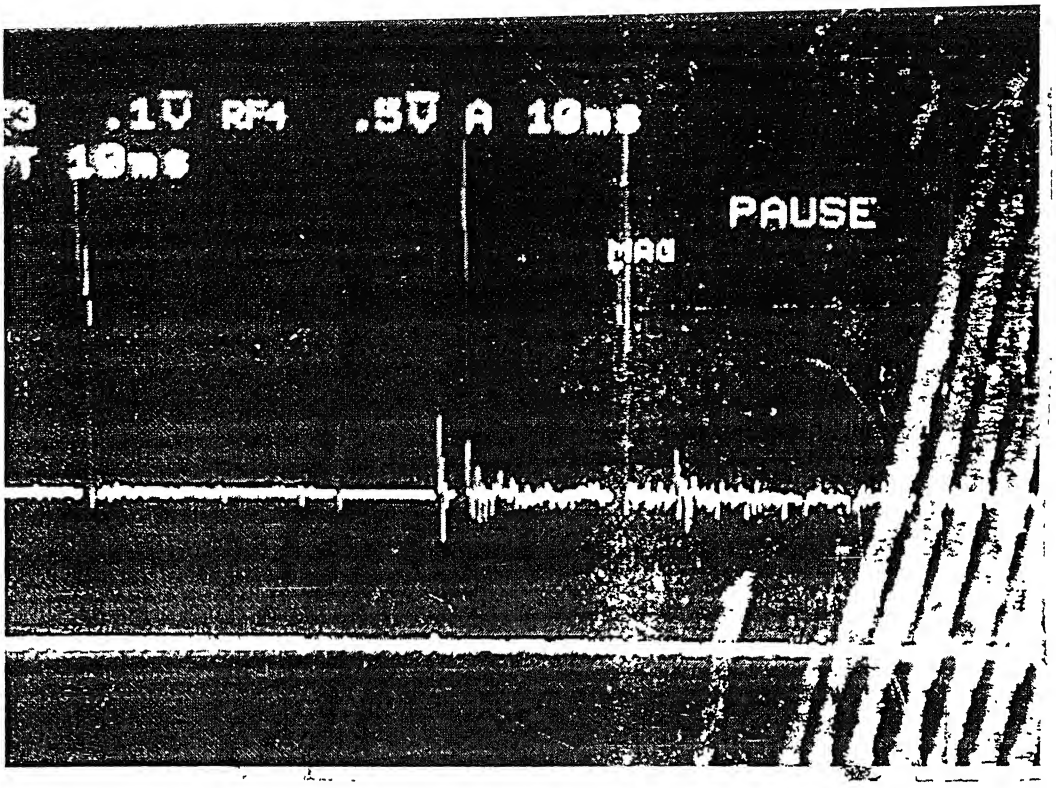

Current

(c) Silicon

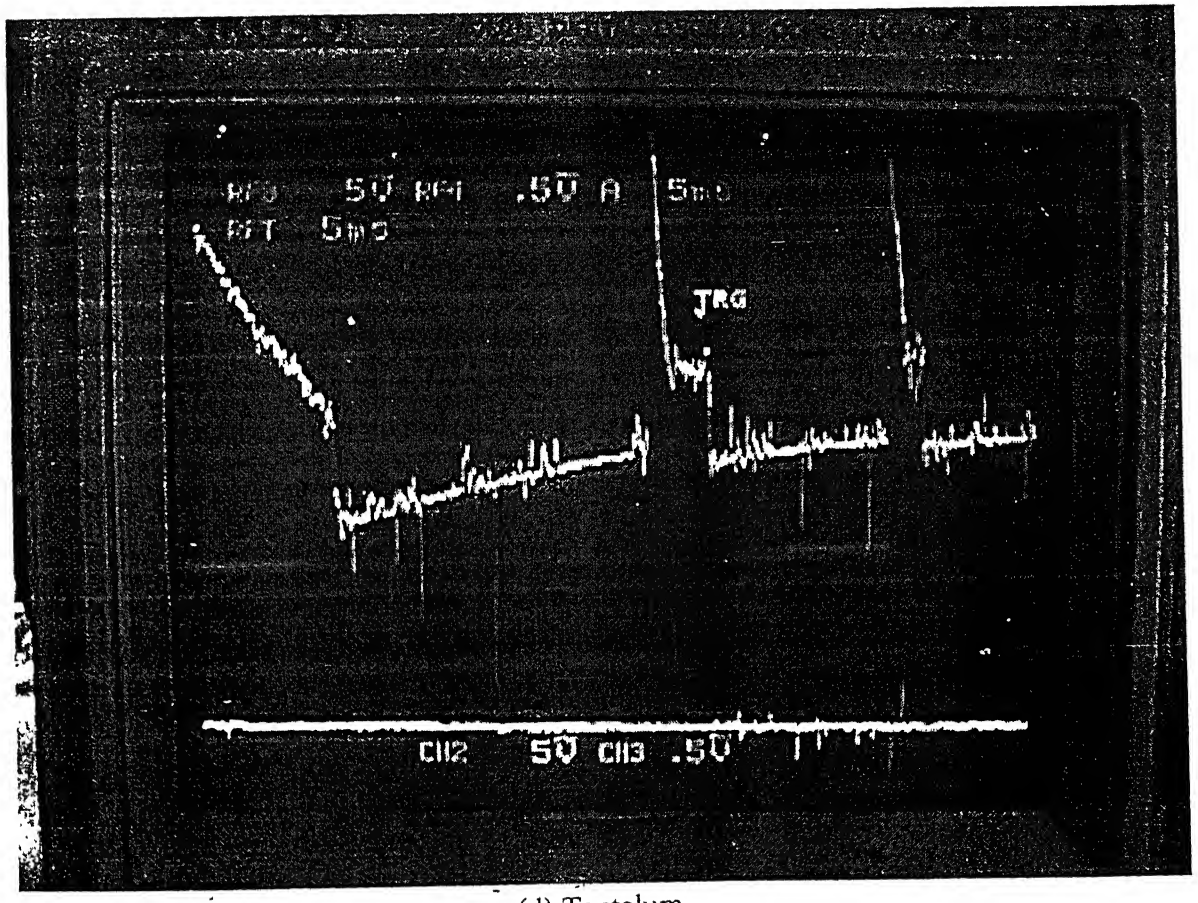

Current

(d) Tantalum

Figure 3. 2 Time varying current at 155 V, 5 % HCl

3.4 Metal Removal Rate (MRR)

The weight of workpiece before and after performing the experiment is recorded. The decrease in the weight shows that the material from the workpiece is removed. In each case, metal removal has taken place. Table 3.4 shows the MRR which resulted in each experiment. With increase in the voltage at the same concentration, the MRR has increased as expected. For 130V and 3% electrolyte concentration combination though the pyrometer did not capture any temperature reading, metal removal has taken place. The MRR is highest at 0.54 mg/sec for supply voltage of 175V and 1.5% electrolyte concentration.

The energy associated with the transformation phenomenon is estimated with the amount of metal removed.

3.5 Simultaneous Time Varying Current and Temperature Waveforms

As mentioned in the previous section, during the discharge, very large variations occur in the current flowing through the circuit giving rise to current spikes. Almost concurrently the pyrometer shows a simultaneous and sudden rise in the temperature of the workpiece in the discharge zone. The current and temperature are simultaneously monitored on two channels of the oscilloscope in ALT mode. The corresponding voltage and time base values are visible on the waveforms. The upper waveform corresponds to current and the lower one shows the temperature sensed by the pyrometer.

Current spikes are observed when discharge takes place. When the discharge hits the workpiece surface, the temperature of workpiece surface increases in the arc stroked zone. Simultaneous current and temperature pulses can be seen in Figure 3.3. It can be noticed that the temperature rises and then falls due to quenching. Once its value becomes lower than 815^0C, the output of pyrometer goes to zero due to its limitation of temperature sensing range. Temperature again rises due to the next arc or discharge hitting the surface of workpiece.

Voltage (V)	C (%v)	MRR (mg/sec)
137	1.5	0.2
173	1.5	0.54
137	4.5	0.05
173	4.5	0.25
130	3	0.012
180	3	0.025
155	1	0.097
155	5	0.16
155	3	0.1
155	3	0.048
155	3	0.083
155	3	0.091
155	3	0.043

Table 3.4 Metal Removal Rate (MRR) for copper.

Simultaneous current and temperature waveforms for copper are shown in Figure 3.3 (a). One can see a temperature pulse occurring between two current pulses. With the arrival of the first pulse, the temperature of the workpiece has increased to 865^0C and then reduces to 815^0C after a time of 2.8ms. After about a 14ms the second current pulse arrives showing that the next discharge has happened. Because of the chosen time scale of the oscilloscope the next pulse is not seen here.

For brass, the current waveform is noisy. Three current pulses and three temperature pulses are visible in Figure 3.3 (b). The current spikes are about 3A peak value with approximately 10-15ms pulse duration. The time between two consecutive pulses is around 50-60ms. The temperature reaches up to 1000^0C as a consequence of each pulse and within a time interval of 40ms the temperature falls from 1000^0C to 815^0C.

Figure 3.3 (c) shows the current and temperature pulses for silicon. In this case the width of temperature pulse seen is much larger (around 50ms) owing to its lower quenching rate due to its lower thermal conductivity. As a result a cumulative effect of several current pulses (hence the discharges) is seen in the figure. The maximum temperature reached is around 1360^0C.

In Figure 3.3 (d), the waveforms are shown for tantalum. The current spike is more than 32A and the temperature reached is 1640^0C. The current pulse duration is about 7-8ms and temperature pulse duration is 5ms.

Another temperature result for tantalum is shown in Figure 3.4. For first 5ms the temperature is about 1500^0C, then suddenly the temperature pulse increases beyond the limit (12V) of the oscilloscope for the chosen voltage base setting (0.2V/division). This indicates that the temperature attained is more than 1700^0C as the pyrometer's upper temperature sensing limit is 1700^0C. These types of pulses are rarely seen. It indicates that at times the high energy discharges do occur and workpiece surface in the discharge affected zone attains temperature of the order of evaporation temperature. The reason of rarely sensing these types of pulses are (i) occlusion of the workpiece surface from the

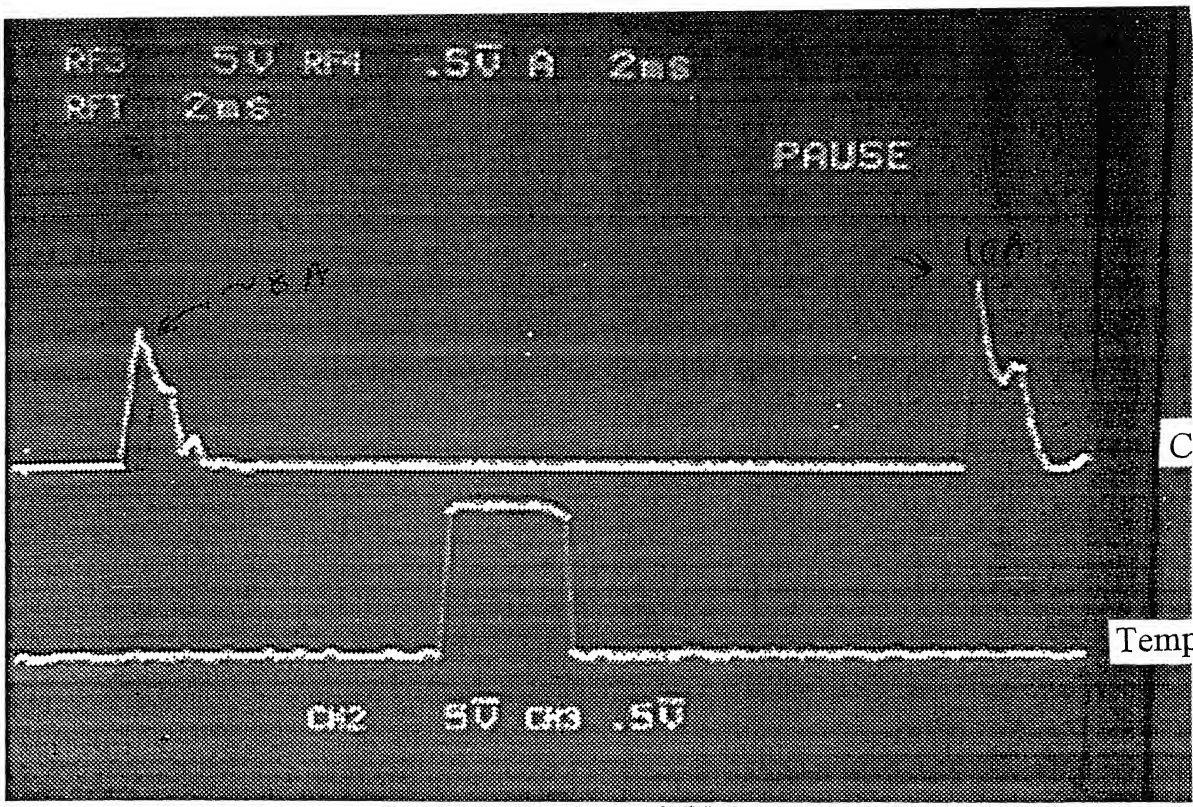

(a) Copper

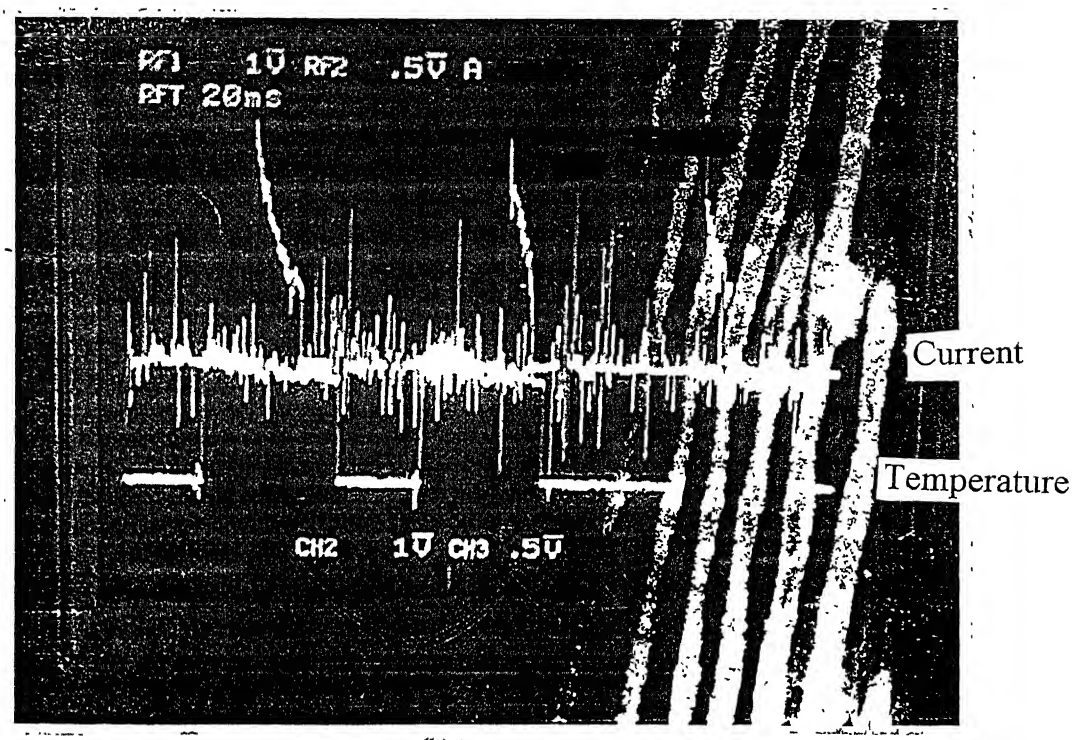

(b) Brass

Figure 3.3 Simultaneous time varying current and temperature at 155 V, 5 % HCl

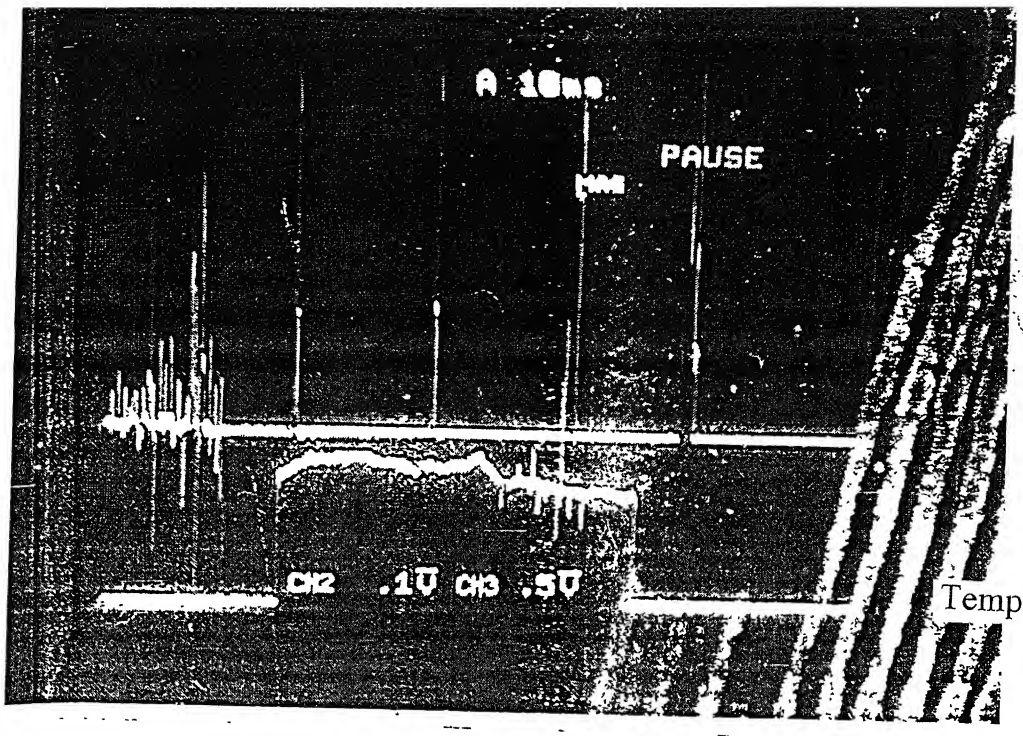

(c) Silicon

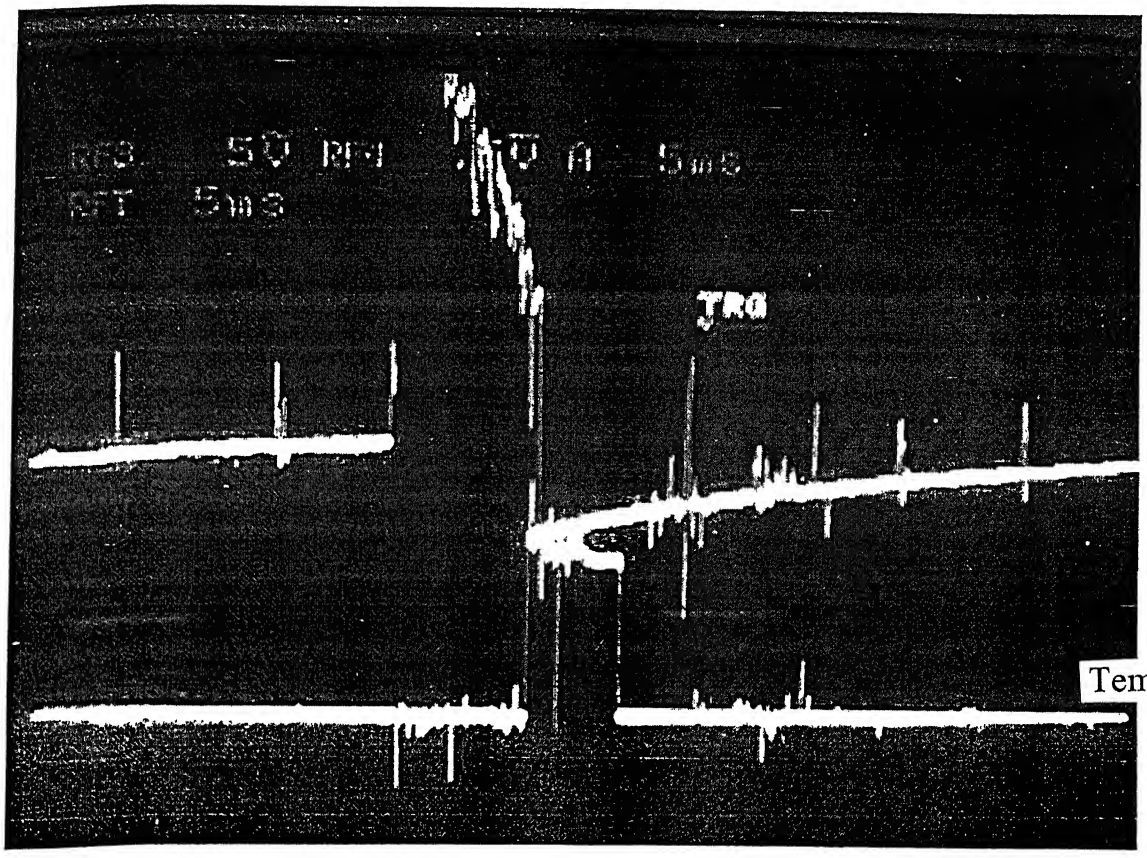

(d) Tantalum

Figure 3.3 Simultaneous time varying current and temperature at 155 V, 5 % HCl

pyrometer (due to shifting of the discharge from the focused area), and (ii) fast rising and quenching. (Time scale involved may become shorter than the response time of pyrometer). Therefore, the oscilloscope may or may not capture this event.

3.6 General Trends

3.6.1 Temperature Distribution in an ECDM Cell

The overall temperature distribution in an ECDM cell in operation is presented in Figure 3.5. The temperature distribution is highly non-linear as expected. As is seen in the figure, there is a small localized area on the workpiece surface where the average temperature is more than 800^{0}C at the center of the workpiece surface where the discharge strikes the surface. At a distance of 4mm away from this point, the temperature is drastically reduced to about 55-200^{0}C. It falls between 30-60^{0}C at a distance of 10mm away from the discharge affected zone. It attains the temperature of the electrolyte at its boundary, 12.5mm away from the discharge-affected zone. The temperature along the same line in the electrolyte in the ECDM cell is also displayed in the figure which shows that the temperature gradually decreases towards the edge of the cell. Temperature distribution is similar at the other side of the workpiece along the same line. This trend is observed for all workpiece materials.

3.6.2 Typical Workpiece Temperature at the Discharge Affected Zone

When discharge strikes the workpiece surface kept very near to the cathode tip, the temperature of the workpiece material increases depending on the striking energy. When it becomes more than 815^{0}C, pyrometer can record it. This temperature starts decreasing due to quenching of the workpiece and when the temperature reduces below 815^{0}C, pyrometer reading shows a sudden drop in its value. This can be seen in Figure 3.6 (a and b). In Figure 3.6 (a), after striking of discharge, the temperature of the workpiece is seen to attain a value of 850^{0}C at 155V with 5% electrolyte concentration. It

pyrometer (due to shifting of the discharge from the focused area), and (ii) fast rising and quenching. (Time scale involved may become shorter than the response time of pyrometer). Therefore, the oscilloscope may or may not capture this event.

3.6 General Trends

3.6.1 Temperature Distribution in an ECDM Cell

The overall temperature distribution in an ECDM cell in operation is presented in Figure 3.5. The temperature distribution is highly non-linear as expected. As is seen in the figure, there is a small localized area on the workpiece surface where the average temperature is more than 800^0C at the center of the workpiece surface where the discharge strikes the surface. At a distance of 4mm away from this point, the temperature is drastically reduced to about 55-200^0C. It falls between 30-60^0C at a distance of 10mm away from the discharge affected zone. It attains the temperature of the electrolyte at its boundary, 12.5mm away from the discharge-affected zone. The temperature along the same line in the electrolyte in the ECDM cell is also displayed in the figure which shows that the temperature gradually decreases towards the edge of the cell. Temperature distribution is similar at the other side of the workpiece along the same line. This trend is observed for all workpiece materials.

3.6.2 Typical Workpiece Temperature at the Discharge Affected Zone

When discharge strikes the workpiece surface kept very near to the cathode tip, the temperature of the workpiece material increases depending on the striking energy. When it becomes more than 815^0C, pyrometer can record it. This temperature starts decreasing due to quenching of the workpiece and when the temperature reduces below 815^0C, pyrometer reading shows a sudden drop in its value. This can be seen in Figure 3.6 (a and b). In Figure 3.6 (a), after striking of discharge, the temperature of the workpiece is seen to attain a value of 850^0C at 155V with 5% electrolyte concentration. It

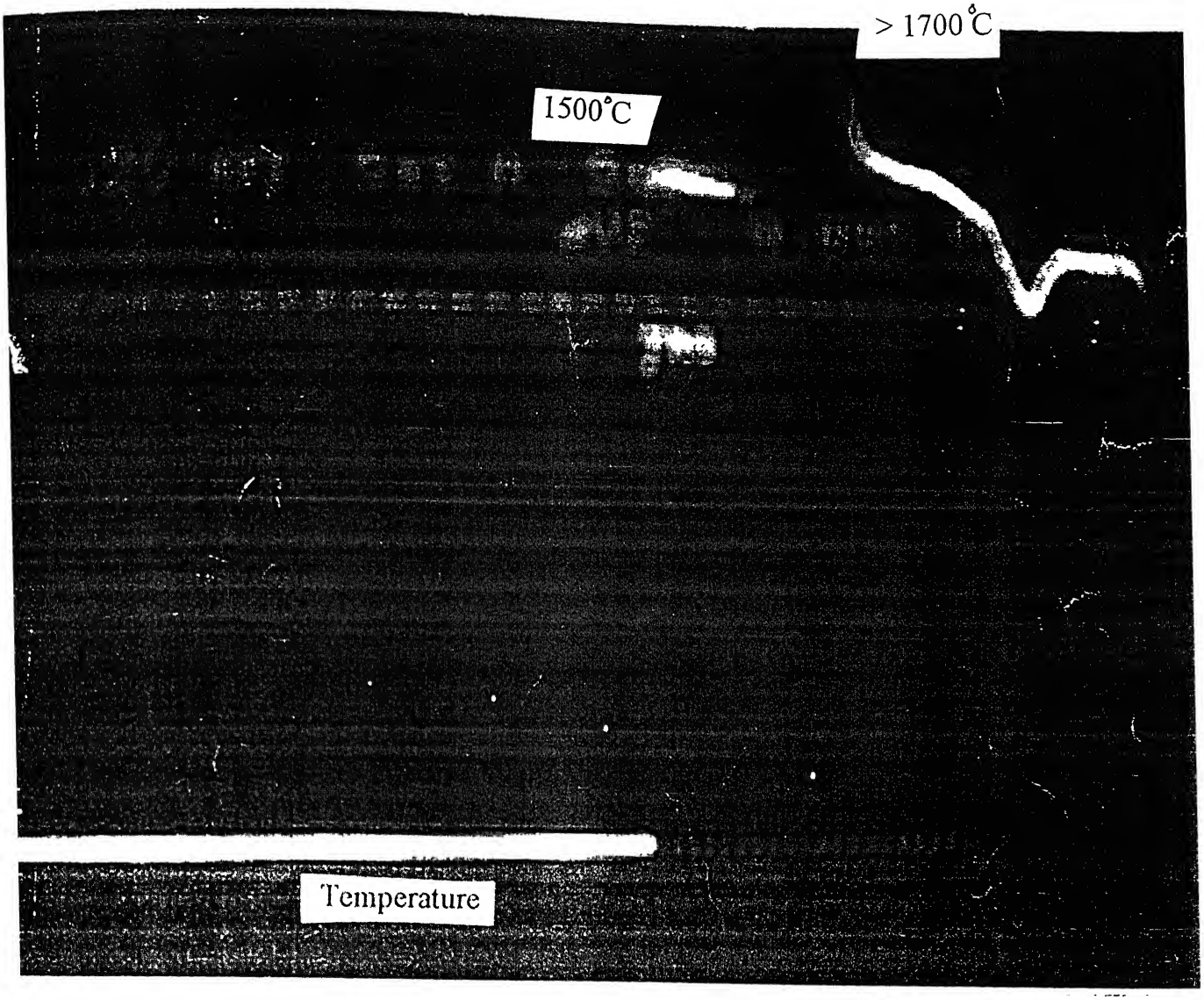

Figure 3.4 A temperature spike recorded for Tantalum workpiece indicating a temperature rise of more than 1700 ^{0}C

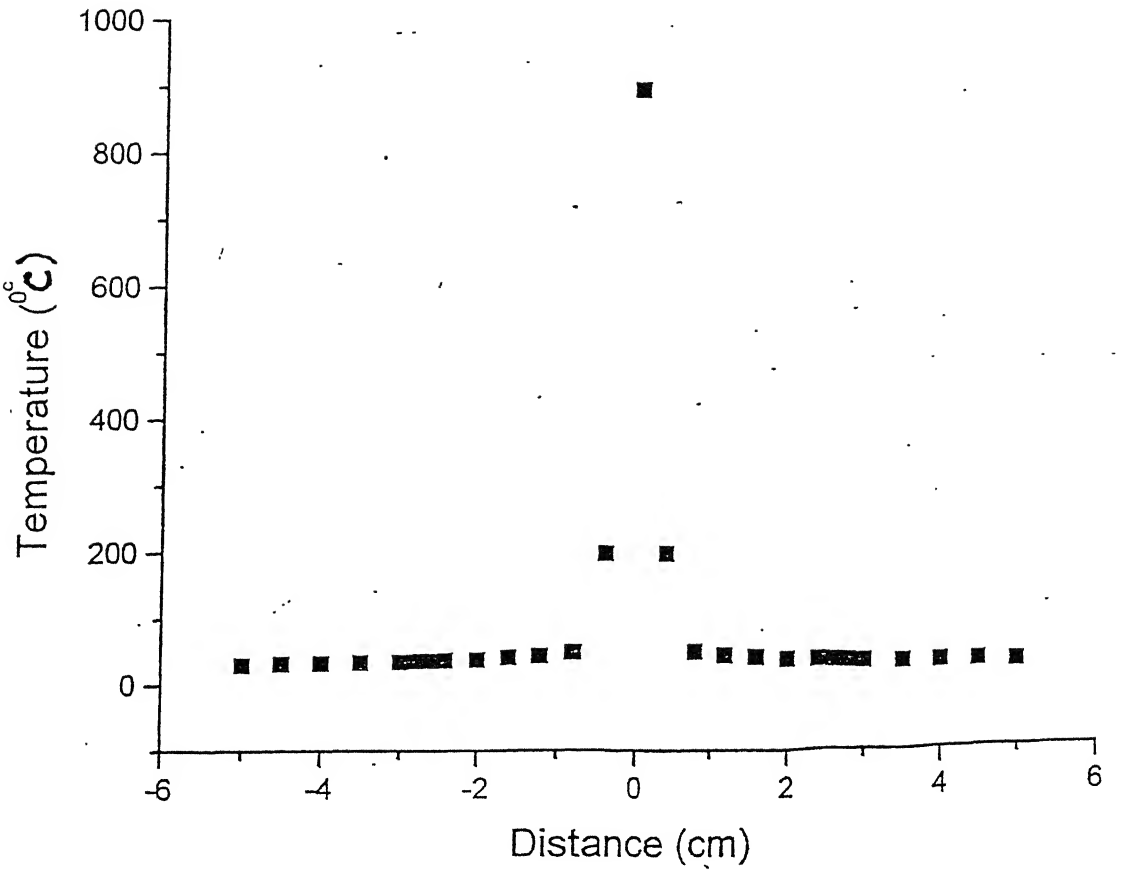

Figure 3.5 Temperature distribution in an ECDM cell

remains at 850^0C about 4.6 ms and then starts cooling. After a time period of around 0.4 ms it reduces below 815^0C and the pyrometer shows zero reading for this temperature. With the next discharge, temperature may further rise. In Figure 3.6 (b), for a voltage of 170V and 5% concentration of electrolyte, workpiece attains a temperature of 950^0C, gradually decreases and after 20 ms it reduces below 815^0C.

In Figure 3.7 (a) and (b) two temperature waveforms are shown for copper and tantalum workpiece materials respectively treated at a supply voltage of 155V and 3% electrolyte concentration. These waveforms show the cumulative effect of discharges taking place at varied time intervals.

3.7 Dimension of Discharge Affected Zone

Normally a cumulative effect of several discharges striking the workpiece surface in the ECDM process is seen. In this work an attempt is made to see the effect of single discharge on the surface topography of the workpiece. The area over which the arc strikes the surface is observed under an optical microscope. For this purpose the ECDM process was carried out for a very short duration to simulate a pulsed power supply and to have least number of discharges striking the workpiece surface so that the effect of single discharge can be studied. The knowledge of the area of the discharge-affected zone on the surface by a single discharge is important in calculating the energy density per discharge. This way, all the parameters, (the voltage pulse, the current pulse at the time of discharge, and the area over which the discharge strikes) can be experimentally determined. These parameters are needed for theoretical evaluation of surface temperature of the workpiece.

Observation of the workpiece under an optical microscope shows clearly the signature of discharges striking the surface, their size, and their distribution over the surface. The discharge-affected region is seen as circular zone in nature. The circular zones and its boundaries appear shiny with wrinkles surrounding it. These features appear to be reminiscent of rapid solidification of the material after melting.

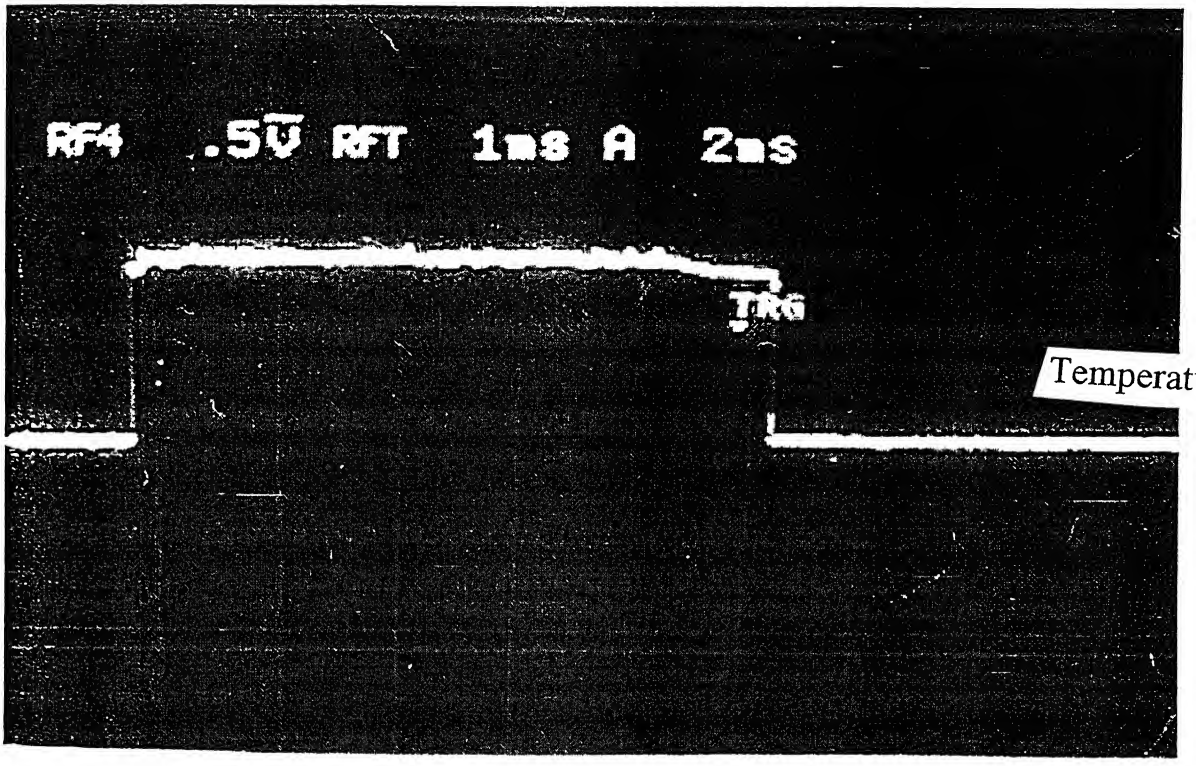

(a) 150 V, 5 %

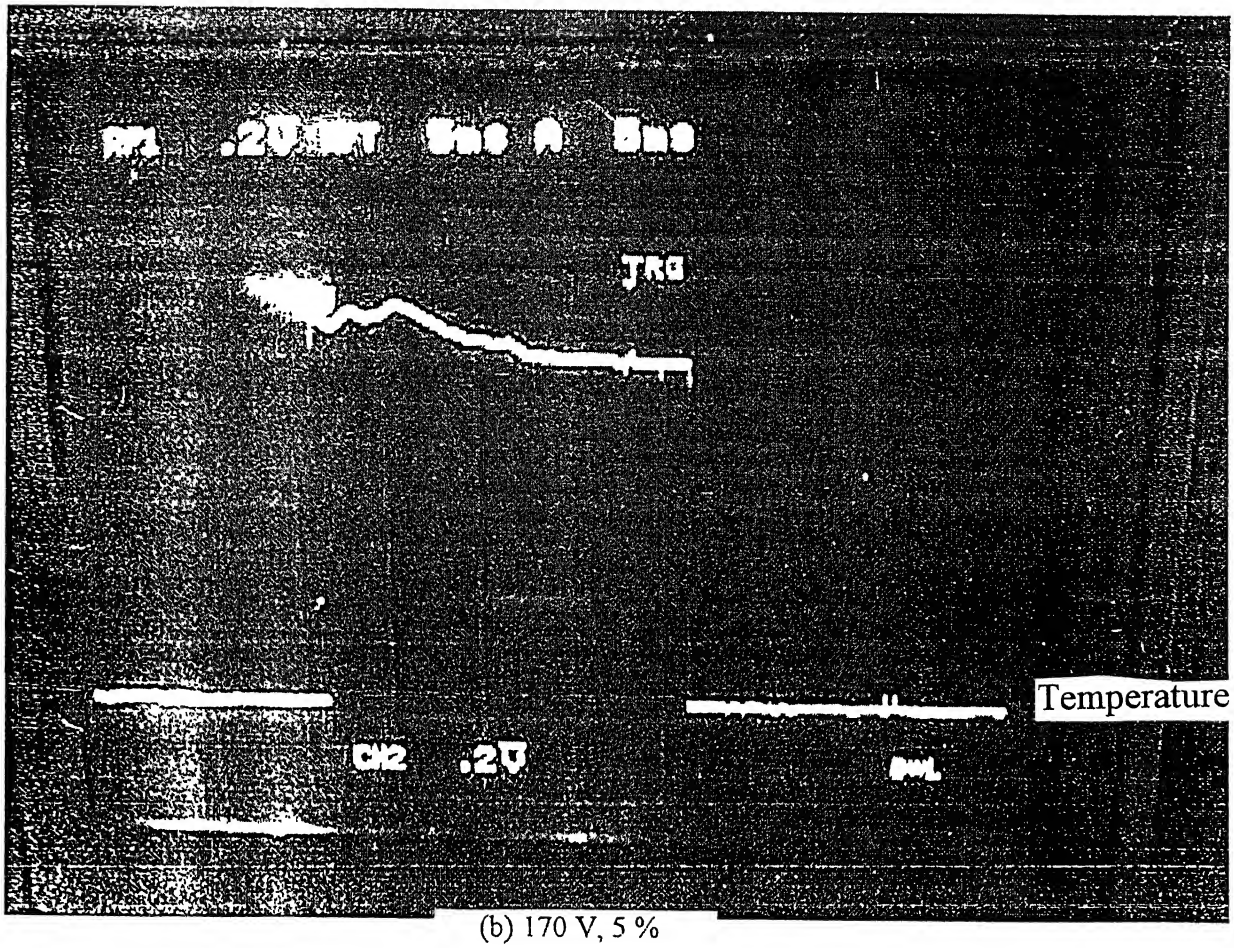

(b) 170 V, 5 %

Figure 3.6 Typical time varying temperature at the discharge affected zone in Copper workpiece

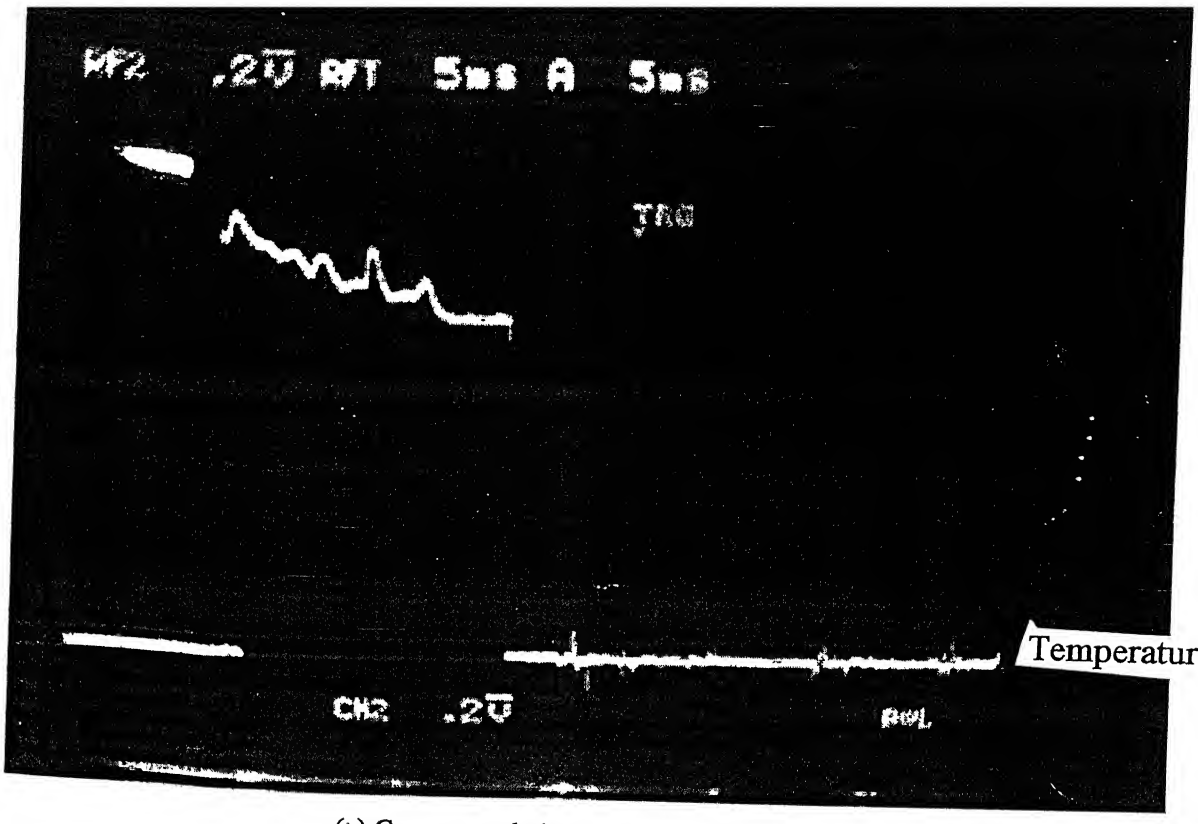

(a) Copper workpiece, 170 V, 5 %

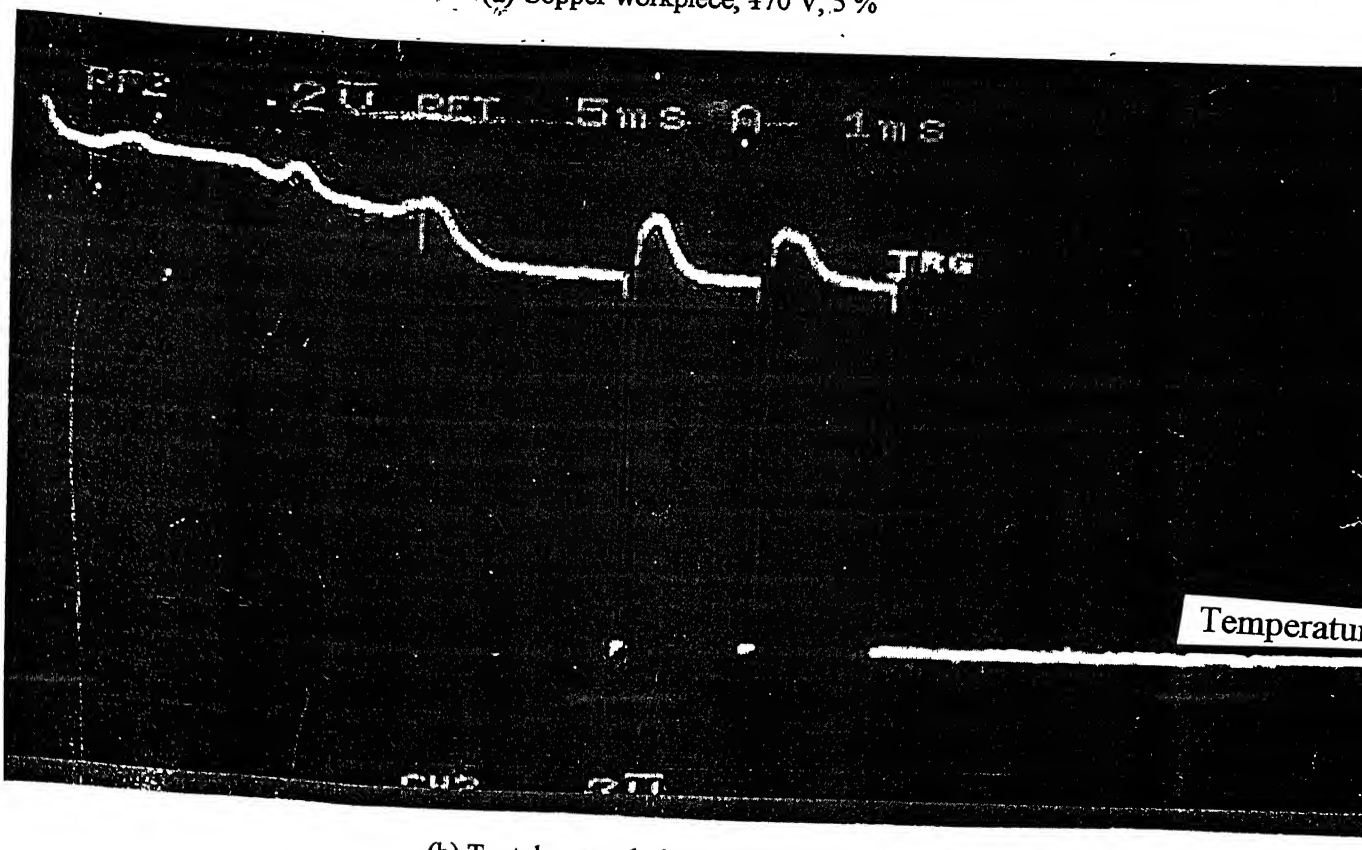

(b) Tantalum workpiece, 170 V, 5 %

Figure 3.7 Temperature pulses showing the cumulative effect of discharges taking place at varied time intervals

In Photograph 3.1, copper workpiece surface is visible. It was kept at a distance of 1000μm from the cathode in the ECDM cell. Experiment was performed for a very short duration of time to have a very few number of discharges striking the surface. Experiment was carried out with supply voltage of 155V, with 1% electrolyte combination. The magnified (100X) surface shows that no discharge striked the copper workpiece as the distance between the workpiece and the cathode tip where the discharge takes place is more. Therefore this surface is similar to that of an untreated workpiece.

Photograph 3.2 shows the copper surface which is treated for about a second at a supply voltage of 155V and 3% electrolyte concentration with the cathode-workpiece separation of 600μm. One can observe about six prominent circular zones on the surface. This number approximately matches with the audio-visual observation of discharges which took place. These affected zones indicate that the striking geometry is circular in nature with an average diameter of 300μm. In this sample, the total affected zone is almost circular in nature and about 1mm diameter.

Photograph 3.3 shows a magnified (200X) view of the discharge affected zone (copper workpiece, 155V, 5% concentration and 600μm distance between cathode-workpiece). It clearly shows the rings formed by melting and solidification due to quenching. The inner shining round spot of 60μm diameter is probably due to the removal of metal from the workpiece surface.

Optical micrograph of tantalum workpiece is shown in Photograph 3.4. One can note the difference in color of the discharge affected zone in copper and that in tantalum. Out of many, three discharges are focused and magnified (100X). Again the ring pattern of melting and solidification is similar to that in copper workpiece. The average diameter of the blackish area is 5000μm. The innermost shining spot is attributed as the metal removal from the workpiece surface.

In general, it can be said that the diameter of the circular regions formed due to striking of the discharges varies from 200 to 500μm for the copper. Discharge location

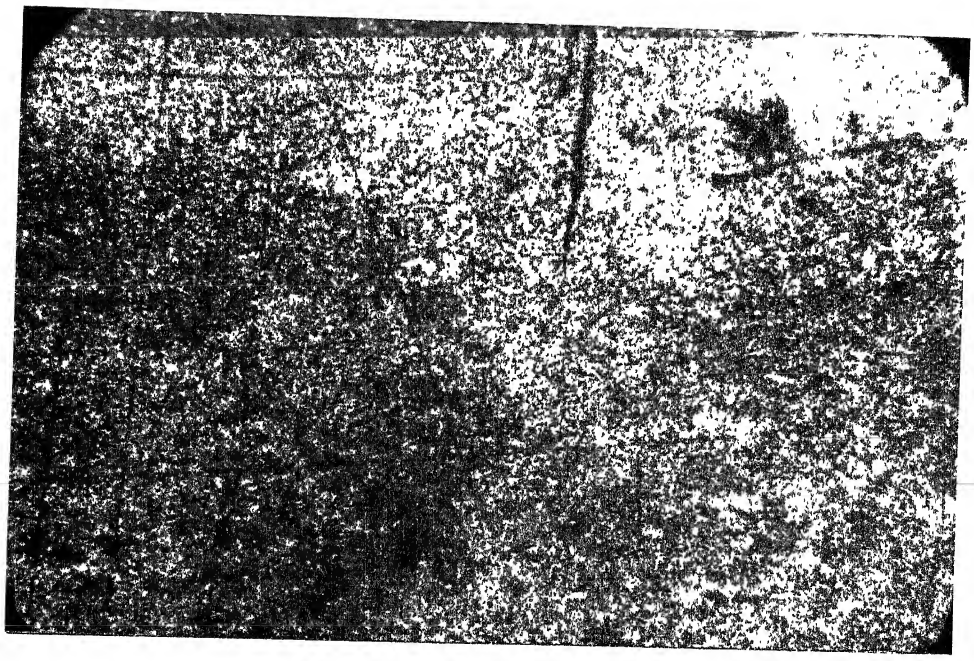

Photograph 3.1 Optical photograph (100X)) showing copper surface where discharge does not strike the surface. (Copper work piece treated at 155V, 1%).

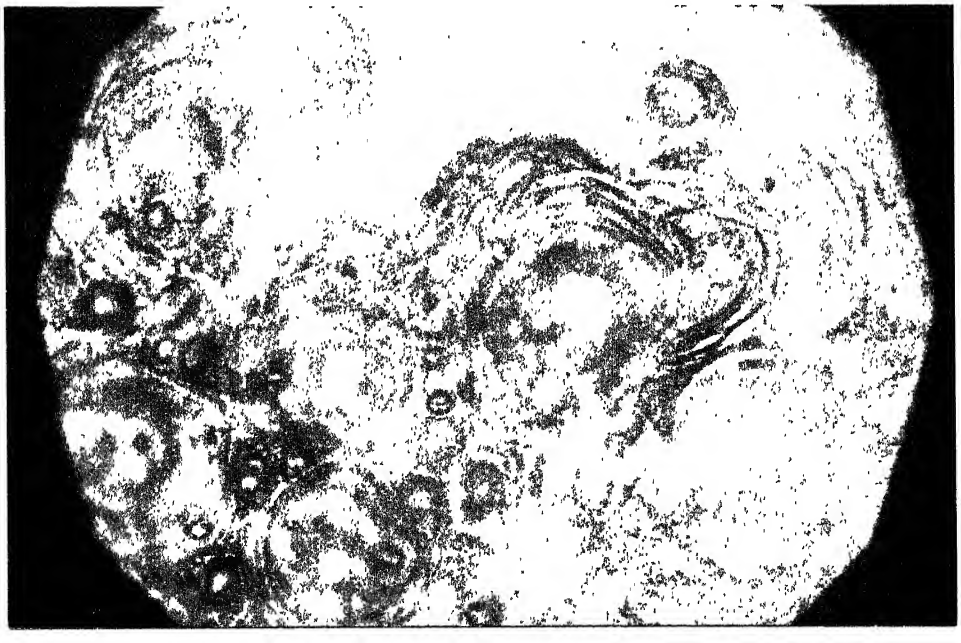

Photograph 3.2 Optical photograph showing discharge affected zone (100X), approximately six prominent circular regions are seen (Copper work piece treated at 155V, 3%).

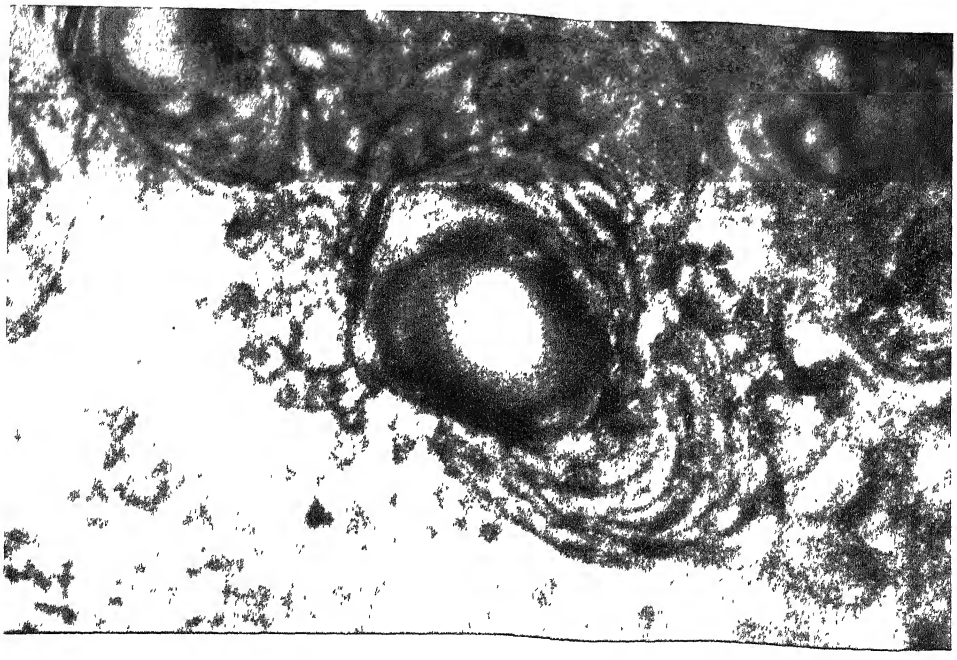

Photograph 3.3 Magnified view (200X) of one of the zones showing effect of an individual discharge
(Copper work piece treated at 155V, 3%).

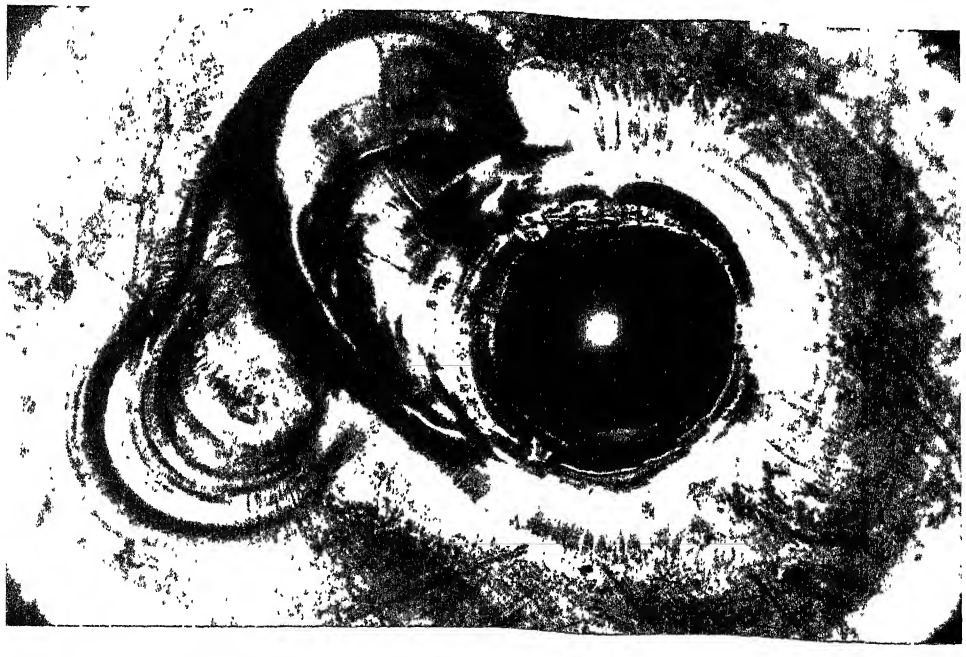

Photograph 3.4 Optical photograph (100X) taken for a tantalum work piece
The affected zone shows a very clear ring pattern
(Tantalum workpiece treated at 155V, 3%).

also vary within a zone of 1000μm diameter. It appears that the discharge affected area is larger in the case of tantalum. Change in the discharge location sometimes occludes the workpiece from pyrometer and proper temperature can not be recorded.

3.8 Energy Balance in ECDM process

There are various phenomena associated with the ECDM process. To understand the contribution of each of the phenomenon, it is necessary to estimate the energy associated with the major phenomena occurring in the process. It was felt that by simple (not too precise) measurements of temperatures at various locations in the ECDM cell one could estimate the energy associated with various phenomena which occur during the discharge process. This will be useful in deriving the efficiency of the process, which is a parameter of utmost importance in manufacturing and industrial applications of the processes.

Various phenomena which occur during the ECDM process when electrical energy supplied to the cell are given below:

- Electrical (input energy, flow of current, potential drops across circuit resistances, I^2R heating of cathode)
- Electrochemical (hydrogen gas bubble generation)
- Discharge (non thermal arc discharge at the cathode-electrolyte interface)
- Thermal (heat conduction in electrolyte, workpiece, etc.)
- Transformation (ablation of workpiece)
- Mechanical (splashing of electrolyte)
- Radiation from cathode and workpiece at elevated temperatures
- Sound

Of these, electrical, thermal and transformation phenomena are those which contribute more to the process and hence are treated for the energy balance. The energy associated with the electrolysis phenomenon contributes very less. The energy input to the system is compared with the total energy associated with thermal and transformation phenomena.

3.8.1 Energy Analysis

Figure 3.8 shows the flow diagram elaborating the steps involved in estimating the energies. Each block in the flow diagram is elaborated in the subsequent discussion.

(i) Input Energy

Input energy to the system is the energy provided by the power supply. This energy is calculated as the product of the DC supply voltage (V), the average current in the circuit (I_{avg}) and the time (t) for which the experiment is performed. Hence,

$$E^{Input}_{ECDMSystem} = E^{Output}_{Power\ sup\ ply} = V * I * time \quad (1)$$

Time values for which the experiments were carried out are mentioned in Table 3.5.

(ii) Energy Associated with the Electrolyte

In the ECDM process, the electrolyte in the ECDM cell gets heated up. The amount of temperature rise is noted by the use of two immersion probes and the average temperature rise is recorded. The weight of the electrolyte used is 200 gm. Neglecting the energy associated in vaporization and splashing of the electrolyte, the total energy utilized in the electrolyte is modelled to be the rise in the stored energy. Therefore,

$$E^{Total}_{Electolyte} = E^{Stored}_{Electrolyte} = m_{\ electrolyte} * C_{\ electrolyte} * \Delta IT \quad (2)$$

where $m_{\ electrolyte}$ is the weight of the electrolyte used in the cell (= 200gm),
$C_{\ electrolyte}$ is the Heat capacity of electrolyte (~ 4000 J/Kg), and ΔIT is the average rise in the temperature of electrolyte measured by immersion thermocouples as indicated in Table 3.5.

where $m_{Workpiece}^{Transformed}$ is the weight of material removed from the workpiece in gm as shown in Table 3.5 and T_m is melting temperature of the workpiece material. E_2, E_3 and E_4 can be evaluated as'

$$E_2 = m_{Workpiece}^{Transformed} * L_f \quad (6)$$

where L_f is the latent heat of fusion.

$$E_3 = m_{Workpiece}^{Transformed} * C' * (T_b - T_m) \quad (7)$$

where C' is the heat capacity of material in liquid phase and T_b is the boiling temperature

$$E_4 = m_{Workpiece}^{Transformed} * L_V \quad (8)$$

where L_V is the latent heat of vaporization. The values of various parameters appearing in the above equations are listed in Appendix C for various materials used in the process. Adding equation (4) to (8) gives the total energy associated with the workpiece.

(iv) Output Energy

The total output energy of the system is approximated by the addition of the above two major components. In so doing, the energies associated with cathode heating, flask heating, splashing of electrolyte are neglected. Also energy associated with radiation is ignored.

Therefore,

$$E_{ECDMsystem}^{Output} = E_{Electolyte}^{Total} + E_{Workpiece}^{Total} \quad (9)$$

(v) Energy Associated with Other Mechanisms of the ECDM process

The sum of the energies associated with the electrolyte and workpiece is treated as total output energy. The difference of the total input energy and output energy can be assigned to the various other mechanisms such as energy required for cathode heating and flask heating, etc. This is indicated in the last column of Table 3.6. This amount of energy is almost comparable to that utilized by the workpiece.

The energy balance is performed by equating the total input energy to that with total output energy. The difference between the input energy and output energy is treated as that associated with the above mentioned phenomena for which the energy is not experimentally estimated. The energy associated with the workpiece contributes towards the efficiency of the system. The calculations for energy balance in different experimental conditions are carried out in the next section.

3.8.2 Energy Calculations

(a) For Copper Workpiece

Table 3.5 gives the values which are needed for calculation of the different types of energy as discussed in the previous section. In this table, column 1 gives the supply voltage, column 2 gives the current values and column 3 shows the time for which the experiment is performed. Column 4 gives the average temperature rise of the workpiece recorded by the two thermocouples and column 5 summarizes the average temperature rise in the electrolyte in the cell measured by the two immersion thermocouples (refer Figure 3.1). The next two columns give the values of the initial workpiece weight and the weight corresponding to the material removed or transformed. Appendix C gives the thermal properties of the copper and other materials used in the experiments..

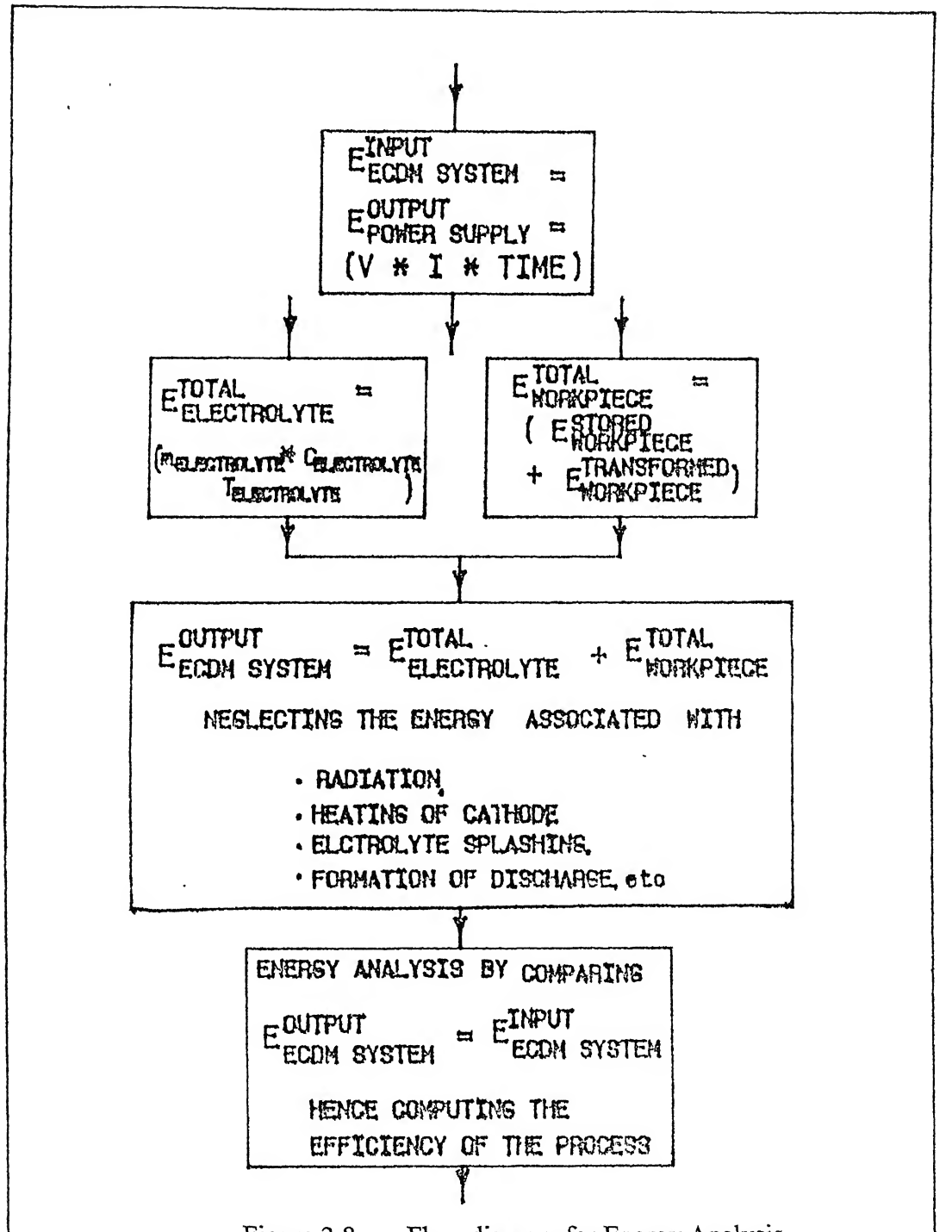

Figure 3.8 Flow diagram for Energy Analysis

Voltage (V)	Current (A)	Time (sec)	ΔT (^0C)	ΔIT (^0C)	$m_{Workpiece}^{Initial}$ (gm)	$m_{Workpiece}^{Transformed}$ (gm)
137	0.35	75	42.5	4	3.374	0.015
173	0.5	50	52.5	5	2.377	0.027
137	0.7	60	57	6.5	2.982	0.003
173	0.8	13	70	2	3.110	0.003
130	0.5	85	67	5.5	3.053	0.001
180	1	80	62.5	14	3.122	0.002
155	1	82	75	12.5	3.161	0.008
155	1.1	75	125	14.5	3.193	0.012
155	0.75	60	100	8	3.111	0.006
155	0.7	62	62.5	8	2.964	0.003
155	0.6	60	62.5	6.5	2.561	0 005
155	0.7	55	67.5	7	3.185	0.005
155	0.7	46	67.5	5.5	3.184	0.002

Table 3.5 Table showing voltage, current, time, average temperature at workpiece and in the electrolyte cell. The initial and lost weight of the copper workpiece are given in last two columns respectively.

(b) Energy Calculations for Other Materials

Similar analysis is carried out for other materials viz., brass and tantalum also. In the case of silicon, the complete analysis is not possible because the workpiece was breaking as it was very fragile. Table 3.7 shows the parameter values and corresponding changes in temperature of the electrolyte and workpiece surface. The last two columns of Table 3.7 show the weight of the workpiece material before carrying out the experiment and that of the transformed material, respectively. The trend is similar to that observed in the case of copper. Table 3.8 shows the energy values and % of energy utilized by the electrolyte in raising its temperature by the workpiece and the remaining energy for other mechanisms involved in the ECDM process for brass and tantalum workpieces.

3.9 Efficiency Evaluation

As mentioned earlier the different energy components effective in ECDM process are evaluated. The approximate total input energy supplied to the system (represented by (1) displayed in column 1 of Table 3.6) is compared to those associated with electrolyte and workpiece. The percentage of total energy utilized by the electrolyte is mentioned in column 3 of Table 3.6. This shows that almost 77 to 95% of input energy is going in heating up the electrolyte. The percentage of total energy input associated with the workpiece is at the most 6%. This energy, in fact, is utilized for carrying out the machining operation and can be treated as the productive energy. Thus the efficiency of the process is about 2-6%.

In the case of brass, out of the total energy supplied to the system by the power supply, around 83% is getting used in raising the temperature of the electrolyte, around 1% only is utilized by the workpiece and around 16% is associated with the other mechanisms involved in the system. The efficiency for tantalum is also around 1.2% .

$E^{Input}_{ECDMsystem}$ (J) (1)	$E^{Total}_{Electrolyte}$ (J) (2)	$E^{Stored}_{Workpiece}$ (J) (3)	$E^{Transformed}_{Workpiece}$ (J) E_1	E_2	E_3	E_4 (4)	$E^{Total}_{Workpiece}$ (J) (3) + (4)	$E^{Output}_{ECDMsystem}$ (J) (1)- [(2)+(3)+(4)]
3596	3200	55.2	6	3.1	10.9	72	147.2	249
4325	4000	48.1	10.7	5.6	19.7	129.6	213.7	111
5754	5200	65.4	1.2	0.6	2.2	14.4	84.2	470
1799	1600	83.8	1.2	0.6	2.2	14.4	102.2	97
5525	4400	78.7	0.4	0.2	0.7	4.8	84.8	240
14400	11200	75.1	0.8	0.4	1.5	9.6	87.4	3112
12710	10000	91.3	3.1	1.7	5.8	38.4	140.3	2570
12787	11600	153.6	3.4	2.5	8.7	57.6	225.8	962
6975	6400	119.7	2.2	1.2	4.4	28.8	156.3	419
6727	6400	71.3	1.2	0.6	2.2	14.4	89.7	237
5580	5200	61.6	1.9	1	3.6	24	92.1	288
5967	5600	82.7	1.9	1	3.6	24	113.2	254
4991	4400	82.7	0.8	0.4	1.46	9.6	95	496

% of total Energy Utilized by Electrolyte	% of total Energy Utilized by Workpiece	% of Energy Associated with the Other Mechanisms
88.9	4	6.9
92.3	4.9	2.6
90.4	1.5	8.2
88.9	5.6	5.5
79.6	1.6	4.3
77.7	0.6	21.6
78.7	1.1	20
90.7	1.8	7.5
91.7	2.2	6
95.1	1.3	3.5
93.1	1.6	5.2
93.8	1.9	4.2
88.2	1.9	9.9

Table 3.6 Table showing results of energy calculations and % of energies utilized by the electrolyte, copper workpiece and other mechanism in the ECDM process for copper workpiece.

Voltage (V)	Current (A)	Time (sec)	ΔT (^{0}C)	ΔIT (^{0}C)	$m_{Workpi}^{Initial}$ (gm)	$m_{Workpiece}^{Transformed}$ (gm)
155	1.4	40	27.5	9	3.009	0.011
155	0.48	--	28.5	5.5	0.282	--
155	0.7	40	37	5	2.028	0.008

Table 3.7 Table showing voltage, current, time, average temperature at workpiece and in the electrolyte cell for Brass, Silicon and Tantalum. The initial and lost weight of workpiece are given in last two columns.

Material	$E_{ECDMsystem}^{Input}$ (J) (1)	$E_{Electrolyte}^{Total}$ (J) (2)	$E_{Workpiece}^{Stored}$ (J) (3)	$E_{Workpiece}^{Transformed}$ (J) E E E E (4)	$E_{Workpiece}^{Total}$ (3) + (4)	$E_{ECDMsystem}^{Output}$ (1)-[(2)+(3)+(4)]
Brass	8680	7200	31.9	4.1 2.3 8.2 52.8	99.3	1380
Silicon	--	4400	5.7			
Tantalum	4340	4000	10.7	3.2 1.5 3.3 34.4	53.1	287

Material	% of total Energy Utilized by Electrolyte	% of total Energy Utilized by Workpiece	% of total Energy Utilized by Other Mechanisms
Brass	82.9	1.1	15.9
Tantalum	92.2	1.2	6.6

Table 3.8 Table showing results of energy calculations and % of energies utilized by the electrolyte, workpiece and other mechanisms in the ECDM process for Brass, Silicon and Tantalum.

In view of these observations, the electrolyte cell should be redesigned to have least energy waste in raising the temperature of the electrolyte. The alternative to use of electrolyte bath in the electrolyte cell could be a jet flow of electrolyte.

3.10 Observations

The observations made during the experiments are summarized below:

1. Discharge initiates at a lower voltage as the concentration of the electrolyte is increased. When the discharge initiates at a particular threshold voltage, it is very much constricted. On increasing the voltage, discharge becomes more agitating and spreads in the area. Further increase in voltage causes splashing of electrolyte. Table 3.9 shows the onset voltage of discharge, voltage corresponding to the constricted discharge and the voltage at which agitating discharge starts, for different values of concentrations.

2. As the electrolyte concentration increases, the average value of current increases. Thus the rate of hydrogen gas bubbles generation increases, and hence the ignition delay decreases.

3. Transient current was observed for different values of series resistance for a particular concentration and supply voltage. Ignition delay decreases for smaller value of series resistance (Figure 3.9). In Figure 3.9 (a), a series resistance of 1 Ohm is connected in series with the cathode while measuring the current. Here it is observed that the duration between the two current pulses is ranging from 10 to 30ms. Current pulses seen in Figure 3.9 (b) are obtained by using a series resistance of 0.15 Ohm. The observed time duration between two current pulses ranges from 2 to 10ms. This shows that with smaller series resistance the ignition delay between two discharges reduces.

4. An important observation is that of the varying frequency of discharge (oscillations) with varying supply voltage. The results obtained are tabulated in Table 3.10. It is clear from the table that when there is no discharge, the difference V_2 - V_1 measured with the multimeter increases with increasing the supply voltage (up to 20V) and it vanishes when

Electrolyte - HCl, Concentration 1.5%

S.N.	VOLTAGE	CURRENT	PHASE
1	20	1.2	Bubbles start growing
2	50	0.15	Constricted Discharge starts
3	120	0.1	Agitated Discharge starts

(a)

Electrolyte - HCl, Concentration 3%

S.N.	VOLTAGE (V)	CURRENT (A)	PHASE
1	7	1.4	Bubbles start growing
2	45	0.2	Constricted Discharge Starts
3	110	0.18	Agitated Discharge starts

(b)

Electrolyte - HCl, Concentration 4.5%

S.N.	VOLTAGE	CURRENT	PHASE
1	6	1.5	Bubbles start growing
2	40	0.45	Constricted Discharge starts
3	90	0.4	Agitated Discharge starts

Table 3.9 Table showing the physical observations (last column) for various values of electrolyte concentration.

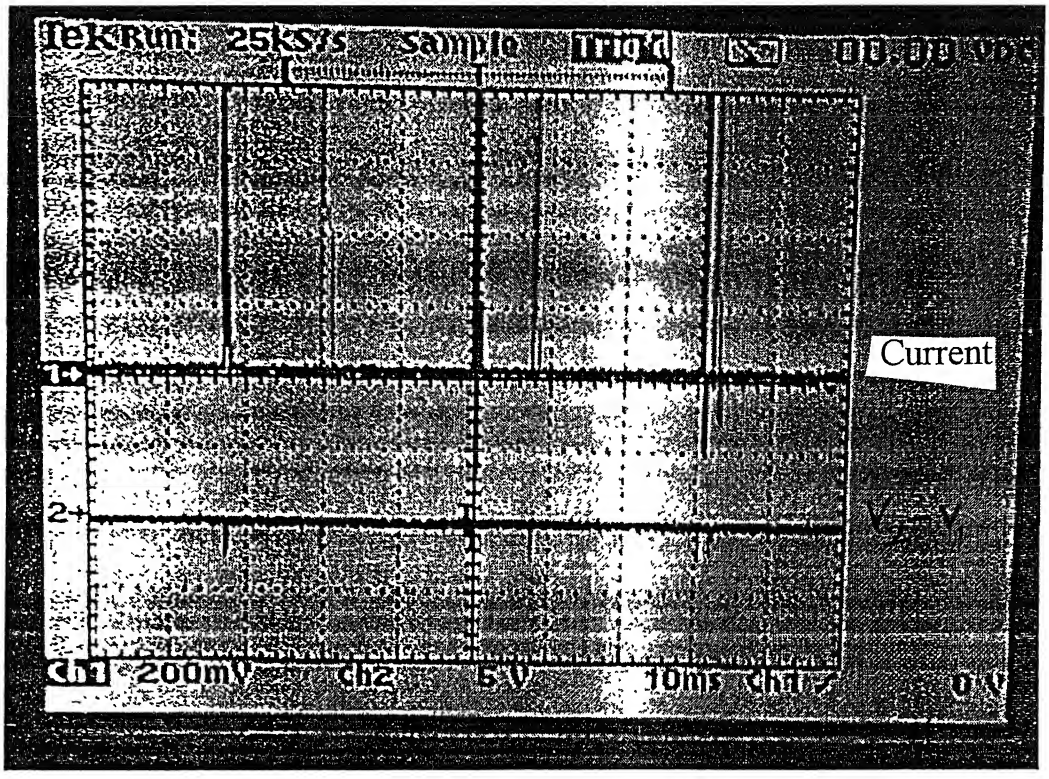

(a) R = 1 Ohm

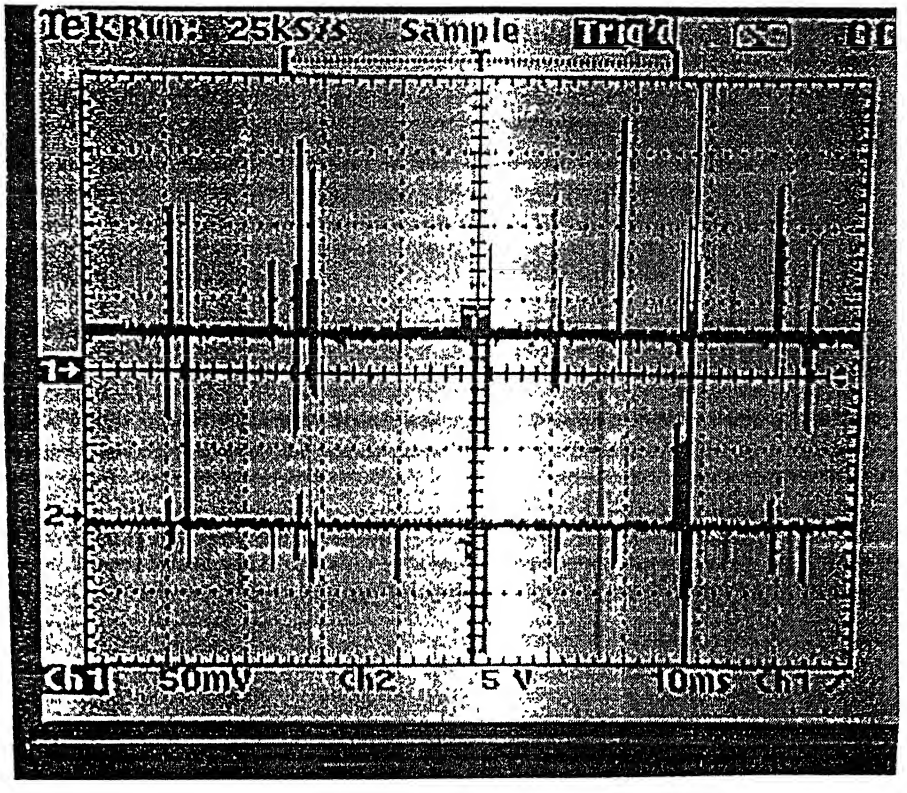

(b) R = 0.15 Ohm

Figure 3.9 Current pulses at the time of discharge with differential voltage V_2 - V_1 for different Resistance values showing the reduction in ignition delay with smaller resistance in series with cathode

discharge starts. Note that the multimeter's response time is quite high to show the spikes occurring at the time of discharge. The discharge occurring at lower voltages is taking place at a higher frequency rate (measured with the oscilloscope). The discharge is restricted over a very small region. Associated temperature change in the workpiece at that region might be very small to be detected by the pyrometer. As the voltage is increased further, the discharge frequency reduces. For voltages greater than 110V, the discharge frequency reduces. It is more agitating and the temperature change associated with this type of discharge is notable by the pyrometer.

Chapter 4 gives the discussion based on time varying current pulses on the development of discharge mechanism for the ECDM process. In view of this mechanism the alternative solution for use of the ECDM process for microwelding purposes is discussed.

APPLIED VOLTAGE	$V_2 - V_1$	FREQUENCY	DISCHARGE
Up to 10V	0.1V		No
Up to 20V	0.2V		No
Up to 40V	Fluctuations		No
Up to 60V	0	8 - 10 MHz	Yes (Constricted)
Up to 80V	0	11 - 15 MHz	Yes
Up to 90	0	1- 2 MHz	Yes
Up to 100V	0	500 - 700 kHz	Yes (Agitating)
Up to 110		200 - 50 kHz	Yes
> 110V	0	4 kHz - 100 Hz	Yes (Agitating with more splashing)

Table 3.10 Correlation the frequencies seen on the oscilloscope and occurrence of arc discharge (machining occurs at lower frequencies).

Chapter 4

BASIC MECHANISM OF ELECTROCHEMICAL DISCHARGE

4.1 Introduction

Although the electrochemical discharge machining process is commercially in use [15], the basic mechanism of the process is not yet completely understood and is still a matter of research investigations. At present the parameters used in the commercial system are empirical in nature. A thorough understanding of the basic mechanism is very important to improve the efficiency of the system and to find out ways for controlling the process parameters.

Understanding of a phenomena depends on the experimental measurements performed. In view of the discrete nature of the arc discharge occurring in the process, an appropriate experimental arrangement was made to capture the time dependence of current and temperature. The details of these are discussed in Chapter 2 and 3. These novel measurements offer deeper insight into the discharge mechanism in the ECDM process.

Before elaborating the mechanism proposed on the basis of measurements done in the present work, a brief outline of the models presented in the literature is given in the next section

4.2 Existing Models of Discharge Mechanism in ECDM

Various researchers have put forth explanations of ECDM phenomenon based on their experimental studies as described in Chapter 1. The main features of these models are presented below for the sake of continuity and completeness. It is understood that when the supply voltage is applied to the ECDM cell, bubble formation takes place at the

interfaces formed at both the electrodes (anode and cathode) due to electrolytic reaction. These electrodes are grossly different in size.

McGough and co-researchers [7] concluded that electrical discharge between cathode tool and electrolyte interface occurs due to

- electrolytic gas generation at the surface of electrodes,
- growth of layers of low ionic concentration near the electrodes and formation of the oxide films on the anode surface, and
- local variations in the electrolyte flow pattern caused by flow stagnation and eddy.

The reasons of the discharge are well identified by these researchers. But the cause of the discharge or the origin of the driving force or extra energy which is needed for discharge to take place has not been dealt with.

Basak [8] treats the discharge phenomenon as a 'switching off' process due to bubble bridges (Figure 1.8). According to Basak et al. [8], when hydrogen bubbles become sufficiently large in number, the resistance at the tool-electrode interface increases substantially due to the constriction effect. This leads to ohmic heating of electrolyte at that region, causing generation of vapour bubbles. When the nucleation site density of bubbles increases, the bubbles cover the maximum possible area of the tool, a blanketing of tool occurs, creating a 'switching off' situation for a short time with zero current. Basak had connected an external inductor in the circuit, so that the spark discharge takes place with large dI/dt. The external inductor has been identified as the key process parameter. The inductor used in the experimental setup appears to be unnecessary since the discharge takes place even in the absence of external inductor.

Jain et al. [9] have considered each gas bubble as a valve (Figure 1.9), which after its breakdown due to high electric field produces discharge in the form of arc. In proposing their 'valve theory' several assumptions regarding diameter of the bubble, electric field intensity, frequency of the spark, etc. have been made. It seems that with overall increase in hydrogen bubble number, the equivalent parallel resistance offered by these valves reduces, which is in contrast with the statement [9] that the overall resistance increases. It is also mentioned that with each bubble break, the discharge takes place. If

this is true then discharge should also occur in case when the tool tip is immersed deeper (say about 4-5mm) in the electrolyte. A crucial observation in the present work is that when cathode is immersed deeper in the electrolyte, discharge does not take place. For a discharge to occur the tool has to be immersed just a fraction of mm below the liquid surface. Thus the above mentioned observations, i.e., absence of inductor and the dependence of arc on the immersion depth of tool, can not be explained by the models proposed by Basak et al.[8] and Jain et al.[9].

Based on the experimental observations of time varying current and temperature a new mechanism for electrochemical discharge is proposed.

4.3 Background of the Proposed Mechanism

In the present context of the ECDM process, the term 'discharge' is related to the breakdown of gases resulting in luminescence. If two electrodes have a gas at low pressure between them and a gradually increasing voltage is applied across them, a series of events take place. First a very small current (microamperes) will flow as the ions and electrons are attracted towards the electrodes. As the voltage is raised, the current increases rapidly as the electrons gain energy and ionizes gas atoms producing more number of electrons. Beyond a critical voltage value the current increases suddenly very rapidly, and at the same time the voltage across the electrodes drops. The value of the voltage at which this occurs is the breakdown voltage and the gas breaks into a self-sustaining discharge called 'glow discharge'. If the current is not limited by circuit resistance, it continues to increase, almost instantaneously. The voltage drops to a low value and the discharge becomes an 'arc'. Thus, glow discharge is characterized by the ability to pass moderate current at moderate values of voltage, while the arc is a low-voltage, high-current electrical discharge [16]. The arc discharge is initiated by phenomenon of field-induced electron emission which requires a voltage gradient of the order of 25V/μm [17].

As discussed above, the discharge in ECDM process can be compared to the 'arc discharge' in gases. When a DC voltage greater than the threshold value that is needed to

produce the discharge is applied to the ECDM cell, electrolysis reactions take place. Reduction of electrolyte at cathode results in hydrogen gas bubbles. These bubbles get accumulated at cathode tip immersed in electrolyte. Bubble generation goes on increasing leading to combining of bubbles to a single large bubble which isolates the tip completely from the electrolyte. This causes the local electric field gradient between the tool and the electrolyte interface to go beyond the breakdown limit of 25V/μm leading to an arc discharge. It should be remembered that the arc discharge occurs even at atmospheric pressure. This is the basis for developing the proposed discharge mechanism in the ECDM process.

4.4 Mechanism in View of Time Varying Current Pulses

Figure 4.1 shows the current pulses captured during typical experiments. Occurrence of each current spike is correlated with each discharge event taking place. This trend of the current spikes is observed for different workpiece materials with different combination of supply voltage and electrolyte concentration as the process parameters.

Based on the time dependence of the current, Figure 4.2 describes the discharge mechanism pictorially. The first column of the figure shows the physical situation existing in the ECDM cell. The second column shows the voltage distribution or potential gradient in the ECDM cell under the respective conditions shown in column one. The third column shows portions of the experimentally obtained current versus time plot from which the situations in column one and two are inferred. The time sequence of the events occurring can now be described as follows :

- When a DC voltage V_{supply} is applied, the potential drop across the cathode-electrolyte interface appears as shown in Figure 4.2 (a). A small ionic current flows (see third column, current vs. time).
- Hydrogen gas bubbles evolve causing the interface resistance to increase. The number and size of bubbles within the interface region grow over the time (Figure 4.2 b).

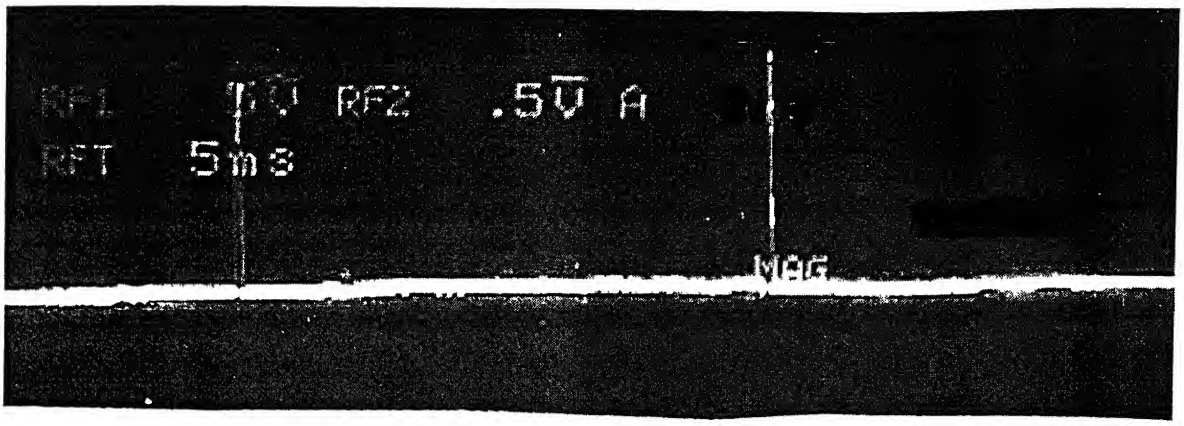

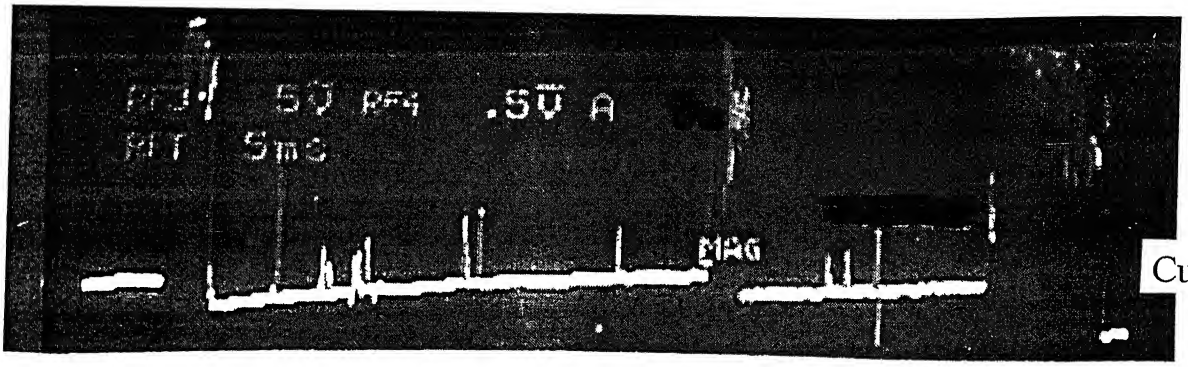

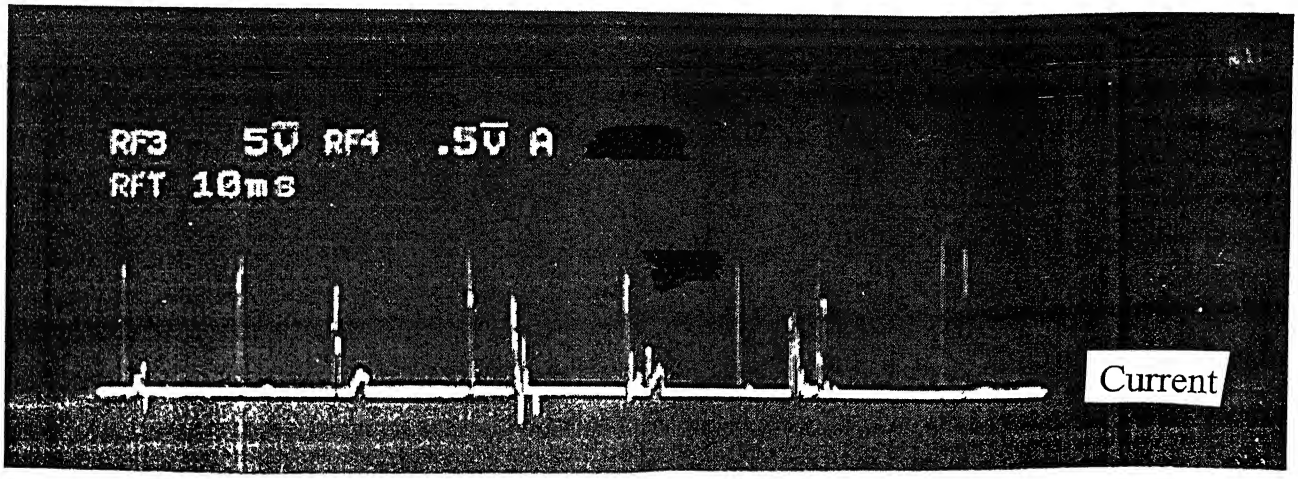

Figure 4.1 Occurrence of Current pulses showing the formation of Arc Discharge

- When an isolating film of hydrogen gas bubbles covers the cathode tip portion in the electrolyte, the tip is covered by a gaseous layer as shown in Figure 4.2 (c), column1. At this time a large dynamic resistance is present and the current through the circuit becomes almost zero (Figure 4.2 c). A high electric field of the order of 10^7 V/m [V_{supply} / d (μm)] gets generated causing an arc discharge within the gas layers covering the tip. The arc should occur between the tip of the tool and the inner surface of the electrolyte.
- At the instant when discharge occurs, a large number of electrons caused by the ionization of gas flow towards anode. Thus a large current $I_{discharge}$ flows through the spark channel (Figure 4.2 d) for a very short duration of time (of the order of few milliseconds). Figure 4.1 shows this current spike captured on a storage oscilloscope. The process is further illustrated in Figure 4.3. The ions flow towards cathode (the tool tip) as shown.

In the published literature, there is a wide variation in reported values of bubble diameter, 1μm [7] and 25 to 55μm [9]. Thus for a V_{supply} = 155V, the electric field could be anywhere between 2.8V/μm to 155V/μm, a value comparable to that specified for the discharge to occur [17]. When the entire process described in Figure 4.2 (a) to 4.2 (d) is completed, the evolution of hydrogen gas bubbles starts again, and when complete isolation of the tool tip with single gas layer occurs the discharge takes place causing a current spike and the process repeats itself.

Hydrogen gas bubbles generate at both the electrodes. But as the anode is much larger in size, the possibility of complete isolation of the immersed anode surface does not take place. Hence discharge can not take place at anode. If the geometry is made same as the one shown in Figure 4.2(a) with the polarities reversed, i.e. the smaller electrode is now made to act as anode, the discharge takes place at anode as well.

The electrons emitted due to the breakdown of gas get bombarded on the workpiece surface which is placed near the cathode as shown in Figure 4.3. This bombardment of electrons increases the workpiece temperature locally. Due to

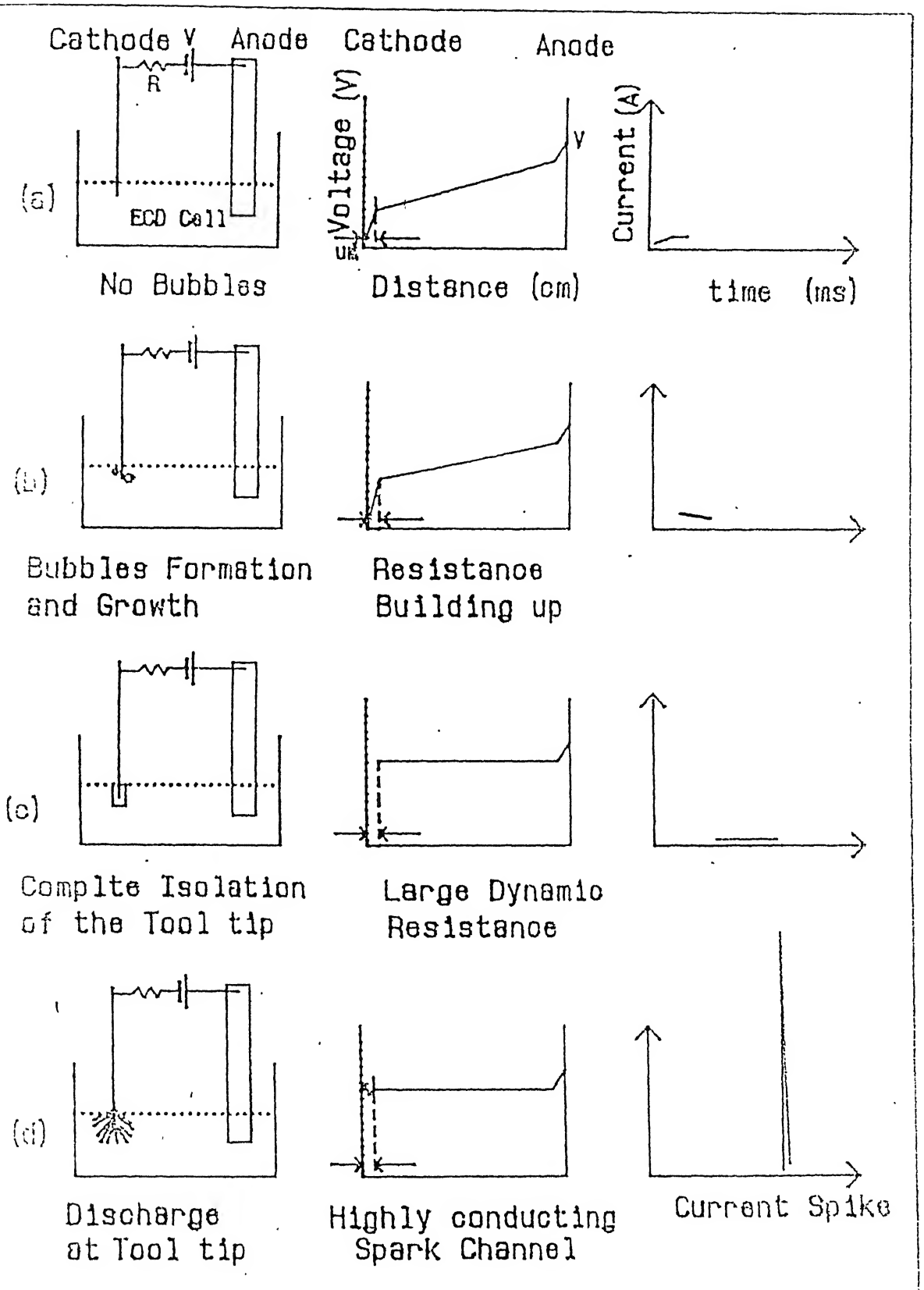

Figure 4.2 Discharge Mechanism elaborating the occurrence of different physical stages together with the voltage distribution and the nature of the current during the discharge in ECDM cell

(a) No bubbles (b) Bubble formation and their growth
(c) Complete isolation of the tool tip (d) Occurrence of discharge

conduction and convection within the electrolyte, the bombarded region immediately cools down. That is each arc produces a temperature spike on the workpiece. These temperature spikes are recorded by the pyrometer as discussed in Chapter 3.

4.4.1 Differential Voltage inside the ECDM Cell

To further validate the present model, specifically the occurrence of a single gas layer surrounding the tip and isolating it from the rest of the electrolyte, voltages V_1 and V_2 in the electrolyte are measured with two separate electrodes (E_1 and E_2) dipped in the electrolyte cell. Their location is shown in Figure 4.4. Electrode E_1 is kept at a distance of 1cm away from the cathode and the other electrode E_2 is near to anode at a distance of 0.5cm from it. These probes and the electrodes, i.e., E_1, E_2, cathode and anode are placed in a straight line. When isolation occurs (Figure 4.2 c) both V_1 and V_2 should be at the same potential. Further, the discharge (Figure 4.2 d) should induce a current pulse through these probes. The differential voltage waveforms recorded between probes E1 and E2 show this expected behavior. The voltage across E_1 and E_2 is measured in differential mode. Figure 4.5 shows the corresponding waveform. It is seen that the difference in V_2 and V_1 is almost zero before it shoots up at the time when discharge takes place. Figure 4.6 (a) and (b) exhibit the events captured at different times and show the actual current pulses observed together with the differential waveform (V_2-V_1). This validates the physical situation predicted in the present model as depicted in Figure 4.2.

4.5 Microwelding Using ECDM

Based on the measurements performed and the mechanism proposed in this work it can now be argued that the geometry which utilizes a fine metallic tip as cathode is very suitable for machining but it is not at all suitable for microwelding. The reason is attributed to the heating mechanism (see Figure 4.3) which is due to electrons getting bombarded on the workpiece. The cathode also gets heated up due to positive ion current but the effect is not as significant as it is on the workpiece. We have observed that the temperature of cathode also increases but it never shows reduction in weight. In order to utilize this ECDM process for microwelding the tool should be made to act as anode

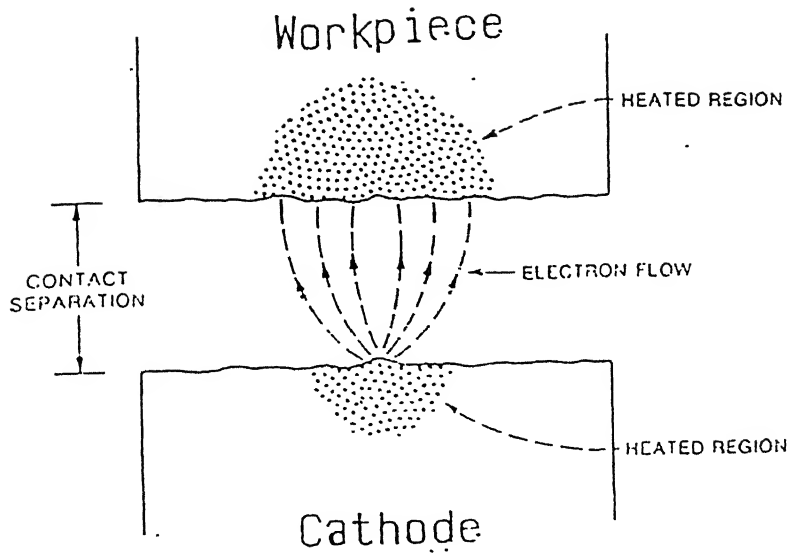

Figure 4.3 Bombardment of electrons on workpiece surface in arc discharge

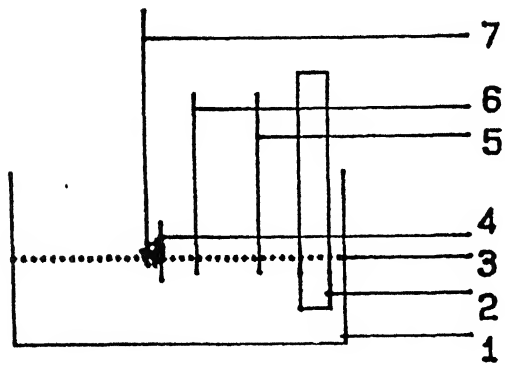

1-ECDM cell. 2-Anode.
3-Electrolyte. 4-Workpiece.
5-Probe2 (E2). 6-Probe1 (E1).
7-Cathode with Discharge at its tip

Figure 4.4 Location of E_1 and E_2 with respect to cathode and anode

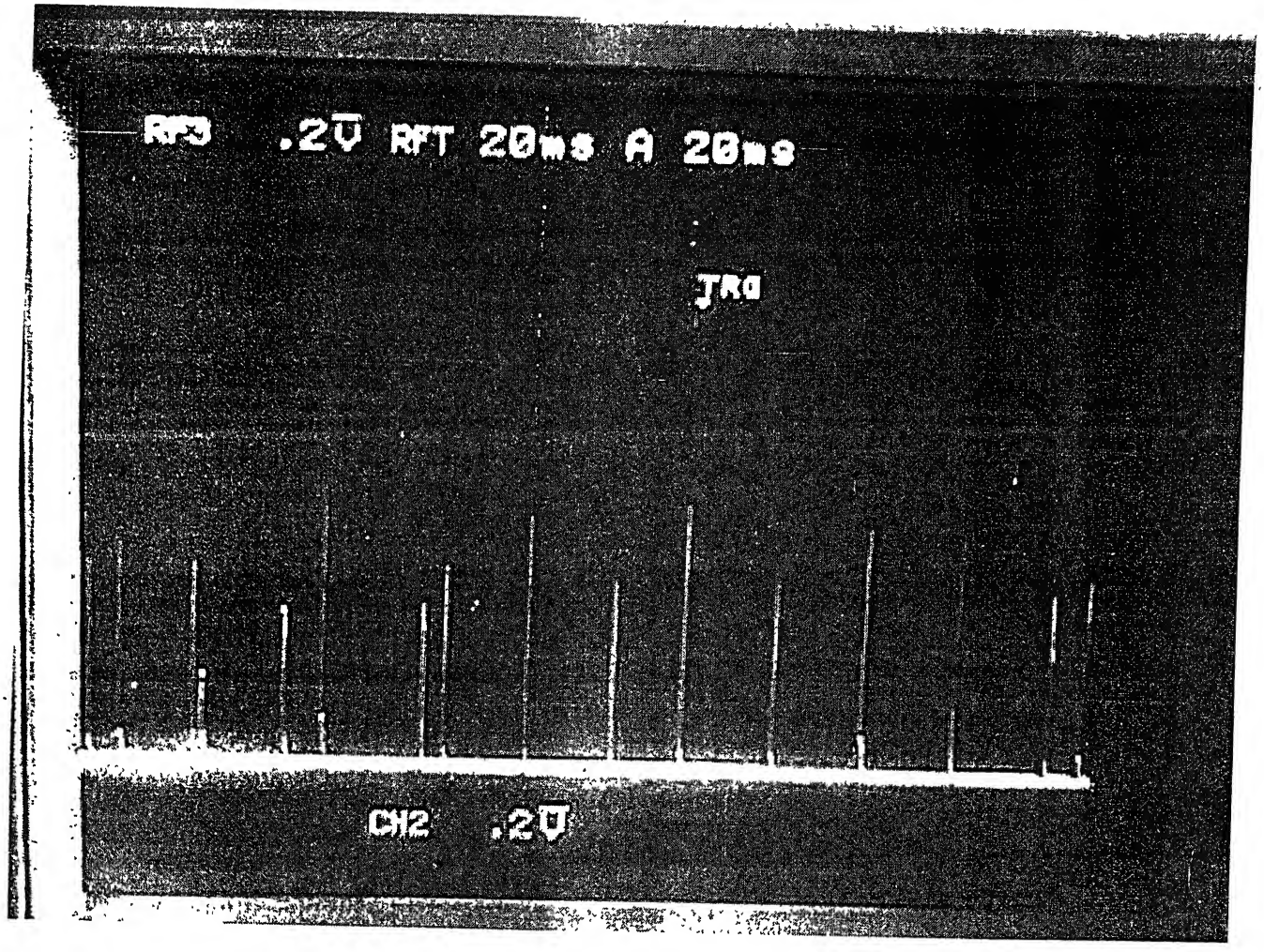

Figure 4.5 Differential voltage V_2 - V_1

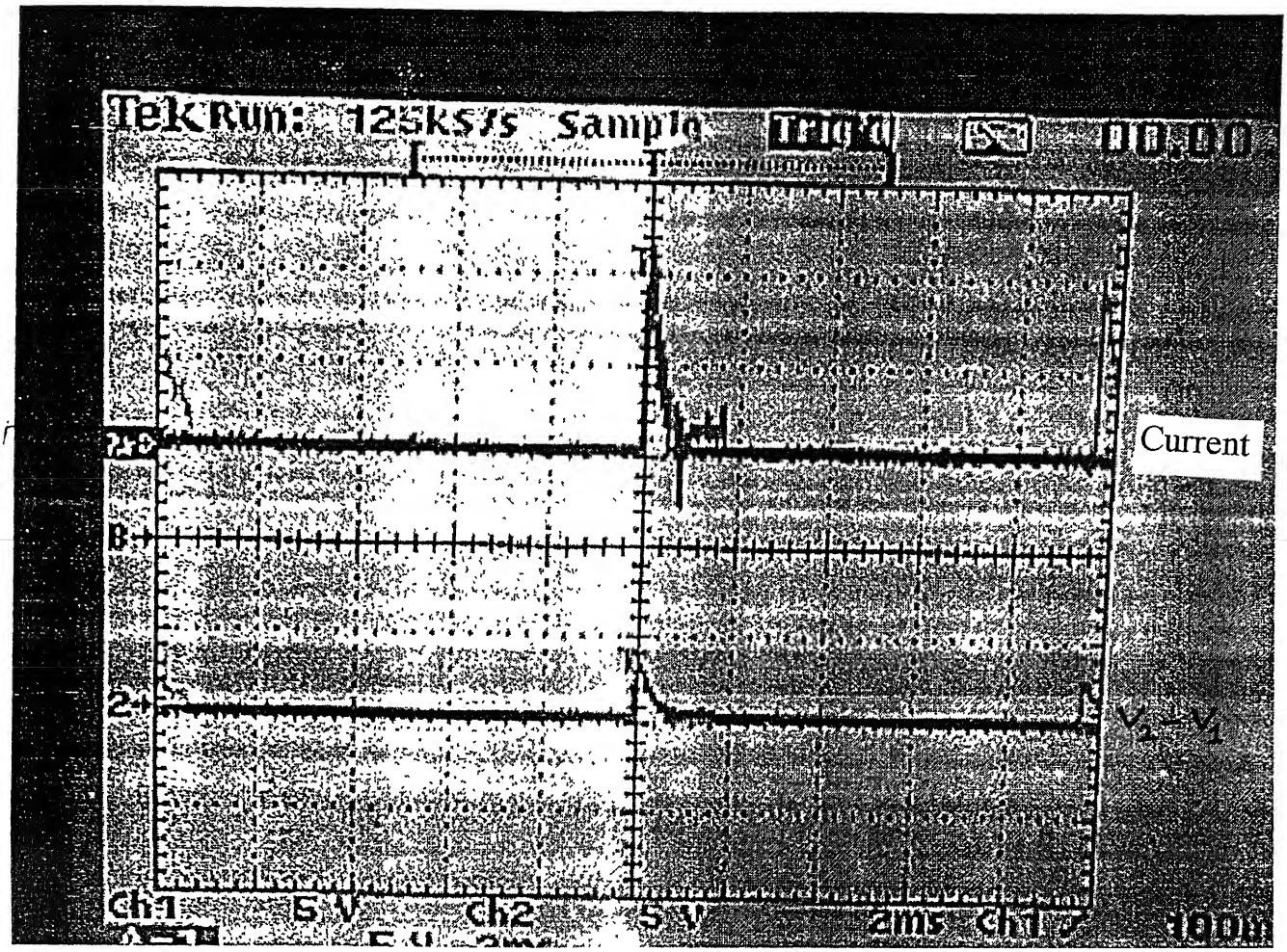

Figure 4.6 (a) Current pulses at the time of discharge with differential voltage $V_2 - V_1$

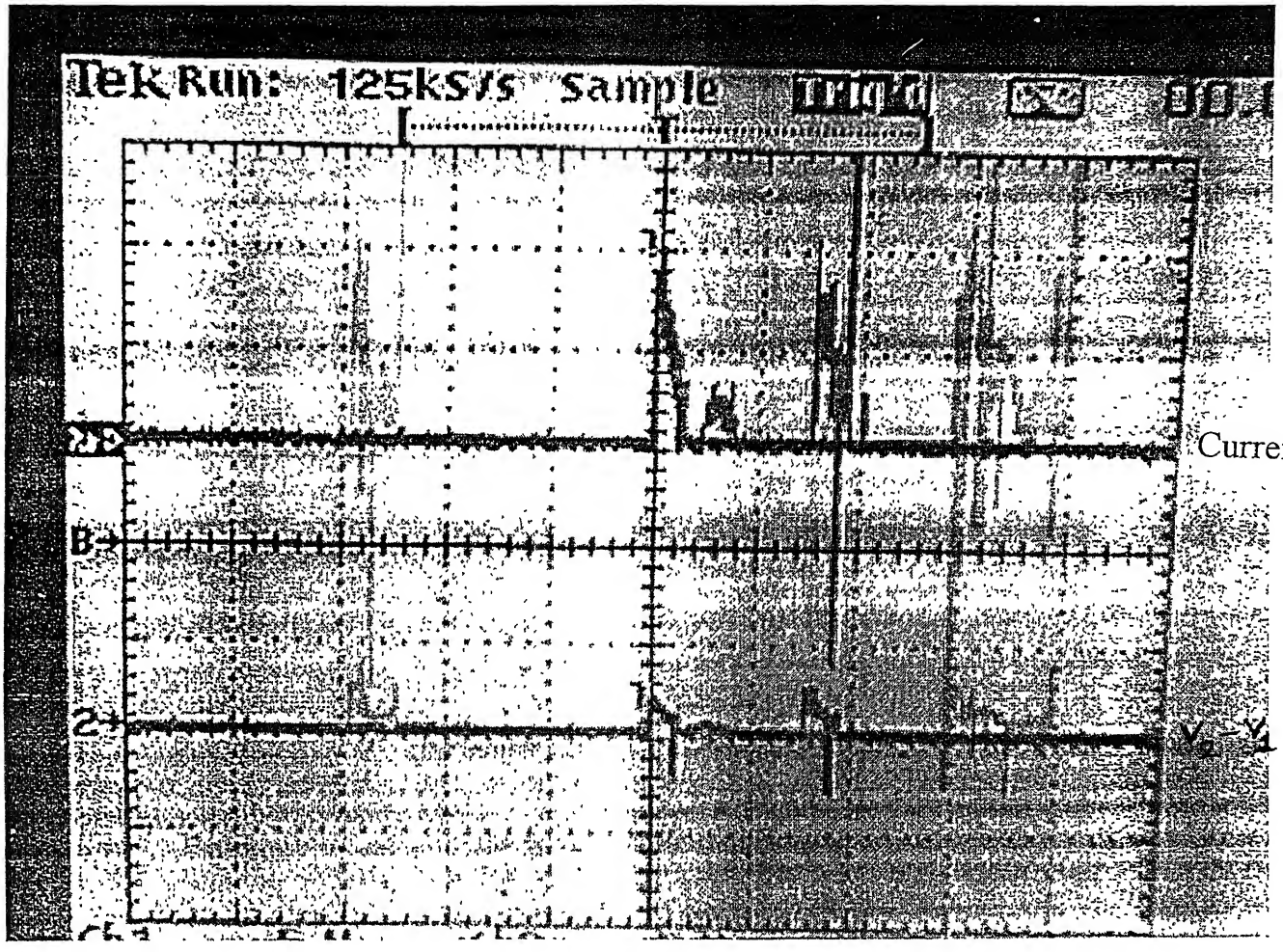

Figure 4.6 (b) Current pulses at the time of discharge with differential voltage $V_2 - V_1$

keeping the geometry same as in the case of ECDM. This arrangement would now lead to discharge with electrons flowing towards the anode(tool) and the ions flowing towards the cathode(workpiece). The overall effect is evaporation of the tool material and temperature rise in the workpiece. This is a favorable situation for welding to occur on the workpiece.

The above geometry is being utilized for welding (using electrolyte jet instead of a bath) by Ghosh et al. [18]. However, the choice of tool as anode has been made only on the basis of empirical observations. The model described in this chapter offers a consistent explanation to both the ECDM process and ECDM based microwelding process.

Chapter 5

CONCLUSIONS

5.1 Conclusions

On the basis of the measurements of time varying current and temperature along with conventional measurements of average current and temperature performed at different locations with different sensors in the ECDM process, following conclusions can be drawn:

- Observation of the discharge treated workpiece under an optical microscope clearly shows the signature of individual discharges striking the surface, their size and their distribution over the surface. The discharge-affected region is seen as circular zone in nature. The circular zones and their boundaries appear shiny with wrinkles surrounding it. These features appear to be reminiscent of rapid solidification of the material after melting.
- Out of the total energy consumed in the process, about 93% of energy is utilized by the electrolyte in raising its temperature. About 4% of total energy is used in the workpiece. The rest gets in other phenomena occurring in the process. Thus the efficiency of the process is very low.
- The discharge is a discrete phenomenon. The breakdown is similar to the one that occurs in a gas due to a large electric field of the order of 10^7 V/m which gets generated locally.
- The discharge frequency for copper, silicon and tantalum is comparable and ranges from 30-100 Hz when the machining occurs.
- A mechanism based on the observations of time varying current and temperature measurements is proposed. When an isolating film of hydrogen gas bubbles covers the cathode tip portion in the electrolyte, a large dynamic resistance is present and the current through the circuit becomes almost zero. A high electric field of the order of 10^7 V/m [V_{supply} / d (μm)] gets generated causing an arc discharge within the gas layers covering the tip. The electrons

flow towards the workpiece kept near the cathode tip. This flow of electron is seen as a current spike of about 20 A or more for a short duration of a few ms.. This bombardment of electrons raises the temperature of the workpiece momentarily and then the temperature decreases due to quenching. This local change in temperature is sensed by the pyrometer which shows a sharp pulse indicating rates of heating (above 815 C) and rapid quenching of the region of the workpiece where the arc strikes the surface.

- Based on the measurements performed and the mechanism proposed in this work it can now be argued that the geometry which utilizes a fine metallic tip as cathode is very suitable for machining but it is not suitable for making microwelding on the workpiece. The reason is attributed to the heating mechanism which is due to electron flow towards the workpiece. In order to utilize this ECDM process for microwelding, the tool should be made to act as anode keeping the geometry same as in the case of ECDM. This arrangement would now lead to discharge with electrons flowing towards the anode (tool) and the ions flowing towards the workpiece. The overall effect is evaporation of the tool material and temperature rise of the workpiece resulting in a good microwelding. Thus the mechanism proposed in this study offers a consistent explanation of the ECDM process and its extrapolation to microwelding purposes.

5.2 Scope for Future Study

There is a large scope for further investigations of the details of the process. Some of which are given below.

1. Effect of single pulse

Study of discharge phenomena in response with a high voltage, short duration single pulse will reveal the effects caused by a single arc discharge.

2. High speed photography

Study of discharge phenomena by performing high speed photography can be useful in capturing the different physical stages in the electrolyte prior to discharge. A direct evidence of stages such as evolution of gas bubbles, their growth, formation of an isolating layer over the cathode tip can be obtained.

3. Theoretical calculation of surface temperature

The temperature profiles on the workpiece surface can be calculated using the experimentally observed current pulses as the source term in the heat diffusion equation. Comparison of the calculated temperature with the one measured by the pyrometer can be done. Such studies would lead to the development of a procedure to predetermine the experimental parameters for machining of a material.

4. Close loop control of the ECDM process

By utilizing the temperature signal sensed by the pyrometer and current pulses measured in this work as feedback parameters, a close loop control of the process can be developed.

References

[1] DeBarr A. E. and Oliver D.A., 'Electrochemical machining', MacDonald and Co. Ltd., 1975.

[2] McGeough, J.A., 'Principles of electrochemical machining', Chapman and Hall, Ltd., London, 1974.

[3] Bhattacharya, A., 'New technology', The Institution of Engineers, Calcutta, 1973.

[4] Allesu, K., ' Electrochemical discharge phenomenon in manufacturing processes', Ph.D. Thesis, IIT, Kanpur, 1988.

[5] Parija, S., 'Thermal model and parameteric investigation of electrochemical discharge micro-welding', M.Tech. Thesis, IIT, Kanpur, 1993.

[6] Ghosh, A. 'Electrochemical discharge machining: Principle and possibilities', Sadhana, Vol 22, 1997, pp 435-447.

[7] Crichton, I.M. and McGough, J.A., 'Studies of the discharge mechanisms in electrochemical arc machining', J of Applied Electrochemistry, Vol 15, pp1985,113-119.

[8] Basak I. and Ghosh, A., 'Mechanism of spark generation during electrochemical discharge machining: a theoretical model and experimental investigation', J. of Materials Processing Technology, Vol 62,1996, pp 46-53.

[9] Jain, V. K., Dixit, P.M. and Pandey, P.M., 'On the analysis of the electrochemical spark machining process', Int. J. of Machine Tools and Manufacture, Vol 39, 1999, pp 165-186.

[10] Basak, I., 'Electrochemical discharge machining: mechanism and a scheme for enhancing material removal capacity', Ph.D. Thesis, IIT, Kanpur, 1992.

[11] Reghuram V., 'Electrical and spectroscopic investigations in electrochemical discharge machining', Ph.D. Thesis, IIT Madras, 1994.

[12] Cocharan, W.G. and Cox, G.M.'Experimental designs', Asia Publishing House, 1957.

[13] Sriram V., 'Preliminary investigations into electrochemical discharge microwelding of thin plates', M.Tech Thesis, IIT Kanpur, 1997

[14] Tse, F.S. and Morse, I.E., 'Measurement and instrumentation in engineering', Dekker Inc. New York, 1989.

[15] Dover, S.J., Bocking, C. And Bennet, 'An Investigation into the suitability of high speed selective jet electrodeposition for rapid prototyping and tooling', Proc. First national Conf. On Rapid Prototyping and Tooling Research , Editor Bennet, G. , Mechanical Engineering Pub. Ltd., 1995, pp 155-173.

[16] Conn, G.K.T. and Fowler, G.N., 'Essays in physics', Academic Press INC., London, 1972.

[17] Ott, H.W., ' Noise reduction techniques', John Wiley and Sons, New York, 1976.

[18] Ghosh, A., Mishra, P.K., Saha, P., Saraf, A., 'A feasibility study using electrochemical deposition for rapid prototyping', Proc. Of 18th All India Manufacturing Technology Design and Research conference, 1998, pp 328-333.

Appendix A

A1.1 Thermocouples

A thermocouple consists of two dissimilar metallic wires A and B. The two junctions of these metals are at different temperatures, T_1 and T_0, as shown in Figure A1.1, three effects are there which describe the functioning of the thermocouple [A1].

These effects are

- Seebeck effect: describes the open-circuit voltage developed in a thermocouple circuit. Figure A.1 shows that in a circuit of two different metallic conductors, current flows round the circuit if the junctions are at different temperatures. The voltage driving this current is found to be

$$E_{AB} = e_{AB} (T_1 - T_0)$$

where e_{AB} is Seebeck coefficient.

- Peltier effect: this relates the reversible heating and cooling that occurs when an electric current crosses a junction between two dissimilar metals. Peltier discovered that the passage of current across the junction of two different metals produces a rejection or absorption of heat, depending on which way the current flows. Heat is rejected at cold junction and absorbed at hot junction. Quantity of heat, Q, rejected or absorbed is given by

$$Q_C = -\pi_{AB} (T_C)$$

- Thompson Effect: relates the reversible heating and cooling in a homogeneous conductor, subjected to a thermal gradient and a current flow. He found that heat could be absorbed by the conductor if current flowed in the same direction as the heat flow. The amount of heat absorbed is proportional to the quantity of electricity and the temperature difference. The constant of proportionality is known as Thompson's coefficient, σ_e, thus

$$Q_A = \sigma_e q_e (T_H - T_C)$$

To design and understand the thermocouple circuits, fundamental thermoelectric laws are evolved. These are, law of homogeneous circuits, the law of intermediate metals, and the law of successive temperatures. These are pictorially illustrated in Figure A1.2.

A1.2 Approximate physical properties of type K thermocouples

Type	+ Wire	- Wire	Temperature Range	Limits of Error
chromel-alumel	$Ni_{90}Cr_{10}$	$Ni_{95}Al_2$	0 to 1250^{0}C	$^+$2.2^{0}C

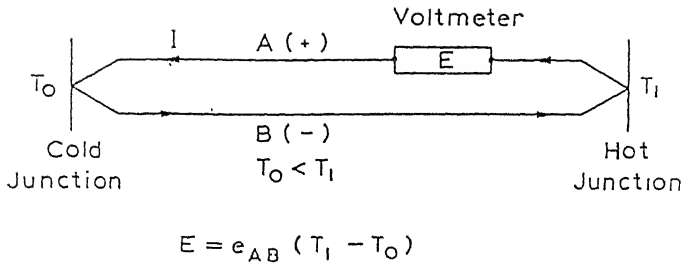

Figure A1.1 circuit of two different metallic conductors

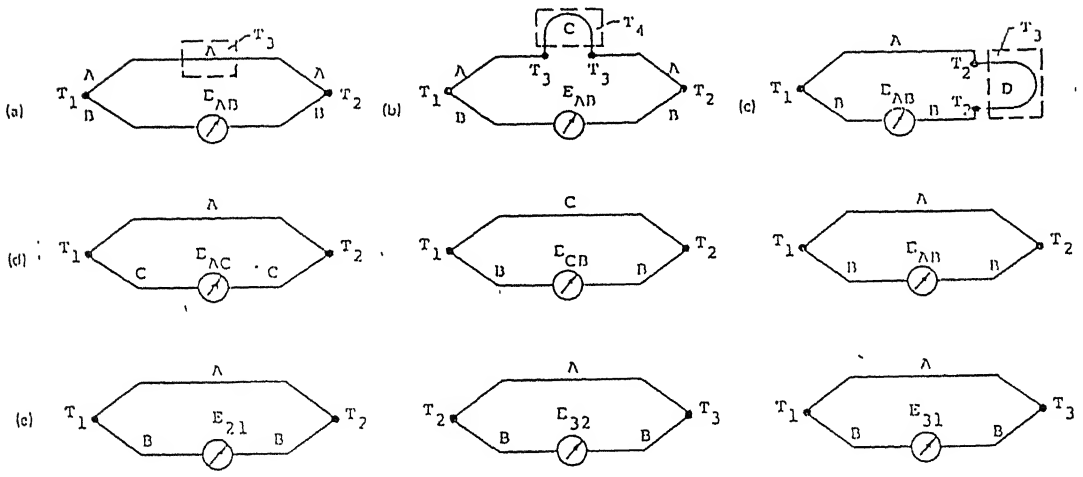

Figure A1.2 Fundamental thermoelectric laws of thermocouple circuits
(a)Homogeneous circuits. (b), (c)Intermediate metals. (d) Successive temperature

[A1] Lawton, B. and Klingenberg, G., 'Transient temperature in engineering and science', Oxford University Press, New York, 1996.

Appendix B

Radiation Thermometer

Temperature of a hot solid body, hot gases, various types of discharges are often difficult to measure with resistance thermometers and thermocouples, especially at the higher temperatures. Determination of temperature from the radiation, is a natural alternative to the use of RTD's and thermocouples. A radiation thermometer determines temperature in a non-intrusive way needing no contact with the hot radiator enabling the sensor to work at room temperature. Also for bodies that are moving, such a non-contacting means of temperature sensing is most convenient. Furthermore, the temperature variations over the surface can be available by 'scanning' over the area. A radiation thermometer is a radiometer calibrated to indicate the temperature of a blackbody, the perfect or ideal radiator. Radiation is emitted continuously by all objects by virtue of their temperature. The radiometer senses radiant flux (electromagnetic radiation) from the target and infers about its temperature through a calibration algorithm. This algorithm involves the spectral emissivity of the surface. The part of the electromagnetic radiation spectrum between 3-40 μm is used for pyrometry.

Radiation is found to exhibit wave characteristics as well as quantum characteristics. The physical law governing the thermal radiation pyrometry is about the distribution of radiant power intensity from a black body at a given temperature for varying wavelengths. Plank's law describes it,

$$W_b(\lambda, T) = \frac{c_1}{\pi\lambda^5[\exp(c_2/\lambda T) - 1]}$$

where $c_1 = 2\pi hc^2$ (W.m^2), $W_b(\lambda, T)$ = radiant power intensity (W/m^2),

λ = wavelength (m), c_2 = hc/k (mK), h = Plank's constant (J/s) and T = temperature (K)

c = speed of light (m/s), k = Boltzmann's constant (J/K).

Wien's law is approximation of the Plank's law. The Stefan-Boltzmann's law relates the radiant power intensity to the 4th power of temperature thus,

$$W_b(T) = \sigma e T^4$$

where σ = Stefan-Boltzmann constant (J m^2 / K^4 s) and e = emissivity.

The concept of black body and emittance are central to the study of pyrometry. A black body is a perfect absorber. By Kirchoff's law, for a black body, absorbvity is equal to emissivity. The emittance of a black body is unity. It is used for calibration of pyrometers.

The general features of a simple radiation thermometer are illustrated in Figure B.1 [B1]. An optical system transfers radiant flux from the target area to a detector having a spectral

responsivity $R(\lambda)$. Apertures within the optical system are used to define the field-of-view parameters: the field defining aperture area (A_d) and the solid angle (w_d); these in turn define the field of view (A_t) and solid angle (w_t) at the target. For properly designed and focused optical systems, the radiant flux reaching the detector is independent of the distance between the instrument and the target. The essential electronic component is an amplifier providing the output signal (S).

The calibration of the radiation thermometer is accomplished as illustrated in Figure B.2. The instrument is sighted upon the blackbody of known temperature (T_b), and the output signal (S) relationship to the target temperature, referred to as the calibration algorithm, is established. Since most commercial radiation thermometers are direct reading, this algorithm is embodied in the electronics and the user does not need to generate the relationship. The calibration process is based upon the target being a blackbody that has a unique characteristic of a known relationship described by Planck's law of radiation, describing the relationship between the spectral distribution of radiant flux and the temperature.

The radiation thermometers are also termed as radiometers, optical pyrometers, radiation pyrometers, spectro radiometers etc. to describe a particular type of instrument. Since this terminology is not standardized, one should know about the basic operating principle of a given instrument to be sure what its characteristics are.

[B1] Dewitt, D.P. and Nutter, G.D., 'Theory and practice of radiation thermometry'. John Wiley and Sons Inc., New York, 1988.

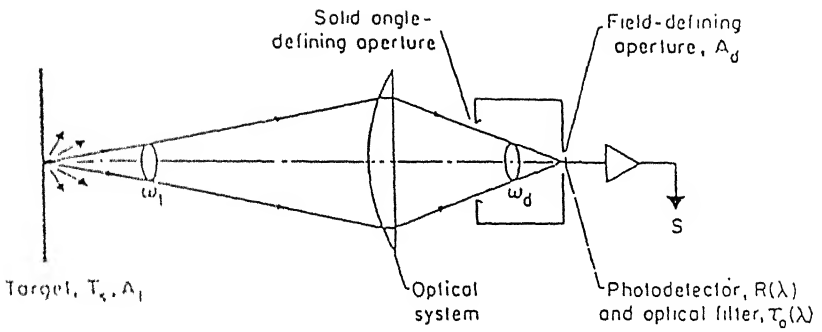

Figure B.1 General features of a simple radiation thermometer

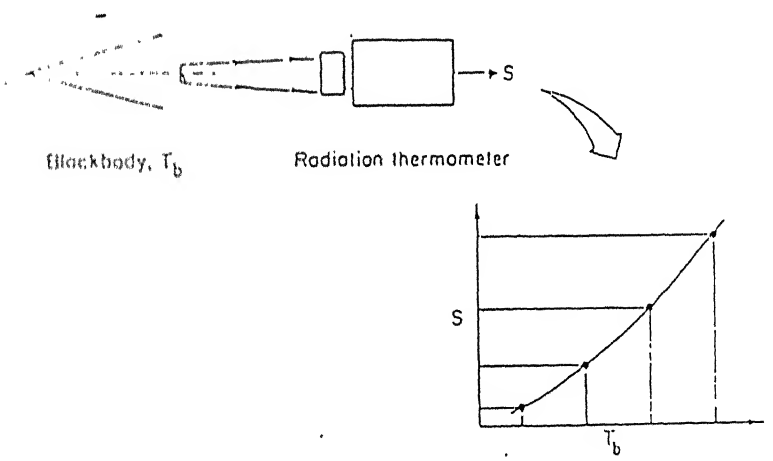

Figure B.2 Calibration of the radiation thermometer

MAURER-Infrared-Radiation Pyrometer Type KTR 85

compact unit

(transducer including objective and electronic process unit with external digital display)

No. 12237

Measuring range: 815 - 1700°C

Operation Instructions

I. Description:

MAURER Infrared radiation pyrometers are partial radiation pyrometers which operate in the region of the spectrum of 900 nm.

The compact unit is protected by suitable screening against electrical and magnetic influences, so that it can even be mounted in direct proximity to inductors, electrodes etc. To enable the compact unit to be exactly aligned with the measuring point, it is equipped with a viewfinder device.

The unit can be used generally for measurement and controll functions. The input of the emission factor and the absorption of the viewing glasses can be carried out directly in %. As the optics can be changed without affecting the calibration, optical matching and the selection of an observation zone of a different size is possible at any time.